

**Boston University**

**OpenBU**

**<http://open.bu.edu>**

Theses & Dissertations

Boston University Theses & Dissertations

2016

# Topics in perturbation analysis for stochastic hybrid systems

---

<https://hdl.handle.net/2144/17075>

*Boston University*

BOSTON UNIVERSITY  
COLLEGE OF ENGINEERING

Dissertation

**TOPICS IN PERTURBATION ANALYSIS FOR  
STOCHASTIC HYBRID SYSTEMS**

by

**JULIA L. FLECK**

B.Eng., Federal University of Rio de Janeiro (UFRJ), 2006  
M.S., Catholic University of Rio de Janeiro (PUC-Rio), 2008

Submitted in partial fulfillment of the  
requirements for the degree of  
Doctor of Philosophy

2016

© 2016 by  
JULIA L. FLECK  
All rights reserved

## Approved by

### First Reader

---

Christos G. Cassandras, PhD  
Professor of Electrical and Computer Engineering  
Professor and Head of Systems Engineering

### Second Reader

---

Ioannis Ch. Paschalidis, PhD  
Professor of Electrical and Computer Engineering  
Professor of Systems Engineering  
Professor of Biomedical Engineering

### Third Reader

---

Calin Belta, PhD  
Professor of Mechanical Engineering  
Professor of Systems Engineering  
Professor of Bioinformatics

### Fourth Reader

---

Pirooz Vakili, PhD  
Associate Professor of Mechanical Engineering  
Associate Professor of Systems Engineering

## Acknowledgments

I would like to thank my advisor, Christos G. Cassandras, for introducing me to the field of discrete event systems. I am most grateful for his willingness to spearhead into a promising albeit essentially unexplored new research direction and for allowing me to develop a work about which I am most passionate.

I am also most thankful to Bud Mishra and Stormy Attaway: the former, for sharing his visionary ideas on cancer research, and the latter for welcoming me time and again into her team of teaching assistants. Both are inspirational faculty members whose passion for research and excellence in teaching have left a profound mark on me.

Many thanks are due to my BU colleagues, in particular my CODES lab mates, who provided invaluable support both inside and outside the academic environment. I am especially thankful to Ana B. Pavel for our successful research partnership and cherished friendship.

Last, but certainly not least, my wholehearted gratitude to my family. I am indebted to my parents, exemplary role models, for helping me become the person I am today. And certainly at least half the credit for my success goes to my boys, João Felipe and Benjamin, without whose help and encouragement I would not have gotten as far as I have.

# TOPICS IN PERTURBATION ANALYSIS FOR STOCHASTIC HYBRID SYSTEMS

**JULIA L. FLECK**

Boston University, College of Engineering, 2016

Major Professor: Christos G. Cassandras, PhD  
Professor of Electrical and Computer Engineering  
Professor and Head of Systems Engineering

## ABSTRACT

Control and optimization of Stochastic Hybrid Systems (SHS) constitute increasingly active fields of research. However, the size and complexity of SHS frequently render the use of exhaustive verification techniques prohibitive. In this context, Perturbation Analysis techniques, and in particular Infinitesimal Perturbation Analysis (IPA), have proven to be particularly useful for this class of systems. This work focuses on applying IPA to two different problems: Traffic Light Control (TLC) and control of cancer progression, both of which are viewed as dynamic optimization problems in an SHS environment.

The first part of this thesis addresses the TLC problem for a single intersection modeled as a SHS. A quasi-dynamic control policy is proposed based on partial state information defined by detecting whether vehicle backlogs are above or below certain controllable threshold values. At first, the threshold parameters are controlled

while assuming fixed cycle lengths and online gradient estimates of a cost metric with respect to these controllable parameters are derived using IPA techniques. These estimators are subsequently used to iteratively adjust the threshold values so as to improve overall system performance. This quasi-dynamic analysis of the TLC problem is subsequently extended to parameterize the control policy by green and red cycle lengths as well as queue content thresholds. IPA estimators necessary to *simultaneously* control the light cycles and thresholds are rederived and thereafter incorporated into a standard gradient based scheme in order to further ameliorate system performance.

In the second part of this thesis, the problem of controlling cancer progression is formulated within a Stochastic Hybrid Automaton (SHA) framework. Leveraging the fact that cell-biologic changes necessary for cancer development may be schematized as a series of discrete steps, an integrative closed-loop framework is proposed for describing the progressive development of cancer and determining optimal personalized therapies. First, the problem of cancer heterogeneity is addressed through a novel Mixed Integer Linear Programming (MILP) formulation that integrates somatic mutation and gene expression data to infer the temporal sequence of events from cross-sectional data. This formulation is tested using both simulated data and real breast cancer data with matched somatic mutation and gene expression measurements from The Cancer Genome Atlas (TCGA). Second, the use of basic IPA techniques for optimal personalized cancer therapy design is introduced and a methodology applicable

to stochastic models of cancer progression is developed. A case study of optimal therapy design for advanced prostate cancer is performed. Given the importance of accurate modeling in conjunction with optimal therapy design, an ensuing analysis is performed in which sensitivity estimates with respect to several model parameters are evaluated and critical parameters are identified. Finally, the tradeoff between system optimality and robustness (or, equivalently, fragility) is explored so as to generate valuable insights on modeling and control of cancer progression.



# Contents

<b>1</b>	<b>Introduction</b>	<b>1</b>
1.1	Stochastic Hybrid Systems . . . . .	2
1.1.1	Models for SHS . . . . .	3
1.1.2	Optimization of SHS . . . . .	6
1.2	Infinitesimal Perturbation Analysis . . . . .	14
1.3	Traffic Light Control . . . . .	16
1.4	Modeling and Control of Cancer Progression . . . . .	27
1.5	Contributions of this Work . . . . .	35
1.6	Document Outline . . . . .	38
<b>2</b>	<b>Traffic Light Control with Fixed Light Cycles</b>	<b>41</b>
2.1	TLC Problem Formulation . . . . .	42
2.2	IPA for TLC with Fixed Light Cycles . . . . .	49
2.2.1	State and Event Time Derivatives . . . . .	51
2.2.2	Cost Derivatives . . . . .	54
2.3	Simulation Results . . . . .	55
<b>3</b>	<b>Traffic Light Control with Quasi-Dynamic Light Cycles and Thresholds</b>	<b>62</b>
3.1	TLC Problem Formulation . . . . .	62

3.2	IPA for TLC with Quasi-Dynamic Light Cycles and Thresholds . . . . .	64
3.3	Simulation Results . . . . .	66
<b>4</b>	<b>Integrating Genomic Data to Infer Cancer Progression</b>	<b>72</b>
4.1	Problem Formulation . . . . .	76
4.2	Results . . . . .	84
4.2.1	Simulated data . . . . .	84
4.2.2	TCGA breast cancer data . . . . .	86
<b>5</b>	<b>Personalized Cancer Therapy Design</b>	<b>98</b>
5.1	Problem Formulation . . . . .	101
5.1.1	Stochastic Model of Prostate Cancer Evolution . . . . .	101
5.1.2	IAS Therapy Evaluation and Optimization . . . . .	109
5.2	IPA for the SHA Model of Prostate Cancer Evolution . . . . .	113
5.2.1	State and Event Time Derivatives . . . . .	114
5.2.2	Cost Derivative . . . . .	122
5.3	Simulation Results . . . . .	123
5.3.1	Achieving Therapy Personalization . . . . .	130
<b>6</b>	<b>Issues in Cancer Therapy Personalization: Robustness vs. Optimal- ity</b>	<b>132</b>
6.1	Problem Formulation . . . . .	132
6.2	IPA for the SHA Model of Prostate Cancer Evolution . . . . .	134
6.2.1	State and Event Time Derivatives . . . . .	134

6.2.2	Cost Derivative . . . . .	144
6.3	Simulation Results . . . . .	145
<b>7</b>	<b>Conclusion</b>	<b>157</b>
7.1	Future Directions . . . . .	159
<b>A</b>	<b>IPA for Stochastic Hybrid Systems</b>	<b>162</b>
<b>B</b>	<b>IPA Algorithm for TLC with Fixed Light Cycles</b>	<b>170</b>
<b>C</b>	<b>Mathematical Proofs</b>	<b>178</b>
C.1	Chapter 2 . . . . .	178
C.1.1	Proof of Lemma 2.1 . . . . .	178
C.2	Chapter 3 . . . . .	179
C.2.1	Proof of Lemma 3.1 . . . . .	179
C.3	Chapter 5 . . . . .	183
C.3.1	Proof of Lemma 5.1 . . . . .	183
C.3.2	Proof of Theorem 5.1 . . . . .	183
	<b>References</b>	<b>186</b>
	<b>Curriculum Vitae</b>	<b>199</b>

# List of Tables

2.1	Optimization results for system with a priori fixed cycle lengths . . .	57
2.2	Optimal cycle lengths obtained in (Geng and Cassandras, 2013) for $\mathbf{s} = [8, 8]$ . . . . .	58
2.3	Optimization results for system with optimal cycle lengths . . . . .	61
2.4	Comparison between three IPA-based approaches to the TLC problem	61
3.1	Optimization results for different traffic intensities . . . . .	67
3.2	Convergence results for different initial configurations . . . . .	70
4.1	Number of mutation and expression genes assigned to each <i>phase</i> of cancer progression using simulated data for $K=2$ . . . . .	85
4.2	Number of mutation and expression genes assigned to each <i>phase</i> of cancer progression using simulated data for $K=3$ . . . . .	85
4.3	Number of mutation and expression genes assigned to each <i>phase</i> of cancer progression using simulated data for $K=4$ . . . . .	86
5.1	Optimization results for different values of $W$ using the clinical model of Patient 1 . . . . .	129
6.1	Sensitivity of model parameters around the optimal therapy configuration	147

6.2	Sensitivity of model parameters around a suboptimal therapy configuration . . . . .	150
-----	---	-----

# List of Figures

1·1	Typical framework of a stochastic simulation optimization . . . . .	10
1·2	Illustrative depiction of a stochastic model of tumor evolution (normal cells in orange and mutated cells in red) . . . . .	34
2·1	A single traffic light intersection with two cross-roads . . . . .	42
2·2	State space representation . . . . .	43
2·3	Illustrative representation of the dynamics of the “clock” state variable	46
2·4	Stochastic Hybrid Automaton for aggregate states $X(t)$ under quasi- dynamic control . . . . .	48
2·5	Typical sample path of a traffic light queue . . . . .	48
2·6	Sample cost and parameter trajectories for $1/\bar{\alpha} = [2, 6], \theta = [10, 30, 10, 30]$ , and $s_0 = [9, 10]$ . . . . .	58
2·7	Cost surface and convergence trajectories for <i>Scenario A</i> (note: the color scale refers to the cost values) . . . . .	59
2·8	Cost surface and convergence trajectories for <i>Scenario B</i> (note: the color scale refers to the cost values) . . . . .	60
3·1	SHA under quasi-dynamic control . . . . .	64
3·2	Sample cost and parameter trajectories for $1/\bar{\alpha} = [1.7, 3]$ . . . . .	69

3.3	Simulated traffic flow variation for $1/\bar{\alpha} = [2.2, 2.7]$ . . . . .	71
4.1	Example of a feasible solution of the MILP formulation proposed in this paper. Red boxes represent genes with mutation. Orange boxes mark genes with altered gene expression levels. White boxes correspond to those entries with no mutations or no expression changes. . . . .	83
4.2	Number of genes assigned to each <i>phase of cancer progression</i> for $K = 2$ (a) cancer mutation genes; (b) cancer expression genes; (c) random mutation genes; (d) random expression genes: 20% of genes were not assigned to any <i>phase</i> . . . . .	89
4.3	Number of genes assigned to each <i>phase of cancer progression</i> for $K = 3$ (a) cancer mutation genes; (b) cancer expression genes; (c) random mutation genes; (d) random expression genes: 20% of genes were not assigned to any <i>phase</i> . . . . .	90
4.4	Number of genes assigned to each <i>phase of cancer progression</i> for $K = 4$ (a) cancer mutation genes; (b) cancer expression genes; (c) random mutation genes; (d) random expression genes: 20% of genes were not assigned to any <i>phase</i> . . . . .	91
4.5	Number of genes assigned to each <i>phase of cancer progression</i> for $K = 5$ (a) cancer mutation genes; (b) cancer expression genes; (c) random mutation genes; (d) random expression genes: 20% of genes were not assigned to any <i>phase</i> . . . . .	92

4.6	Optimal solution of the MILP algorithm for cancer mutation and expression genes (K=3). Shown here is the assignment of mutation genes to each <i>phase of cancer progression</i> . . . . .	93
4.7	MILP model identifies causal relationships from PI3K/AKT and TP53 pathways (KEGG) (a) PI3K/AKT pathway is altered in <i>phase 1</i> of breast cancer progression; (b) TP53 pathway is altered in <i>phase 2</i> of breast cancer progression. . . . .	96
5.1	Schematic representation of Intermittent Androgen Suppression (IAS) therapy . . . . .	104
5.2	Stochastic Hybrid Automaton model of prostate cancer evolution under IAS therapy . . . . .	109
5.3	Convergence plots of average cost and PSA threshold values for initial configuration $[\theta_1^{init}, \theta_2^{init}] = [2.5, 14.0]$ (Patient #15) . . . . .	125
5.4	Convergence plots of average cost and PSA threshold values for initial configuration $[\theta_1^{init}, \theta_2^{init}] = [7.0, 12.5]$ (Patient #15) . . . . .	125
5.5	Convergence plots of average cost and PSA threshold values for initial configuration $[\theta_1^{init}, \theta_2^{init}] = [6.5, 9.0]$ (Patient #15) . . . . .	126
5.6	Convergence plots of average cost and PSA threshold values for initial configuration $[\theta_1^{init}, \theta_2^{init}] = [5.5, 14.5]$ (Patient #1) . . . . .	126
5.7	Convergence plots of average cost and PSA threshold values for initial configuration $[\theta_1^{init}, \theta_2^{init}] = [7.0, 15.0]$ (Patient #1) . . . . .	127



5·8	Convergence plots of average cost and PSA threshold values for initial configuration $[\theta_1^{init}, \theta_2^{init}] = [4.5, 11.5]$ (Patient #1) . . . . .	127
5·9	Response surface and convergence trajectories (Patient #15) . . . . .	128
5·10	Response surface and convergence trajectories (Patient #1) . . . . .	128
6·1	Sensitivity of $\theta_3$ as a function of the values of $\theta_1$ and $\theta_2$ (Patient #15)	151
6·2	Sensitivity of $\theta_4$ as a function of the values of $\theta_1$ and $\theta_2$ (Patient #15)	152
6·3	Sensitivity of $\theta_5$ as a function of the values of $\theta_1$ and $\theta_2$ (Patient #15)	153
6·4	Sensitivity of $\theta_6$ as a function of the values of $\theta_1$ and $\theta_2$ (Patient #15)	154
6·5	Sensitivity of $\theta_3$ as a function of the values of $\theta_1$ and $\theta_2$ (Patient #1)	155
6·6	Sensitivity of $\theta_4$ as a function of the values of $\theta_1$ and $\theta_2$ (Patient #1)	155
6·7	Sensitivity of $\theta_5$ as a function of the values of $\theta_1$ and $\theta_2$ (Patient #1)	156
6·8	Sensitivity of $\theta_6$ as a function of the values of $\theta_1$ and $\theta_2$ (Patient #1)	156

## List of Abbreviations

ACS	.....	Adaptive Control Software
ANN	.....	Artificial Neural Networks
BF	.....	Brute Force
BRCA	.....	Breast Invasive Carcinoma
CAS	.....	Continuous Androgen Suppression
CHA	.....	Cancer Hybrid Automaton
CNV	.....	Copy Number Variation
CPLEX	.....	Simplex Method in C
CRC	.....	Castration Resistant Cell
DES	.....	Discrete Event System
DNA	.....	Deoxyribonucleic Acid
ELCP	.....	Extended Linear Complementary Problem
EP	.....	Empty Period
ES	.....	Expert Systems
FL	.....	Fuzzy Logic
HSC	.....	Hormone Sensitive Cell
IAS	.....	Intermittent Androgen Suppression
ILP	.....	Integer Linear Program
IPA	.....	Infinitesimal Perturbation Analysis
KEGG	.....	Kyoto Encyclopedia of Genes and Genomes
MDP	.....	Markov Decision Process
MILP	.....	Mixed Integer Linear Program
NEP	.....	Non-Empty Period
ONG	.....	Oncogene
OPAC	.....	Optimized Policies for Adaptive Control

PA	.....	Perturbation Analysis
PRODYN	.....	Programming Dynamic
PSA	.....	Prostate-Specific Antigen
RHDP	.....	Rolling Horizon Dynamic Programming
RHODES	.....	Real-Time Hierarchical Optimized Distributed and Effective System
RL	.....	Reinforcement Learning
SCATS	.....	Sydney Coordinated Adaptive Traffic System
SCOOT	.....	Split Cycle Offset Optimization Technique
SFM	.....	Stochastic Flow Model
SHA	.....	Stochastic Hybrid Automaton
SHS	.....	Stochastic Hybrid Systems
TCGA	.....	The Cancer Genome Atlas
TLC	.....	Traffic Light Control
TRANSYT	.....	Traffic Network Study Tool
TSG	.....	Tumor Suppressor Gene
UTCS	.....	Urban Traffic Control System
$\mathbb{R}^2$	.....	The Real plane

## Chapter 1

# Introduction

A dynamical system is characterized by a set of mathematical rules that define how elements of the system evolve throughout time. Much of the theory developed in this field was initially motivated by the study of classical mechanical systems, whose behavior is usually described by ordinary differential equations. Such systems are commonly referred to as *continuous* dynamical systems, and contrast with *discrete* dynamical systems, whose evolution is driven by the occurrence of instantaneous events. With the advent of computers and ensuing modern technologies, a new generation of *hybrid* systems was identified by researchers. Hybrid systems comprise an interesting, albeit challenging, class of systems that combine continuous and discrete dynamics, and provide a useful abstraction for describing several complex systems.

Hybrid systems theory has roots in various fields of science; in fact, motivation for the study of hybrid systems has spawn from several different lines of research. At present the reverse is also seen to hold, as hybrid systems theory is seen to increasingly contribute to the development of more established fields such as computer science, mathematical programming, and control theory. Indeed, researchers in software verification, in search of a more precise description of the processes in which computers

play a role, have begun to incorporate continuous dynamics to their discrete systems. Similarly, hybrid systems theory has influenced the introduction of differential equations in mathematical programming problems. Additionally, switching control has frequently proven advantageous over smooth control, and various types of switching have been used for nonlinear control, as in the case of sliding mode control, gain scheduling, programmable-logic controllers, and even fuzzy control (to the extent that fuzzy schemes are composed of different operating regimes).

At present it is becoming increasingly clear that many problems of interest can be cast within a hybrid system framework. Several such problems also frequently share additional features, such as stochasticity, which render their analysis, control and optimization particularly challenging. At the same time, recent technological developments in system control and optimization call for data driven techniques that can be easily implemented online. These challenges motivate our study of efficient control and optimization techniques (such as perturbation analysis) that can be applied to such complex stochastic hybrid problems.

## 1.1 Stochastic Hybrid Systems

A great deal of work has been undertaken in the field of hybrid systems using deterministic models that fully describe system dynamics. Nevertheless, the fact that uncertainty may be an inherent part of such complex systems has recently motivated the study of non-deterministic models, in which stochastic processes may affect discrete state transitions or may be present within the continuous state dynamics.

Stochastic Hybrid Systems (SHS) comprise a family of models that incorporate several types of randomness which, in its most general form, is associated with probability distributions for both discrete and continuous transitions (Bujorianu, 2012).

Simple SHS models were introduced in control engineering a few decades ago, being initially used to describe, with high accuracy, the corrective actions taken to prevent significant deviations in plane trajectories due to turbulence. Since then, SHS analysis has been increasingly used in all activities that relate to systems engineering, and the modeling, control, and optimization of such systems constitute increasingly active fields of research (Cassandras and Lygeros, 2007).

### 1.1.1 Models for SHS

Models are the ultimate tools for representing knowledge about phenomena, and much effort has been undertaken to develop appropriate mathematical models for hybrid systems not only in engineering, but also in other fields such as philosophy, biology, and economics (Schutter et al., 2009). A suitable modeling language for hybrid systems should be descriptive, composable, and abstractable. The descriptive power of these languages allows for *(i)* capturing different types of continuous and discrete dynamics; *(ii)* modeling different ways in which discrete evolution affects and is affected by continuous evolution; *(iii)* capturing the inherent uncertainty of non-deterministic models. Furthermore, it should be possible to construct large models by composing different simple ones. Finally, abstraction is desirable both in allowing composite models to be refined down to design problems for individual components,

as well as in allowing performance results of individual components to be used to study the performance of the overall system (Lygeros et al., 2008).

To date, many models have been proposed which possess at least some subset of these properties; different languages emphasize different aspects, depending on the applications that they are designed to address. Some of the most well-known modeling frameworks proposed for hybrid systems include switched systems, hybrid Petri nets, and hybrid automata.

Switched systems (Liberzon, 2003) seek to represent hybrid systems as continuous systems with switching, and hence place more emphasis on the properties of the continuous state. A complete switched system model specifies the dynamics governing the evolution of the system's continuous and discrete states, where the latter is termed a switching signal, which is a piecewise constant function of time. The use of such models is motivated by the fact that a continuous feedback law capable of stabilizing a continuous-time control system may not exist. In such situations, logic-based decisions are incorporated into the control law so as to implement switching among a family of controllers, resulting in a switched (hybrid) closed-loop system. Classes of problems for which switched systems techniques are particularly appropriate include nonholonomic systems, systems with large-scale modeling uncertainty, as well as systems with sensor and/or actuator limitations.

Petri nets (David and Alla, 2001) are widely used to model discrete systems, being frequently applied in areas such as manufacturing, communications, software design,

and reliability engineering, among others. A Petri net is a directed bipartite graph in which the nodes represent transitions (i.e., events that may occur) and places (i.e., conditions for the occurrence of events), and directed arcs describe conditions for each transition. Places in a Petri net may contain a discrete number of marks (termed tokens), and the marking of a place may correspond either to the Boolean state of a device (e.g., availability of a certain resource) or to an integer number (e.g., the number of parts in a buffer). This implies, however, that the number of reachable states explodes as the number of tokens increases. Hybrid Petri nets address this limitation by representing the firing of transitions as continuous processes and allowing for the number of tokens to be a real value.

The concept of hybrid Petri nets was introduced in (David and Alla, 1987) and subsequently developed in (Bail et al., 1991). Two distinct parts are defined in a hybrid Petri net: a discrete part (formed by a set of discrete places and a set of discrete transitions), and a continuous part (formed by a set of continuous places and a set of continuous transitions). These parts are connected through arcs such that one part may affect the behavior of the other without changing its own marking. The model of a hybrid Petri net was extended to account for a stochastic discrete part in (Dubois and Alla, 1993), and applications of hybrid Petri nets models were reported in (Alla et al., 1992) for production systems and in (Alla and David, 1998) for water supply systems. Although such models may be designed intuitively, their quantitative analysis is a substantially more complex task.



Hybrid automata (Cassandras and Lafortune, 2008) are the most commonly used modeling framework for hybrid systems due to a great extent to their power of analysis. The Alur automaton (Alur et al., 1995), developed primarily for algorithmic analysis of hybrid systems model checking, remains one of the most popular hybrid automaton model. A hybrid automaton is a finite state machine with a finite set of continuous variables whose evolution is described by ordinary differential equations. An extension of such models exists in the form of stochastic hybrid automaton models, which are especially suited for cases where state evolution may not be fully determined. Since we make use of stochastic hybrid automata throughout our work, we will presently limit ourselves to this brief introduction; a more detailed account this modeling framework will be presented in later parts of this document.

### **1.1.2 Optimization of SHS**

In essence, Stochastic Hybrid System (SHS) control is a class of stochastic optimization problems, whose solution relies on models and methods capable of optimizing system performance while explicitly accounting for uncertainty. In recent years, the area of stochastic optimization has evolved considerably due, to a great extent, to new theoretical developments and advances in computational power. As a result, stochastic optimization techniques are being increasingly applied to problems in energy planning, national security, supply chain management, health care, finance, transportation, revenue management, among others. The problem of optimizing a

general stochastic system can be formulated as

$$\min_{\theta \in \Theta} J(\theta) \tag{1.1}$$

where  $\theta$  is a vector of all the decision variables,  $\Theta$  is the feasible region and  $J(\theta)$  is the objective function (note that (1.1) may also represent deterministic optimization problems, in which no randomness is considered, but since we are interested in systems with inherent uncertainty, we will henceforth assume that (1.1) is defined in a stochastic setting). If the objective function  $J(\theta)$  is linear in  $\theta$  and the feasible region can be written as a set of linear equations in  $\theta$ , (1.1) reduces to a stochastic linear programming problem. Similarly, if some of the constraints that make up  $\Theta$  contain integer restrictions, (1.1) is referred to as a stochastic integer programming problem. Nonlinear versions of (1.1) also exist, but many algorithms developed for the linear case carry over to stochastic nonlinear programming (Sahinidis, 2004). Robust stochastic optimization is a variant of (1.1) in which the underlying assumption that the decision-maker is risk-neutral is relaxed. On the other hand, (1.1) is defined as a probabilistic programming problem when the focus is on the system's ability to meet feasibility in a stochastic environment.

In the above approaches, uncertainty is modeled through discrete or continuous probability functions, in contrast with fuzzy programming (Sahinidis, 2004), where random parameters are represented by fuzzy numbers and constraints are treated as fuzzy sets. Different types of fuzzy programming techniques exist to deal with ran-

domness in the objective function coefficients and/or constraint coefficients, and all such approaches allow for constraints to be violated to a certain extent. Membership functions are thus used to represent the degree to which a certain constraint is satisfied, as well as the range of uncertainty of the coefficients.

Stochastic dynamic programming (Bertsekas, 2005) constitutes yet another approach to optimization under uncertainty where randomness is considered as an integral part of the dynamic multi-stage decision process. In this context, system uncertainty follows some probability distribution that depends on the current state and control action. The procedure for solving (1.1) involves many subproblems and suffers from the curse of dimensionality, i.e., computational time and storage requirements grow exponentially in the number of state and control variables. In order to bypass such limitations, various approximation techniques have been developed, which make use of heuristic learning schemes or simulation.

The aforementioned methods apply to instances of (1.1) where the objective function can be evaluated in closed form so that the optimal solution may be determined by solving the necessary and/or sufficient conditions. However, it may be desirable or even unavoidable not to make any assumptions about the structure of  $J(\theta)$ , in which case the goal becomes to choose  $\theta$ , frequently through some form of random search, so as to find a solution with desirable properties such as asymptotic optimality or probabilistic optimality guarantees. Indeed, in many applications, little is known regarding the convexity, continuity, or differentiability of  $J(\theta)$ , and the system must

inevitably be repeatedly simulated under different values of  $\theta$  in order to ultimately approximate the value of the objective function as

$$J(\theta) = \mathbb{E}[L(\theta, \omega)] \quad (1.2)$$

where  $L(\theta, \omega)$  is the sample performance function,  $\omega \in \Omega$  denotes an observed sample path, and  $\Omega$  represents the set of all possible sample paths. This approach is known as *stochastic simulation optimization* (Chen and Lee, 2010), and the estimation algorithms that fall into this category generally consist of a sequence of (i) stochastic simulations, from which the values of the sample performance function are obtained for several sample paths; (ii) performance estimation, where (1.2) is computed for different  $\theta$ ; (iii) optimality search, whereby the decision variables yielding the best estimated performance are chosen. A schematic representation of this estimation procedure is shown in Figure 1.1.

In (1.2), the sample mean performance is commonly computed as an estimate of the objective function. If the observed sample paths are independent so that the sequence  $\{L(\theta, \omega_1), \dots, L(\theta, \omega_n)\}$  is iid (Cassandras and Lafortune, 2008), the strong law of large numbers can be applied to yield

$$J(\theta) = \lim_{n \rightarrow \infty} \left[ \frac{1}{n} \sum_{i=1}^n L(\theta, \omega_i) \right] \quad (1.3)$$

At this point, it is clear that two primary efficiency concerns in stochastic simulation optimization relate to the fact that (i) the quality of the estimate of  $J(\theta)$



**Figure 1.1:** Typical framework of a stochastic simulation optimization

increases with the number of sample paths  $n$ , and (ii)  $J(\theta)$  must be evaluated for many different values of  $\theta$  before the best one can be determined. For instances where the feasible region  $\Theta$  is relatively small, enumeration can, in principle, be used to find the optimum. This eliminates the need to repeatedly estimate system performance, but multiple simulation replications are still required. In most cases of interest, however, the system's size and complexity frequently render the use of exhaustive verification techniques prohibitive, so that efficient simulation methods must be used. Such methods can be broadly classified as *metaheuristics* and *model-based approaches* (Chen and Lee, 2010). The former do not assume that an underlying response function exists for  $J(\theta)$ ; in fact, such methods frequently start with an initial population of decision variables, from which elite variable(s) is(are) selected, and then improve upon this selection at each iteration. Some of the approaches that fall within

this category include evolutionary and genetic algorithms (Boesel et al., 2003), simulated annealing (Alrefaei, 1999), model reference adaptive search (Hu et al., 2008), as well as population-based algorithms from nonlinear optimization (Kim and Zhang, 2010), (Barton and Ivey, 1996).

In contrast to metaheuristics, model-based approaches consist of iterative algorithms that use statistical methods to search the feasible region, and implicitly assume that an underlining response function exists for  $J(\theta)$ . Gradient-based approaches are a class of model-based methods in which the local search for optimality is carried out using the gradient of the performance measure with respect to the decision variables. There are several ways in which the gradient of the performance measure, or some estimate of it, can be used for analysis and control of stochastic systems. In the case where  $\theta$  is a scalar parameter, the gradient of  $J(\theta)$  with respect to  $\theta$  is simply the derivative  $\frac{dJ}{d\theta}$ , and we note that, for notational simplicity, and without loss of generality, we will assume this to be the case in the remainder of this discussion. The derivative  $\frac{dJ}{d\theta}$  at  $\theta = \theta_0 \in \Theta$  is a measure of the sensitivity of  $J(\theta)$  with respect to  $\theta$  at the point  $\theta = \theta_0$ , thus providing some local information regarding the effect of this decision variable on the system's performance (Cassandras and Lafortune, 2008). Such information could include, for instance, the sign of the derivative, which reveals the direction in which  $\theta$  should be changed. Additionally, the magnitude of the derivative is also useful in determining how sensitive  $J(\theta)$  is to changes in the decision variable; a very small derivative value, for example, indicates that the performance would not

be significantly improved by changes in the current parameter and that it would be more advantageous to consider other decision variables.

Another useful type of information that may be obtained through sensitivity analysis relates to the structural properties of the system, such as monotonicity and convexity. A case in point is when the derivative of the sample function  $\frac{dL}{d\theta}$ , which represents an estimate of  $\frac{dJ}{d\theta}$ , is found to be always positive (or negative) for any given sample path. In this setting,  $J(\theta)$  can be seen to be monotonically increasing (or decreasing), although its actual value may not be determined.

Finally, the value of  $\frac{dJ}{d\theta}$  can also be used to improve current operating conditions or (under certain conditions) to compute an optimal  $\theta^*$  through an iterative optimization algorithm of the form

$$\theta_{n+1} = \theta_n - \rho_n \left( \frac{dJ}{d\theta} \right)_{\theta=\theta_n} \quad n = 1, 2, \dots \quad (1.4)$$

where  $\rho_n$  is the step size at the  $n$ th iteration. Since the objective function  $J(\theta)$  is not known, we must approximate its derivative by the derivative of the sample function  $\frac{dL}{d\theta}$ . There are two main techniques for obtaining such derivative estimates: methods based on finite differences, and direct approaches. The former rely on computing a finite difference approximation as

$$\frac{dL}{d\theta} \approx \frac{L(\theta + \Delta\theta) - L(\theta)}{\Delta\theta} \quad (1.5)$$

This approach requires simulating the system under two different but very close values

of  $\theta$ , i.e., it is necessary to generate one sample path under  $\theta$  (from which  $L(\theta)$  is computed), and subsequently change the parameter by a small amount  $\Delta\theta$ , thus obtaining  $L(\theta + \Delta\theta)$  from a second sample path. The difference between the objective function estimates is then used to compute an estimate of  $\frac{dL}{d\theta}$ . Such procedure is clearly inefficient; moreover, it is possible that, in an attempt to improve the estimate, a decrease in  $\Delta\theta$  could make it necessary to evaluate a ratio of two small numbers, thus leading to numerical problems.

More efficient alternatives to computing  $\frac{dL}{d\theta}$  exist in the form of direct approaches, such as the likelihood ratio method (Rubinstein and Shapiro, 1993) and perturbation analysis (Glasserman, 1991), (Ho and Cao, 1991), (Fu and Hu, 1997). Perturbation Analysis (PA) techniques monitor a single unperturbed (nominal) sample path of the simulation and subsequently attempt to predict what would have happened if the values of the parameters had actually been changed. The attractive feature of such techniques is that the derivative estimates are extracted from a single sample path in a non-intrusive manner, so that the computational cost of doing so is, in most cases of interest, minimal. One of the basic assumptions underlying the use of PA methods is that any changes made to the parameter of interest may lead to event order changes as long as the final state of the system is the same. This property is referred to as the *commuting condition* (Glasserman, 1991), being important for ensuring the unbiasedness of PA-based derivative estimates.



## 1.2 Infinitesimal Perturbation Analysis

The simplest class of PA algorithms is Infinitesimal Perturbation Analysis (IPA), which constitutes a set of techniques for explicitly evaluating sample derivative values. The central idea behind IPA, and PA in general, involves two distinct, but complementary, issues: perturbation generation and perturbation propagation. Determining local generation of perturbations amounts to finding the realized difference between the nominal and perturbed values of the decision variable. Interestingly, however, explicit knowledge of the value of  $\Delta\theta$  is never used by IPA to compute the instantaneous derivative of the objective function. In fact, it suffices to keep track of the state of the system under the nominal value of the parameter  $\theta$ , so that little additional effort is needed beyond the computation required for one simulation of the system.

Although perturbation generation can be carried out independently of the magnitude of  $\Delta\theta$ , the way in which such perturbation propagates is nevertheless dependent on the system, parameter, and objective function of interest. Hence, instead of an underlying theory of propagation, a collection of algorithms exist that share a common thread yet have individual modifications for different applications. This, in turn, makes it more difficult for such algorithms to be incorporated into general-purpose simulation environments, constituting the main factor hindering the application of IPA to more general problems.

Much of the theory of infinitesimal perturbation generation and propagation was

originally developed for evaluating gradients of sample performance functions in queueing systems (Cassandras and Lafortune, 2008),(Glasserman, 1991), (Ho and Cao, 1991). The unbiasedness of such gradient estimates is guaranteed as long as the commuting condition holds. However, several aspects of queueing systems such as multiple user classes, blocking due to limited resource capacities, as well as various forms of feedback control, cause significant discontinuities in the sample function, thus leading to the violation of the commuting condition.

These limitations can frequently be overcome when IPA is applied to some classes of Stochastic Hybrid Systems (SHS), in particular Stochastic Flow Models (SFMs) (Cassandras et al., 2010),(Wardi et al., 2010), for which, under mild technical conditions, simple unbiased gradient estimates of useful metrics can be obtained, thus making tractable many classes of problems which would not previously have been solved directly using IPA. SFMs are fluid models in which flow rates are treated as stochastic processes, and were introduced in (Cassandras et al., 2002) to carry out IPA for a queueing system. Although the use of fluid models may not necessarily allow for accurately predicting the performance of the underlying system, such models are nevertheless capable of capturing those system features needed for designing an effective controller. As a result, it is possible to optimize system performance without the need to precisely estimate the corresponding optimal value of the system performance.

Over the past decade, SFMs and IPA have been successfully applied in several

different settings, including those comprising serial networks (Sun et al., 2004a), systems with feedback control mechanisms (Yu and Cassandras, 2006), multi-class models (Sun et al., 2003),(Panayiotou, 2004),(Sun et al., 2004b), systems with blocking due to limited capacity (Sun et al., 2003), fluid scheduling (Kebbarighotbi and Cassandras, 2009),(Kebbarighotbi and Cassandras, 2011a), and systems with delay thresholds (Kebbarighotbi and Cassandras, 2011b). Current results on the application of IPA to SFMs are encouraging enough to motivate the search for extensions to more complicated problems. This thesis focuses on developing IPA-based optimization schemes for SHS representations of two challenging problems, namely traffic light control and control of cancer progression. Since IPA is at the core of the work presented here, a technical introduction to this technique is included in Appendix A; we thus proceed by introducing each of the aforementioned problems separately in the sections that follow.

### 1.3 Traffic Light Control

The Traffic Light Control (TLC) problem involves dynamically adjusting roads' green and red light cycle lengths in order to control the traffic flow through an intersection. In its broader conception, the TLC problem encompasses a set of intersections and traffic lights, which are monitored with the objective to minimize congestion in the urban perimeter within which they are located. There exist two types of control strategies for the TLC problem: *fixed-cycle strategies* and *traffic-responsive strategies* (Papageorgiou et al., 2003).

Traffic signals are typically regulated through fixed-cycle strategies, whereby several timing plans covering different traffic-intensity scenarios are periodically interchanged. The most popular such systems are the Urban Traffic Control System (UTCS) (Wey, 2000), TRANSYT (Robertson, 1969), and MAXBAND (Little et al., 1981). UTCS was developed by the Federal Highway Administration in the 1970s and is to this day the most commonly used TLC system in the United States. This system generates signal timing schedules off-line and subsequently implements them according to the time of day. The chosen timing schedules are the ones that either *(i)* maximize the period of time available for traffic flow on arterial streets (i.e. maximize bandwidth), or *(ii)* minimize a disutility index, which is defined as a measure of traffic delay and number of stops.

The TRANSYT system is the most well-known and frequently used TLC strategy worldwide, serving as an unofficial international standard against which other methods that operate at constant and common cycle lengths can be compared. The system makes use of average traffic flow information along any given network of roads to generate optimal fixed-cycle plans and hence coordinate the corresponding traffic light signals. Finally, MAXBAND also operates off-line by setting traffic light signals on arterial roads so as to achieve maximal bandwidth. Some distinguishing features of this system include *(a)* allowing a queue clearance time for secondary flow accumulated during a red light; *(b)* accepting user-specified weights for the green bands in each direction; and *(c)* handling a simple network in the form of a three-artery

triangular loop.

The main limitation of all such fixed-cycle methods has to do with the fact that they use historical traffic flow data to determine light cycle settings off-line, and are thus incapable of adapting in real time to evolving traffic conditions. Traffic-responsive strategies address this limitation by making use of current traffic information to determine optimal signal settings online. To date, most adaptive traffic control systems have been developed and/or deployed in Europe; in fact, in the United States, only about 1% of all traffic signals have been estimated to operate adaptively (NTS, 2007). Traffic-responsive systems consist of algorithms that adjust a signal's phase length and phase sequences so as to minimize delays and reduce the number of stops, and require transit surveillance, typically implemented using pavement loop detectors, in order to adjust signal timing in real time (Stevanovic, 2010). The two most widely used such systems are the Sydney Coordinated Adaptive Traffic System (SCATS) (Lowrie, 1982) and the Split Cycle Offset Optimization Technique (SCOOT) (Hunt et al., 1982).

SCATS operates in real time by reacting to changes in traffic demand and system capacity. Instead of adjusting signal timings for isolated intersections, the system simultaneously manages groups of intersections (i.e. subsystems). Each subsystem typically consists of any number between one and ten intersections that are coordinated as a group. Coordination is also enforced among adjacent subsystems by dividing traffic flow on major roads into platoons (groups of vehicles). Network ca-

capacity is then maximized by allowing just enough time for each platoon to progress through the system while ensuring the required amount of green time for competing flows.

In SCOOT optimal traffic control in a given network of roads is achieved through small, regular variations in signal timings, so as to avoid major disturbances of traffic flow. The system generates a model for estimating queue lengths based on flow-occupancy profiles from upstream detectors, thus maintaining a detailed, real-time representation of the traffic network. Such model is run repeatedly online to determine the effects of incremental changes in signal timing on the overall performance of the region's network. When the changes lead to a reduction in vehicle delays and number of stops, they are transmitted to the local signal controllers.

Recent technological developments, which exploit the ability to collect traffic data in real time, have made it possible for new methods to be applied to the TLC problem, hence several other traffic-responsive methods have been under development, including ACS Lite (Shelby et al., 2008), OPAC (Gartner et al., 2002), PRODYN (Henry and Farges, 1990), and RHODES (Sen and Head, 1997). Leveraging the fact that TLC is fundamentally a form of scheduling for systems operating through simple switching control actions, numerous solution algorithms have been proposed using artificial intelligence techniques (including fuzzy logic, expert systems, evolutionary algorithms, artificial neural networks, and reinforcement learning), game theory, mixed integer linear programming, as well as perturbation analysis techniques.

Fuzzy Logic (FL) is a computational approach based on degrees of truth rather than the most common Boolean logic, being originally developed to simulate the understanding of natural language. The main idea behind FL is that data can be aggregated into a number of partial truths, which are subsequently aggregated into higher truths, which ultimately produce some outcome when certain thresholds are exceeded. The use of fuzzy logic is particularly relevant in cases where it is unlikely that an exact mathematical model of the phenomenon of interest may be obtained (Niittymäki et al., 2002). In fact, its underlying principle is that the knowledge of a human expert can be taught to the FL system, whose behavior then closely resembles that of an intelligent biological system. In the context of adaptive traffic signal control, FL was first used in (Pappis and Mamdani, 1977) for a single intersection without turning traffic. Subsequent applications expanded upon this work by incorporating left-turning traffic and oversaturated conditions for single intersections (Murat and Gedizlioglu, 2005), (Trabia et al., 1996), (Wei et al., 2001), and considering two consecutive intersections with one-way movements (Nakatsuyama et al., 1984), as well as multiple intersections (Lee et al., 1995), (Chiu, 1992), (Chou and Teng, 2002). Considering multiple intersections and relying on sensor information regarding traffic congestion, a first-order Sugeno fuzzy model was developed and incorporated into a fuzzy logic controller in (Choi et al., 2002).

Expert Systems (ES) emulate the decision-making ability of a human expert and constitute some of the first artificial intelligence softwares to be successfully deployed.

An ES is composed of two sub-systems: the knowledge base and the inference engine. The former consists of facts and *if-then* rules, while the latter evaluates the current state of the knowledge base and feeds new knowledge into it by applying relevant rules. Expert systems were used in (Findler and Strapp, 1992) to design a distributed control network where each intersection was equipped with a processor that runs an identical ES and communicates directly with its four adjacent processors. A dynamic and automatic ES-based TLC system focusing on the road congestion problem was also presented in (Wen and Hsu, 2006). Additionally, a flexible and general online method was proposed in (Findle et al., 1997) to determine whether protected left-turns are required for certain traffic flow scenarios.

Evolutionary algorithms, such as genetic algorithms, ant algorithms, and particle swarm optimization, are population-based metaheuristic optimization algorithms inspired by the principles of biological evolution, namely reproduction, mutation, recombination, and selection. Candidate solutions to the optimization problem are treated as individual members of a population; in this sense, the quality of any given solution is equated to an individual's chance of survival, which is determined by a fitness function. Population evolution is driven by the fittest solutions, which are determined through random search. As a result, these methods are capable of converging to a global optimal solution in spite of the existence of several local minima. In the context of TLC, an improved immunity genetic algorithm was proposed in (Liu, 2007), a chaos-particle swarm optimization algorithm was presented in (Dong, 2004),



a catastrophe-particle swarm optimization algorithm was used in (Dong, 2006), and an ant algorithm was proposed in (Wen and Wu, 2005).

Artificial Neural Networks (ANN) are computational models designed to reproduce the functioning of the animal brain. The basic unit of these models is termed a neuron, which is capable of evaluating input information and transmitting the corresponding result throughout the network. Some of the main uses of ANN include machine learning, pattern recognition, and automatic control. Several approaches to applying ANN for traffic signal control have been reported. In (Spall and Chin, 1997) and (Henry et al., 1998), an ANN-based model is used for TLC, while in (Dong et al., 2005) ANN are used to improve the generalization capability of other methods, which are simultaneously applied to the TLC problem. In yet another instance, the precision of fuzzy controller is enhanced through the use of ANN to map fuzzy relations and implement fuzzy reasoning (Liu et al., 1997),(Xu et al., 1992).

Reinforcement Learning (RL) is a class of machine learning techniques that focuses on determining which actions should be taken by certain agents within a given environment in order to maximize some cumulative reward. The environment is frequently formulated as a Markov Decision Process (MDP), which is a particularly appropriate framework for dealing with sequential decision making problems whose complexity prohibits the straightforward computation of optimal solutions. An MDP was used to model traffic light intersections in (Yu and Recker, 2006), and in (Abdulhai et al., 2003) a method for controlling a single traffic intersection was proposed based on

RL with full state representation. An RL algorithm with function approximation and feedback policies was used in (Prashant and Bhatnagar, 2011) for traffic signal control, and additional RL approaches to the TLC problem have been presented in (Thorpe, 1997), (Wiering et al., 2004), and (Bazzan, 2009).

Numerous other solution algorithms have also been proposed for the TLC problem. A game theoretic approach was applied to a finite controlled Markov chain model in (Alvarez and Poznyak, 2010). In (Porche et al., 1996), a decision tree model was used with a Rolling Horizon Dynamic Programming (RHDP) approach, while a multiobjective Mixed Integer Linear Programming (MILP) formulation was proposed in (Dujardin et al., 2011). The optimal traffic light control problem was also stated as a special case of an Extended Linear Complementarity Problem (ELCP) in (Schutter, 1999), and formulated as a hybrid system optimization problem in (Zhao and Chen, 2003). Robust optimization methods that take into account uncertain traffic flows have also been proposed. For example, in (Ukkusuri et al., 2010), a semidefinite programming routine for model predictive control is used; in (Wen and Hsu, 2006), a robust optimal signal control problem is formulated as a linear program; in (Zhao and Chen, 2003), signal timings were determined so as to minimize the mean delay per vehicle under daily traffic flow variations.

At this point, it is worthwhile to point out that the aforementioned real-time adaptive traffic control approaches differ mainly with regards to how they address the issues of developing a mathematical model for a stochastic and highly nonlinear

traffic system, as well as the design of appropriate control laws. Although most of the signal control strategies previously described implicitly recognize that variations in traffic conditions are caused by random processes, some resort to using deterministic models that significantly simplify the description of vehicle flow. In addition to this, some TLC methods (e.g. those that are based on artificial intelligence techniques) employ heuristic control strategies, which rely on historical data, without an embedded traffic flow model. Such applications are consequently better suited for analyzing traffic systems in steady state, which is a state seldom attained due to the random nature of vehicle flow. Stochastic control approaches address this limitation by explicitly accounting for the random variations in traffic flow, but the methods presented thus far do so within a Markov Decision Process (MDP) framework, which requires assumption of specific probability models. Furthermore, many of these approaches, such as those based on dynamic or linear programming, are computationally inefficient and learning rate dependent, and thus not immediately amenable to online implementations. Conversely, perturbation analysis techniques allow for stochastic control without the need for limiting assumptions on the stochastic processes that represent vehicle flow, and have proven to be adaptive and simple to implement online.

Perturbation analysis techniques were used in (Head et al., 1996) and (Fu and Howell, 2003) for modeling a traffic light intersection as a stochastic Discrete Event System (DES), while an Infinitesimal Perturbation Analysis (IPA) approach, which

made use of a Stochastic Flow Model (SFM) to represent the queue content dynamics of roads at an intersection, was presented in (Panayiotou et al., 2005). In (Geng and Cassandras, 2012), IPA was applied with respect to controllable green and red cycle lengths for a single isolated intersection and in (Geng and Cassandras, 2015) for multiple intersections. Traffic flow rates need not be restricted to take on deterministic values, but may be treated as stochastic processes (Cassandras et al., 2002), which are suited to represent the continuous and random variations in traffic conditions. Using the general IPA theory for SHS in (Wardi et al., 2010),(Cassandras et al., 2010), on-line gradients of performance measures are estimated with respect to several controllable parameters with only minor technical conditions imposed on the random processes that define input and output flows. These IPA estimates have been shown to be unbiased, even in the presence of blocking due to limited resource capacities and of feedback control (Yao and Cassandras, 2011a). It should be emphasized that IPA is not used to estimate performance measures, but only their gradients, which may be subsequently incorporated into standard gradient-based algorithms in order to effectively control parameters of interest.

Hence, there are several advantages associated with the use of IPA for the TLC problem. First, IPA estimates have been shown to be unbiased under very mild conditions; second, IPA estimators are robust with respect to the stochastic processes used to model random traffic processes. Furthermore, IPA is event driven and hence scalable in the number of events in the system, and does not explode with the space

dimensionality. Finally, IPA possesses a decomposability property (Cassandras, 2015) and can be easily implemented online, thus taking advantage of directly observed data.

In contrast to earlier works where the adjustment of light cycles did not make use of real-time state information, the authors in (Geng and Cassandras, 2013) proposed an SFM model within a quasi-dynamic control setting in which partial state information is used to adjust the light cycle lengths conditioned upon a given queue content threshold being reached. Our work is also based on modeling traffic flow through an intersection controlled by switching traffic lights as an SFM, which conveniently captures the system’s inherent hybrid nature: while traffic light switches exhibit event-driven dynamics, the flow of vehicles through an intersection is best represented through time-driven dynamics. Moreover, we also draw upon a quasi-dynamic setting, but rather than controlling only the light cycle lengths as in (Geng and Cassandras, 2013), here we initially focus on the threshold parameters and derive IPA performance measure estimators necessary to optimize these parameters, while assuming fixed cycle lengths. In this first step, our goal is to compare the relative effects of the threshold parameters and the light cycle length parameters on our objective function. Building upon these results, we then derive IPA estimators necessary to *simultaneously* optimize light cycle lengths and queue content threshold values within a quasi-dynamic control setting. By incorporating the IPA estimators into a gradient-based optimization algorithm, we show that the quasi-dynamic control approaches proposed in this work offer considerable improvements over prior results.

## 1.4 Modeling and Control of Cancer Progression

In spite of significant scientific advances, cancer remains one of the deadliest diseases known to mankind. Recent critical biological discoveries, such as the existence and function of the DNA molecule, have not only led to the view of cancer as a genetic disease, but also fueled important undertakings such as the mapping of the cancer genome. Nevertheless, the knowledge that tumors arise due to genetic malfunctioning has yet to be adequately translated into therapy design. In fact, cancer treatment protocols have traditionally been devised based on the results of clinical trials averaged over a cohort of patients. Consequently, the current standard of care consists of applying a common therapy to any given patient; unfortunately, tumor recurrence (accompanied by drug resistance) frequently ensues. By shifting the paradigm of cancer treatment to genetically tailored protocols, the concept of personalized medicine is emerging as the state-of-the-art in cancer care.

Personalized cancer treatments involve therapies whose design (choice of drug(s), dosage, duration of treatment, etc.) is based on the unique set of genetic abnormalities found in each patient's tumor. However, tumors harboring a common genetic mutation do not respond consistently to the same therapy. For example, approximately 25% of breast cancer patients with a particular amplification or overexpression of the ERBB2 growth factor receptor tyrosine kinase may be assigned trastuzumab (Vogel et al., 2001). Unfortunately, less than half of patients with ERBB2-positive breast cancer actually respond positively to this drug (Park et al., 2008). Such limited suc-

cess is largely due to our incomplete understanding of the mechanisms that drive tumor initiation, growth and recurrence.

Tumorigenesis (i.e., the production or formation of a tumor) is frequently depicted as a multistep process along which normal cells acquire a succession of traits. Such traits, also termed hallmarks of cancer (Hanahan and Weinberg, 2011), have been described as distinctive and complementary capabilities that must be acquired in order for cancer cells to be able to survive, replicate and eventually spread from one part of the body to another. The process of acquiring such capabilities varies with regards to the order in which each is attained, as well as the time spent by the system in each distinctive state. As a result, the number and type of mutated genes can vary significantly not only across different tumor types (inter-patient heterogeneity), but also within different regions of the same tumor and different stages of the disease (intra-tumor heterogeneity).

The existence of intra-tumor heterogeneity (Dexter and Leith, 1986),(Somasundaram et al., 2012) is now widely accepted, albeit seldom explored in practice due to insufficient knowledge regarding how different molecular subtypes correlate with clinical behavior and hence treatment options. Moreover, intra-tumor heterogeneity has been frequently associated with the acquisition of drug resistance (Zahreddine and Borden, 2013),(Wadhwa et al., 2002), a highly undesirable phenomenon that has been linked to ephemeral treatment response and eventual tumor recurrence. A deeper understanding of both such phenomena is expected to facilitate the development of the

next generation of personalized therapies (Lee and Swanton, 2012); indeed, oncologists already make use of molecular information extracted from tumor samples to aid in the selection of appropriate therapies. Such samples, however, represent a limited proportion of the cancer tissue and may, therefore, not be representative of the several different types of cells that populate the tumor (Bedard et al., 2013). Moreover, clinicians also face time constraints for trying out different therapies, and only a small number of the available combination protocols end up being tested. In addition to these limitations, the use of targeted therapies, in which drugs are chosen to target the single most common population of cancer cells, currently prevails in the clinic. However, the fact that other less frequently occurring cell populations are not accounted for during therapy design significantly limits predictions of treatment response (Turner and Reis-Filho, 2012).

In this context, much effort has been undertaken to collect, organize and make publicly available data obtained from genetic analysis of tumor samples (e.g., in The Cancer Genome Atlas). Effectively analyzing such data for the purposes of prognosis and therapy design remains one of the biggest challenges in modern cancer research mainly because samples are usually only obtained from patients at one point in time (commonly that of initial diagnosis). Furthermore, significant variations are observed in the patterns of somatic mutations across different patients. In light of this, much of the research currently being undertaken using cross-sectional data aims at determining whether the order in which somatic mutations occur in tumors follows common



progression paths. Although not all patients with the same type of cancer harbor the exact same set of mutated genes, there seems to exist at least a subset of such genes that are consistently mutated across a large set of different patients. This suggests that different underlying sequences of events can drive tumor progression along equivalent evolutionary paths; in other words, different sequences of mutations can lead to similar phenotypes or disease states.

Recent pilot studies (e.g., (TCGA, 2008),(TCGA, 2014)) have investigated how genomic changes affect genetic pathways that, in turn, determine cancer phenotypes, thus suggesting common pathways of cancer progression. Driver genes (i.e., genes that, when mutated, drive tumorigenesis) have been identified and classified into signaling pathways that regulate core cellular processes (e.g., (Vogelstein and Kinzler, 2004),(Vogelstein et al., 2013)). These findings are well aligned with the view of cancer as a “disease of stages” in which tumors must progress through a series of “states” in order to ultimately become malignant. Existing datasets of cross-sectional data have been extensively used to derive temporal models capable of inferring sequences of mutational events and/or sequences of affected pathways responsible for driving cancer progression (e.g., (Gerstung et al., 2011), (Loohuis, 2013), (Raphael and Vandin, 2015)), and the importance of connecting different genomic alterations (as opposed to a single type of genomic data) was recognized in (Vaske et al., 2010). The aforementioned approaches analyze cancer development on a molecular level. Hence, they cannot explicitly account for the effect of the tumor microenvironment on tumor

progression, and do not provide suitable frameworks for analyzing the evolution of different cancer cell subpopulations that coexist within any given tumor.

Addressing this limitation, population-level approaches yield mathematical models for tumor population evolution considering mutations as the driving force behind cancer. Most of the work done in this area (e.g., (Michor et al., 2004), (Beerenwinkel et al., 2007), (Dingli et al., 2007), (Rodriguez-Brenes et al., 2011), (Werner et al., 2011), (Gentry and Jackson, 2013), (Werner et al., 2013), (Rodriguez-Brenes et al., 2014)) propose valid formalisms for investigating cancer evolution within a multi-step framework, but do not incorporate information obtained from genetic analyses of tumor samples. The model derived in (Michor et al., 2004) provided a quantitative understanding of the dynamics of tumorigenesis with respect to mutation, selection, genetic instability, and tissue architecture. The authors in (Beerenwinkel et al., 2007) developed a model of somatic evolution of colorectal cancer based on published data and used it to investigate the effect of different parameters on tumor evolution on a global scale, while those in (Dingli et al., 2007) suggested that stochastic dynamics alone might be responsible for either remission or rapid growth of tumors in the hematopoietic systems. In (Rodriguez-Brenes et al., 2011), evolutionary computational models were used to study the dynamics of feedback escape and their role in the progression of stem cell-driven cancer. Using a hierarchical multi compartment model, the authors in (Werner et al., 2011) analyzed the dynamics of mutant cells based on their origin and specific proliferation properties. A model of mutation acqui-

sition was developed in (Gentry and Jackson, 2013) to investigate how deregulation of the mechanisms preserving stem cell homeostasis contributes to tumor initiation. In (Werner et al., 2013), a model was developed to predict the average number of passenger mutations acquired from a single cell at any stage of hierarchy of organized tissues. Using a stem cell-based model, the authors in (Rodriguez-Brenes et al., 2014) suggested that the risk of cancer progression may be associated with the type of cell where mutations originate, such that mutations occurring in the stem cells are much more capable of driving tumor evolution than those occurring in progenitor cells.

More recently, efforts at deriving mathematical models that take into account tumor cellular heterogeneity and acquired resistance in order to determine optimal treatment schedules have been reported in (Leder et al., 2014) and (Liu et al., 2015). However, such approaches frequently rely on simplifying assumptions (and hence fail to include several potential important biological factors) and do not take into account noise and fluctuations that are inevitably involved in cell population dynamics. In short, most attempts to mathematically represent cancer evolution are capable of generating descriptive (open-loop), but not prescriptive, tools for inferring the behavior of cancer evolution, while recent attempts at personalized therapy design have relied on deterministic and often overly simplified models.

In order to address these limitations, we propose an integrative closed-loop framework capable not only of describing the progressive development of cancer, but also ultimately determining optimal personalized therapies. The aforementioned model-

ing and optimization framework incorporates a complex stochastic model of tumor evolution based on which effective computer simulation tools for cancer progression can be developed to quantify the effects of alternative courses of action and to analyze the outcomes of different therapies in a timely and minimally invasive manner. While this approach does not focus on finding a cure, it can help overcome current issues of intra-tumor heterogeneity, being ultimately also useful to the development of robust clinical biomarkers.

Adopting the view that (i) cell-biologic changes necessary for cancer development may be schematized as a series of discrete states, and (ii) transitions between states may be delayed or prevented by appropriate treatment, the critical observation that motivates this work is that these are precisely the characteristics of a Discrete Event System (DES). In other words, DES models are ideally suited to the view of cancer as a “disease of stages” and can subsequently lead to more elaborate Stochastic Hybrid Automata (SHA) models capturing additional details.

In this context, we ultimately envision the development of a Stochastic Hybrid Automaton (SHA) model representation of cancer progression in which cell-biologic changes necessary for cancer development are schematized as a series of discrete steps, and the stages of disease progression can be conveniently represented by distinct states of the automaton. Furthermore, the fact that transitions between such stages may be delayed or prevented by appropriate treatment can be accounted for within a SHA framework. An illustrative depiction of a general stochastic model of tumor

progression is given in Figure 1-2.

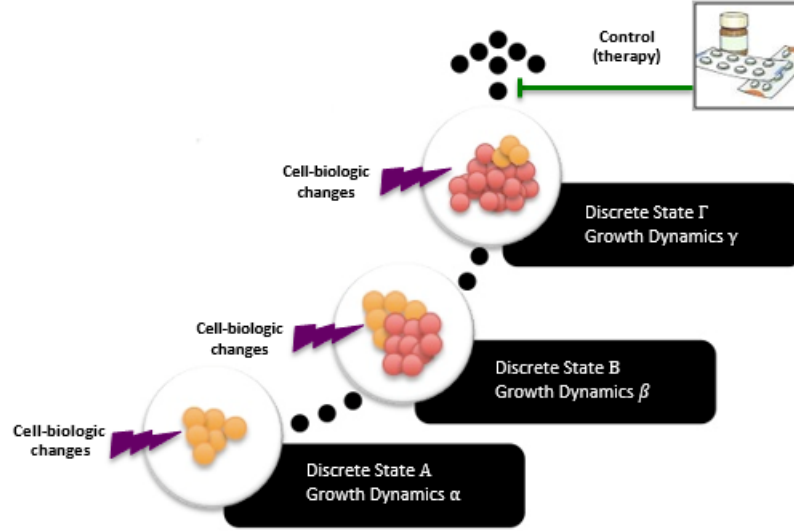


**Figure 1-2:** Illustrative depiction of a stochastic model of tumor evolution (normal cells in orange and mutated cells in red)

Hence, a well-designed integrative framework must be founded upon two pillars. The first one is a SHA model of tumor evolution whose development is based on multiple data types obtained from genetic analysis of tumor samples. In particular, cross-sectional data can be used to infer temporal reconstructions of cancer progression, which can then be abstracted to specify the components of the SHA model. The second pillar consists of system analysis, control, and optimization techniques that can be used to evaluate and design personalized cancer treatment schemes. More specifically, the inherent nature of SHA dynamics allows for the use of Perturbation Analysis (PA), specially Infinitesimal Perturbation Analysis (IPA) techniques to predict the system's behavior under different therapy regimes before such therapies are actually assigned to patients, thus aiding in the design of optimal personalized treat-

ment schemes. The elaboration of such framework is clearly an ambitious multistep undertaking whose completion lies outside the scope of this work. Nevertheless, given the incipient state of current research in the field, this thesis represents an important effort towards laying the foundations for such development.

In this context, the contributions of this thesis are twofold. First, we address the problem of cancer heterogeneity by proposing a novel Mixed Integer Linear Programming (MILP) formulation that integrates somatic mutation and gene expression data to infer the temporal sequence of events from cross-sectional data. This formulation is tested using both simulated data and real breast cancer data with matched somatic mutation and gene expression measurements from The Cancer Genome Atlas (TCGA). Second, we set the stage for the use of basic IPA techniques for optimal personalized cancer therapy design by advancing a methodology applicable to stochastic models of cancer progression and subsequently illustrating our analysis with a case study of optimal prostate cancer therapy design.

## 1.5 Contributions of this Work

The main contributions of this thesis are as follows.

- We consider the Traffic Light Control (TLC) problem for a single intersection modeled as a Stochastic Hybrid System (SHS) and study a quasi-dynamic policy based on partial state information defined by detecting whether vehicle backlogs are above and below certain controllable thresholds. We initially focus on

controlling the threshold parameters, rather than the light cycle lengths, and derive online gradient estimates of a cost metric with respect to controllable queue content thresholds using Infinitesimal Perturbation Analysis (IPA). These estimators are subsequently used to iteratively adjust the threshold values so as to improve overall system performance.

- We compare the relative effects of the threshold parameters and the light cycle length parameters on our objective function, and extend our methodology to parameterize the control policy by green and red cycle lengths as well as the queue content thresholds. We then derive online gradient estimates of a cost metric with respect to controllable cycle lengths and thresholds using IPA. By incorporating these estimators in quasi-dynamic control setting, we consistently obtain reductions in the mean queue content of the roads in the order of 50% with respect to static IPA approaches to the TLC problem.
- We address the problem of cancer heterogeneity by proposing a novel Mixed Integer Linear Programming (MILP) formulation that integrates somatic mutation and gene expression data to infer the temporal sequence of events from cross-sectional data. We test this formulation using both simulated data and real breast cancer data with matched somatic mutation and gene expression measurements from The Cancer Genome Atlas (TCGA). First, we classify the genes as oncogenes or tumor suppressors based on the frequency of driver mutations and select those genes with the most frequent driver mutations. Then,

we apply the MILP to identify the temporal order in which genes mutate and, simultaneously, the changes they produce at the gene expression level during cancer progression. Finally, we identify known causal relationships between mutations and gene expression changes in important breast cancer pathways.

- We set the stage for the use of basic IPA techniques for optimal personalized cancer therapy design by proposing a methodology applicable to stochastic models of cancer progression and illustrating our analysis with a case study of advanced prostate cancer. We develop a threshold-based policy for optimal prostate cancer therapy design that is parameterized by lower and upper threshold values and is associated with a cost metric that combines clinically relevant measures of therapy success. We initially focus on controlling the threshold parameters and derive online gradient estimates of our cost metric using IPA. These estimators are subsequently used to iteratively adjust the threshold values so as to improve therapy outcomes. Results obtained by applying our methodology to clinical data from real prostate cancer patients suggest that optimal treatment schemes are those in which both the lower and upper thresholds take values as small as possible.
- We extend our analysis of the stochastic model of prostate cancer evolution and focus on the importance of accurate modeling in conjunction with optimal therapy design. In particular, we evaluate sensitivity estimates with respect to several model parameters and identify critical ones. We use IPA to explore



the tradeoff between optimality and robustness (or, equivalently, fragility) and verify the extent to which our model is robust to certain critical parameters. Assuming that an underlying, and most likely poorly understood, equilibrium of prostate cancer cell subpopulation dynamics exists at suboptimal therapy settings, we verify that relaxing the optimality condition in favor of increased robustness to modeling errors provides an alternative objective to therapy design for at least some patients.

## 1.6 Document Outline

The rest of this document is organized as follows. Chapters 2 and 3 address the Traffic Light Control (TLC) problem for a single isolated intersection. In Chapter 2, we study a quasi-dynamic policy based on partial state information defined by detecting whether vehicle backlogs are above or below certain controllable thresholds. A Stochastic Flow Model (SFM) representation of the traffic light intersection is detailed in Section 2.1. In Section 2.2, we use Infinitesimal Perturbation Analysis (IPA) to derive gradient estimators with respect to the threshold parameters; by incorporating these estimators into a gradient-based algorithm, we iteratively adjust the threshold values so as to improve overall system performance under various traffic conditions. Simulation results are presented in Section 2.3. In Chapter 3, we extend our quasi-dynamic analysis to parameterize the control policy by green and red cycle lengths as well as the road content thresholds. We reintroduce the TLC problem formulation in Section 3.1 and derive the corresponding IPA estimators in Section

3.2. Results obtained by applying this methodology to a simulated urban setting are included in Section 3.3.

In Chapter 4, we address the problem of cancer heterogeneity by modeling cancer progression using somatic mutation and gene expression cross-sectional data. In Section 4.1, we propose a MILP formulation for stratifying molecular events such as mutation and gene expression changes. Results obtained using both simulated data and real breast cancer data are presented in Section 4.2. Chapters 5 and 6 address the challenge of optimal personalized cancer therapy design. In Chapter 5, we present a framework for IPA applications to personalized cancer therapy design which is illustrated with a case study of advanced prostate cancer. A SHA model of prostate cancer evolution is detailed in Section 5.1.1. In Section 5.1.2, we introduce a threshold-based policy for optimal prostate cancer therapy design that is associated with a cost metric which combines clinically relevant measures of therapy success. We use IPA to derive gradient estimators of this cost metric with respect to controllable threshold parameters and subsequently use these estimators to iteratively adjust the threshold values so as to improve therapy outcomes. Results obtained using clinical data from real prostate cancer patients are given in Section 5.3. In Chapter 6, we extend our analysis of the SHA model of prostate cancer evolution and focus on the importance of accurate modeling in conjunction with optimal therapy design. The derivation of IPA estimators of our cost metric with respect to several additional model parameters is detailed in Section 6.2. In Section 6.3, we present the ensuing

sensitivity analysis results. In Chapter 7, we summarize the main results and discuss future research directions.

## Chapter 2

# Traffic Light Control with Fixed Light Cycles

In this chapter, we consider the Traffic Light Control (TLC) problem for a single intersection modeled as a Stochastic Hybrid System (SHS) and study a quasi-dynamic policy based on partial state information defined by detecting whether vehicle backlogs are above and below certain controllable thresholds. In contrast to (Geng and Cassandras, 2013), where real-time partial state information was used to adjust light cycles conditioned upon a fixed queue content threshold being reached, here we focus on controlling the threshold parameters rather than the light cycle lengths. Our goal is to compare the relative effects of the threshold parameters and the light cycle length parameters on our objective function, build upon these results, and ultimately control both the light cycle lengths and the queue content thresholds simultaneously.

In what follows, we formulate the TLC problem for a single intersection as a Stochastic Flow Model (SFM) and subsequently detail the derivation of an Infinitesimal Perturbation Analysis (IPA) estimator for the cost function gradient with respect to a controllable parameter vector defined by the queue content thresholds. The IPA estimator is then incorporated into a gradient-based optimization algorithm and we

present simulation results showing that, by controlling the threshold parameters, performance improvements are obtained over prior quasi-dynamic and static approaches.

## 2.1 TLC Problem Formulation

The system we consider comprises a single intersection, as depicted in Figure 2.1. For simplicity, left-turn and right-turn traffic flows are not considered and yellow light cycles are implicitly accounted for within a red light cycle. Within the quasi-dynamic setting considered in this chapter, the controllable parameter vector of interest is given by  $\mathbf{s} = [s_1, s_2]$ , where  $s_n \in \mathbb{R}^+$  is the queue content threshold value for road  $n$ ,  $n = 1, 2$ . Let us then define a state vector  $x(\mathbf{s}, t) = [x_1(t), x_2(t)]$ , where  $x_n(\mathbf{s}, t) \in \mathbb{R}^+$  is the content of road  $n$ . Although we stress the dependence of the state variable on the queue content threshold values, for notational simplicity, we will henceforth write  $x(t)$  when no confusion arises.

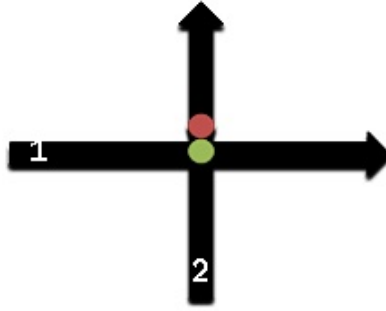


**Figure 2.1:** A single traffic light intersection with two cross-roads

Let us now partition the queue content state space into the following four regions

(as illustrated in Figure 2.2):

$$X_0 = \{(x_1, x_2) : x_1(t) < s_1, x_2(t) < s_2\}$$

$$X_1 = \{(x_1, x_2) : x_1(t) < s_1, x_2(t) \geq s_2\}$$

$$X_2 = \{(x_1, x_2) : x_1(t) \geq s_1, x_2(t) < s_2\}$$

$$X_3 = \{(x_1, x_2) : x_1(t) \geq s_1, x_2(t) \geq s_2\}$$

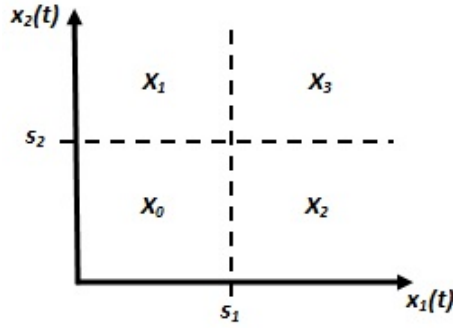


**Figure 2.2:** State space representation

Let us also define a left-continuous clock state variable  $z_n(t) \in [0, \theta_{n,\max}]$ , which measures the time elapsed since the last light switch from RED to GREEN on road  $n$ . It is thus reset to 0 as soon as the GREEN light switches to RED, and remains at this value while the light is GREEN for road  $\bar{n}$ , where  $\bar{n}$  is the index of the road perpendicular to road  $n$ . In this context, each road is guaranteed a minimum GREEN cycle length  $\theta_{n,\min}$ , which may be prolonged up to  $\theta_{n,\max}$  depending on the queue content of both roads. At any time  $t$ , let the control be defined as:

$$u(x(t), z(t)) \equiv \begin{cases} 1 & \text{set road 1 GREEN and road 2 RED} \\ 2 & \text{set road 2 GREEN and road 1 RED} \end{cases} \quad (2.1)$$

Although the queue content of any given road is usually not observable (i.e. there is no way of knowing the full state of the system in real time), it is feasible to obtain information regarding whether such content is above or below some threshold value. Therefore, it is possible to use partial state feedback in order to quasi-dynamically control the traffic light switches. In this context, we shall define a quasi-dynamic controller of the form  $u(X(t), z(t))$ , with  $X(t) \in \{X_0, X_1, X_2, X_3\}$ , as follows:

For  $X(t) \in \{X_0, X_3\}$ :

$$u(z(t)) = \begin{cases} 1 & \text{if } z_1(t) \in (0, \theta_{1,\max}) \text{ and } z_2(t) = 0 \\ 2 & \text{otherwise} \end{cases} \quad (2.2)$$

For  $X(t) = X_1$ :

$$u(z(t)) = \begin{cases} 1 & \text{if } z_1(t) \in (0, \theta_{1,\min}) \text{ and } z_2(t) = 0 \\ 2 & \text{otherwise} \end{cases} \quad (2.3)$$

For  $X(t) = X_2$ :

$$u(z(t)) = \begin{cases} 2 & \text{if } z_2(t) \in (0, \theta_{2,\min}) \text{ and } z_1(t) = 0 \\ 1 & \text{otherwise} \end{cases} \quad (2.4)$$

The stochastic processes involved in this system are defined on a common probability space  $(\Omega, F, P)$ . Each road is treated as a queue with arrival flow process  $\{\alpha_n(t)\}$ ,  $n = 1, 2$ , such that  $\alpha_n(t)$  corresponds to the instantaneous vehicle arrival rate at time  $t$ . Furthermore, the departure flow process on road  $n$  is defined as:

$$\beta_n(t) = \begin{cases} h_n(t) & \text{if } x_n(t) > 0 \text{ and } u = n \\ \alpha_n(t) & \text{if } x_n(t) = 0 \text{ and } u = n \\ 0 & \text{otherwise} \end{cases} \quad (2.5)$$

where  $h_n(t)$  corresponds to the instantaneous vehicle departure rate at time  $t$ . We can now write the dynamics of the state variables  $x_n(t)$  and  $z_n(t)$  as follows, where we adopt the notation  $\bar{n}$  to denote the index of the road perpendicular to road  $n = 1, 2$ , and note that the symbols  $t^+$  ( $t^-$ , respectively) denote the time instant immediately following (preceding, respectively) time  $t$ :

$$\dot{x}_n(t) = \begin{cases} \alpha_n(t) & \text{if } z_n(t) = 0 \\ 0 & \text{if } x_n(t) = 0 \text{ and } \alpha_n(t) \leq h_n(t) \\ \alpha_n(t) - \beta_n(t) & \text{otherwise} \end{cases} \quad (2.6)$$

$$\begin{aligned} \dot{z}_n(t) &= \begin{cases} 1 & \text{if } z_{\bar{n}}(t) = 0 \\ 0 & \text{otherwise} \end{cases} \\ z_n(t^+) &= 0 \text{ if } z_n(t) = \theta_{n,\max} \\ &\quad \text{or } z_n(t) = \theta_{n,\min}, x_n(t) < s_n, x_{\bar{n}}(t) \geq s_{\bar{n}} \\ &\quad \text{or } z_n(t) > \theta_{n,\min}, x_n(t^-) > s_n, x_n(t^+) = s_n, x_{\bar{n}}(t) \geq s_{\bar{n}} \\ &\quad \text{or } z_n(t) > \theta_{n,\min}, x_n(t) < s_n, x_{\bar{n}}(t^-) < s_{\bar{n}}, x_{\bar{n}}(t^+) = s_{\bar{n}} \end{aligned} \quad (2.7)$$

The dynamics of the “clock” state variable can be more easily understood graphically, and an illustrative representation of (2.7) is given in Figure 2.3.

In this context, the traffic light intersection illustrated in Figure 2.1 can be viewed as a hybrid system in which the time-driven dynamics are given by (2.6) and (2.7), and the event-driven dynamics are associated with light switches and with events that cause the value of  $x_n(t)$  to change from strictly positive to zero or vice-versa. It is then possible to derive a Stochastic Hybrid Automaton (SHA) model (Cassandras and Lafortune, 2008) containing 14 modes, which are defined by combinations of  $x_n(t)$  and  $z_n(t)$  (details of this derivation may be found in (Geng, 2013)). The event set for



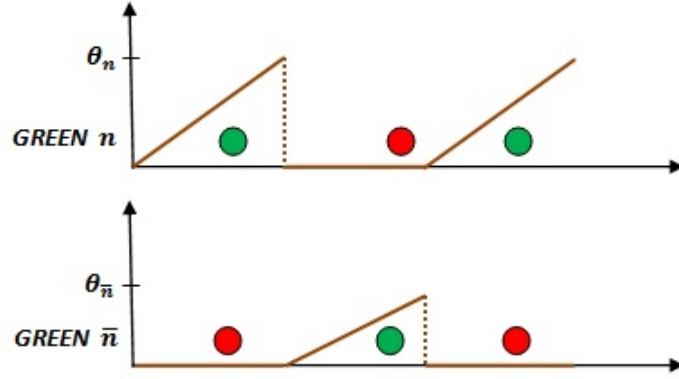


**Figure 2-3:** Illustrative representation of the dynamics of the “clock” state variable

this SHA is  $\Phi_n = \{e_1, e_2, e_3, e_4, e_5, e_6, e_7\}$ , where:

$e_1$  is the guard condition  $[x_n = s_n \text{ from below}]$

$e_2$  is the guard condition  $[x_n = s_n \text{ from above}]$

$e_3$  is the guard condition  $[z_n = \theta_{n,\min}]$

$e_4$  is the guard condition  $[z_n = \theta_{n,\max}]$

$e_5$  is the guard condition  $[x_n = 0 \text{ from above}]$

$e_6$  is a switch in the sign of  $\alpha_n(t) - h_n(t)$  from non-positive to strictly positive

$e_7$  is a switch in the sign of  $\alpha_n(t)$  from 0 to strictly positive

For easier reference, we shall rename events  $e_1$  through  $e_4$  as  $\zeta_n$ ,  $\gamma_n$ ,  $\lambda_n$ , and  $\mu_n$ , respectively, where the subscript  $n$  refers to the road where the event occurred. This notation is especially convenient for defining the control rules which must be met in order for traffic light switches to take place. In fact, if we label light switching events from RED to GREEN and GREEN to RED as  $R2G_n$  and  $G2R_n$ , respectively (the subscript  $n$  once again refers to the road where the event occurred), we can specify

the following simple hysteresis control rules:

**Rule 1** The occurrence of event  $\zeta_n$ , while  $z_{\bar{n}} > \theta_{\bar{n},\min}$  and  $x_{\bar{n}} < s_{\bar{n}}$ , results in event

$$R2G_n.$$

**Rule 2** The occurrence of event  $\gamma_n$ , while  $z_n > \theta_{n,\min}$  and  $x_{\bar{n}} \geq s_{\bar{n}}$ , results in event

$$G2R_n.$$

**Rule 3** The occurrence of event  $\lambda_n$ , while  $x_n < s_n$  and  $x_{\bar{n}} \geq s_{\bar{n}}$ , results in event

$$G2R_n.$$

**Rule 4** The occurrence of event  $\mu_n$  always results in event  $G2R_n$ .

We present the SHA of this system, defined in terms of the queue content state  $X(t)$ , in Figure 2-4 and concentrate on analyzing a typical sample path of any one of the queue contents, which is shown in Figure 2-5. Such sample path consists of alternating Non-Empty Periods (NEPs) and Empty Periods (EPs), which correspond to time intervals when  $x_n(t) > 0$  (i.e. queue  $n$  is non-empty) and  $x_n(t) = 0$  (i.e. queue  $n$  is empty), respectively. Let us then label the events corresponding to the end and to the start of an NEP as  $E_n$  and  $S_n$ , respectively, and note that  $E_n$  is induced by event  $e_5$ , while  $S_n$  may be induced by events  $e_6$  or  $e_7$  or  $G2R_n$ .

The purpose of our analysis is to apply IPA to sample path data in order to obtain unbiased gradient estimates of a system performance measure, and subsequently incorporate such estimates into a gradient-based optimization scheme. In this context, let us choose our performance metric to be the weighted sum of the mean queue

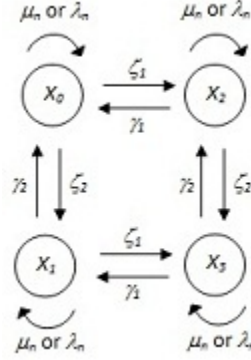


**Figure 2.4:** Stochastic Hybrid Automaton for aggregate states  $X(t)$  under quasi-dynamic control

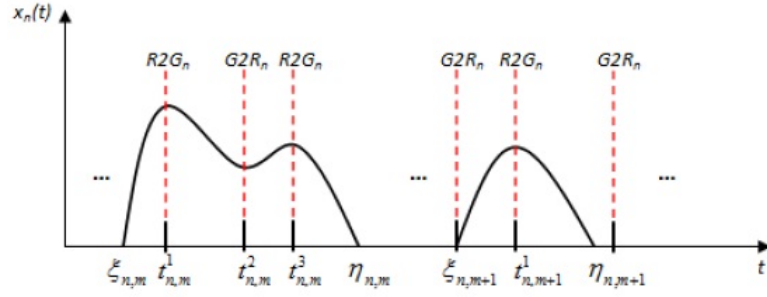


**Figure 2.5:** Typical sample path of a traffic light queue

lengths over a fixed time interval  $[0, T]$ . Since we wish to adjust the controllable parameter vector  $\mathbf{s}$  in such a way as to minimize the chosen cost function, let the sample function be defined as

$$L(\mathbf{s}; x(0), z(0), T) = \frac{1}{T} \sum_{n=1}^2 \int_0^T w_n x_n(\mathbf{s}, t) dt \quad (2.8)$$

where  $w_n$  is a cost weight associated with road  $n$ , and  $x(0)$ ,  $z(0)$  are given initial

conditions. Since the queue content is null during EPs, (2.8) can be rewritten as

$$L(\mathbf{s}; x(0), z(0), T) = \frac{1}{T} \sum_{n=1}^2 \sum_{m=1}^{M_n} \int_{\xi_{n,m}}^{\eta_{n,m}} w_n x_n(\mathbf{s}, t) dt \quad (2.9)$$

where  $M_n$  is the total number of NEPs during the sample path of road  $n$ . Finally, let us define the overall performance metric as

$$J(\mathbf{s}; x(0), z(0), T) = E[L(\mathbf{s}; x(0), z(0), T)] \quad (2.10)$$

Recall that it is not possible to derive a closed-form expression of  $J(\mathbf{s}; x(0), z(0), T)$  without imposing limitations on the processes  $\{\alpha_n(t)\}$  and  $\{\beta_n(t)\}$ . Nevertheless, by assuming that  $\alpha_n(t)$  and  $\beta_n(t)$  are piecewise continuous w.p. 1, and that  $\{\alpha_n(t)\}$  and  $\{\beta_n(t)\}$  are stationary random processes over  $[0, T]$ , we can successfully apply IPA to obtain an estimate of  $\nabla J(\mathbf{s})$  and then determine  $\mathbf{s}^*$  through (A.4). We will further assume that the derivatives  $\frac{dL}{ds_i}$  exist for all  $s_i \in \mathfrak{R}^+$  w.p. 1, and proceed to derive the IPA estimators of  $\frac{dJ}{ds_i}$ ,  $i = 1, 2$ .

## 2.2 IPA for TLC with Fixed Light Cycles

For simplicity of notation, let us define the derivatives of the states  $x_n(\mathbf{s}, t)$  and  $z_i(\mathbf{s}, t)$  and event times  $\tau_k(\mathbf{s})$  with respect to  $s_i$ ,  $i = 1, 2$ , as follows:

$$x'_{n,i}(t) \equiv \frac{\partial x_n(\mathbf{s}, t)}{\partial s_i}, \quad z'_{i,i}(\mathbf{s}, t) \equiv \frac{\partial z_i(\mathbf{s}, t)}{\partial s_i}, \quad \tau'_{k,i} \equiv \frac{\partial \tau_k(\mathbf{s})}{\partial s_i} \quad (2.11)$$

Using the definition of  $L(\mathbf{s})$  in (2.9), we may obtain the sample performance

derivatives  $\frac{dL}{ds_i}$  as follows:

$$\frac{dL(\mathbf{s})}{ds_i} = \frac{1}{T} \sum_{n=1}^2 \sum_{m=1}^{M_n} \left[ w_n x_n(\eta_{n,m}) \frac{\partial \eta_{n,m}}{\partial s_i} - w_n x_n(\xi_{n,m}) \frac{\partial \xi_{n,m}}{\partial s_i} + \frac{\eta_{n,m}}{\xi_{n,m}} w_n x'_{n,i}(t) dt \right]$$

Note that, at the start and end of an NEP, we have that  $x_n(\xi_{n,m}) = x_n(\eta_{n,m}) = 0$ . Moreover, based on (2.6), we will have  $\frac{\partial f_{n,k}(t)}{\partial x_n} = \frac{\partial f_{n,k}(t)}{\partial s_i} = 0$ ,  $n, i = 1, 2$ , so that in (A.7) we have  $\frac{d}{dt}x'(t) = 0$  for  $t \in [\tau_k, \tau_{k+1})$ . This means that the value of the state derivative of any road remains unaltered while the system is in a given discrete mode, i.e.

$$x'_{n,i}(t) = x'_{n,i}(\tau_k^+), t \in [\tau_k, \tau_{k+1}) \quad (2.12)$$

which, in turn, implies that we can decompose each NEP into time intervals of the form  $[\xi_{n,m}, t_{n,m}^1), [t_{n,m}^1, t_{n,m}^2), \dots, [t_{n,m}^{J_{n,m}}, \eta_{n,m})$ . Letting

$$L_{n,m}(\mathbf{s}) = \int_{\xi_{n,m}}^{\eta_{n,m}} x_n(\mathbf{s}, t) dt$$

we get

$$\begin{aligned} \frac{dL_{n,m}(\mathbf{s})}{ds_i} &= x'_{n,i}((\xi_{n,m})^+) \cdot (t_{n,m}^1 - \xi_{n,m}) \\ &\quad + x'_{n,i}((t_{n,m}^{J_{n,m}})^+) \cdot (\eta_{n,m} - t_{n,m}^{J_{n,m}}) \\ &\quad + \sum_{j=2}^{J_{n,m}} x'_{n,i}((t_{n,m}^j)^+) \cdot (t_{n,m}^j - t_{n,m}^{j-1}) \end{aligned} \quad (2.13)$$

In what follows, we derive the IPA state and event time derivatives for the events identified in our SHA model.

### 2.2.1 State and Event Time Derivatives

We shall proceed by considering each of the event types  $(E_n, G2R_n, R2G_n, S_n)$  identified in the previous section and deriving the corresponding event time and state derivatives. We begin with a general result which applies to all light switching events  $G2R_n$  and  $R2G_n$ . Let us denote the time of the  $j$ th occurrence of a light switching event by  $\sigma_j$  and define its derivative with respect to the control parameters as  $\sigma'_{j,i} \equiv \frac{\partial \sigma_j}{\partial s_i}$ ,  $i = 1, 2$ .

**Lemma 2.1** *The derivative  $\sigma'_{j,i}$ ,  $i = 1, 2$ , of light switching event times  $\sigma_j$ ,  $j = 1, 2, \dots$  with respect to the control parameters  $s_1, s_2$  satisfies:*

$$\sigma'_{j,i} = \begin{cases} \frac{1}{\alpha_n(\sigma_j)} \cdot \mathbf{1}[n = i] - x'_{n,i}(\sigma_j^-) & \text{if } \zeta_n \text{ occurs at } \sigma_j \\ \frac{1}{\alpha_n(\sigma_j) - h_n(\sigma_j)} \cdot \mathbf{1}[n = i] - x'_{n,i}(\sigma_j^-) & \text{if } \gamma_n \text{ occurs at } \sigma_j \\ \sigma'_{j-1,i} & \text{otherwise} \end{cases} \quad (2.14)$$

where  $\mathbf{1}[\cdot]$  is the usual indicator function.

*Proof:* See Appendix C.

We now proceed by considering each of the event types  $(G2R_n, R2G_n, E_n, S_n)$ .

#### (1) Event $G2R_n$

Two cases must be considered: (a)  $G2R_n$  occurs at  $\tau_k$  while road  $n$  is undergoing an NEP; (b)  $G2R_n$  occurs at  $\tau_k$  while road  $n$  is undergoing an EP. In case (a), the fact that  $x_n(\tau_k^-) > 0$  means that  $f_{n,k-1}(\tau_k^-) = \alpha_n(\tau_k) - h_n(\tau_k)$ . Additionally, since road  $n$  is undergoing a RED cycle at time  $\tau_k^+$ , we must have  $f_{n,k}(\tau_k^+) = \alpha_n(\tau_k)$ . It follows from (A.8) that  $x'_{n,i}(\tau_k^+) = x'_{n,i}(\tau_k^-) - h_n(\tau_k)\tau'_{k,i}$ ,  $n = 1, 2$ ,  $i = 1, 2$ . In case (b),  $x_n(\tau_k^-) = 0$ , so that  $f_{n,k-1}(\tau_k^-) = 0$ , and it is simple to verify that  $x'_{n,i}(\tau_k^+) = x'_{n,i}(\tau_k^-) - \alpha_n(\tau_k)\tau'_{k,i}$ ,

$n = 1, 2$ ,  $i = 1, 2$ . Moreover, if the  $k$ th event corresponds to the  $j$ th occurrence of a light switching event, we have  $\tau'_{k,i} = \sigma'_{j,i}$  for some  $j = 1, 2, \dots$ . Combining these results, we get, for  $n = 1, 2$  and  $i = 1, 2$ ,

$$x'_{n,i}(\tau_k^+) = x'_{n,i}(\tau_k^-) - \begin{cases} h_n(\tau_k)\sigma'_{j,i} & \text{if } x_n(\tau_k) > 0 \\ \alpha_n(\tau_k)\sigma'_{j,i} & \text{if } x_n(\tau_k) = 0 \end{cases} \quad (2.15)$$

where  $\sigma'_{j,i}$  is given by (2.14) in Lemma 2.1 with  $\sigma_j = \tau_k$ .

## (2) Event $R2G_n$

Once again, two cases must be considered: (a)  $R2G_n$  occurs at  $\tau_k$  while road  $n$  is undergoing an NEP; (b)  $R2G_n$  occurs at  $\tau_k$  while road  $n$  is undergoing an EP. In case (a), the fact that road  $n$  is undergoing a RED cycle within an NEP at time  $\tau_k^-$  means that  $f_{n,k-1}(\tau_k^-) = \alpha_n(\tau_k)$ . Additionally, since road  $n$  is undergoing a GREEN cycle at time  $\tau_k^+$ , we must have  $f_{n,k}(\tau_k^+) = \alpha_n(\tau_k) - h_n(\tau_k)$ , and (A.8) reduces to  $x'_{n,i}(\tau_k^+) = x'_{n,i}(\tau_k^-) + h_n(\tau_k) \cdot \tau'_{k,i}$ ,  $n = 1, 2$ ,  $i = 1, 2$ . In case (b), the fact that road  $n$  is empty while undergoing a RED cycle at time  $\tau_k^-$  implies that  $f_{n,k-1}(\tau_k^-) = \alpha_n(\tau_k)$  with  $0 < \alpha_n(\tau_k) \leq h_n(\tau_k)$ , while  $f_{n,k}(\tau_k^+) = 0$ . Substituting these expressions into (A.8) yields  $x'_{n,i}(\tau_k^+) = x'_{n,i}(\tau_k^-) + \alpha_n(\tau_k) \cdot \tau'_{k,i}$ ,  $n = 1, 2$  and  $i = 1, 2$ . Combining these two cases, we get, for  $n = 1, 2$  and  $i = 1, 2$ ,

$$x'_{n,i}(\tau_k^+) = x'_{n,i}(\tau_k^-) + \begin{cases} \alpha_n(\tau_k)\sigma'_{j,i} & \text{if } x_n(\tau_k) = 0 \text{ and } 0 < \alpha_n(\tau_k) \leq h_n(\tau_k) \\ h_n(\tau_k)\sigma'_{j,i} & \text{otherwise} \end{cases} \quad (2.16)$$

where again  $\sigma'_{j,i}$  is given by (2.14) in Lemma 2.1 with  $\sigma_j = \tau_k$ .

### (3) Event $E_n$

This event corresponds to the end of an NEP on road  $n$  and is induced by  $e_5$ , which is an endogenous event at  $\tau_k$  with  $g_k = x_n = 0$ . Since at time  $\tau_k^-$  road  $n$  is in an NEP, we must have  $f_{n,k-1}(\tau_k^-) = \alpha_n(\tau_k) - h_n(\tau_k)$ , and (A.12) implies that  $\tau'_{k,i} = \frac{-x'_{n,i}(\tau_k^-)}{\alpha_n(\tau_k) - h_n(\tau_k)}$ . Moreover, the fact that road  $n$  is in an EP at time  $\tau_k^+$  implies that  $f_{n,k}(\tau_k^+) = 0$ , and (A.8) reduces to  $x'_{n,i}(\tau_k^+) = x'_{n,i}(\tau_k^-) - x'_{n,i}(\tau_k^-)$  so that

$$x'_{n,i}(\tau_k^+) = 0, \quad n = 1, 2 \text{ and } i = 1, 2 \quad (2.17)$$

### (4) Event $S_n$

This event corresponds to the start of an NEP and can be induced by a  $G2R_n$ ,  $e_7$  or  $e_6$  event. These three cases are analyzed in what follows.

1.  $S_n$  is induced by a  $G2R_n$  event. Suppose that this  $G2R_n$  event initiated the  $m$ th NEP on road  $n$ . Therefore, during the preceding EP, i.e. during the time interval  $[\eta_{n,m-1}, \xi_{n,m})$ , we have  $x_n(t) = 0$  for  $t \in [\eta_{n,m-1}, \xi_{n,m})$ , and, consequently,  $x'_{n,i}(t) = 0$  for  $t \in [\eta_{n,m-1}, \xi_{n,m})$  and  $i = 1, 2$ . As a result,  $x'_{n,i}(\eta_{n,m-1}^+) = x'_{n,i}(\xi_{n,m}^-) = 0$ , and since  $\tau_k = \xi_{n,m}$  it follows that  $x'_{n,i}(\tau_k^-) = x'_{n,i}(\xi_{n,m}^-) = 0$ . Therefore, (2.15) reduces to

$$x'_{n,i}(\tau_k^+) = -\alpha_n(\tau_k)\tau'_{k,i} \quad (2.18)$$

The value of  $\tau'_{k,i}$  above depends on the event inducing  $G2R_n$ . If the  $k$ th event corresponds to the  $j$ th occurrence of a light switching event, then  $\tau'_{k,i} = \sigma'_{j,i}$  which is obtained from (2.14). Note, however, that event  $S_n$  cannot be induced by  $\gamma_n$  due to



the fact that the occurrence of  $\gamma_n$  is conditioned upon road  $n$  being in an NEP, which cannot be the case here. As a result, the second case in (2.14) is excluded.

2.  $S_n$  is induced by an  $e_7$  event. Recall that  $e_7$  corresponds to a switch from  $\alpha_n(t) = 0$  to  $\alpha_n(t) > 0$  while road  $n$  is undergoing a RED cycle, i.e.  $z_n(t) = 0$ . Since this is an exogenous event,  $\tau'_{k,i} = 0$ ,  $i = 1, 2$ , and (A.8) reduces to  $x'_{n,i}(\tau_k^+) = x'_{n,i}(\tau_k^-)$ . We know that  $\tau_k$  corresponds to the time when the NEP starts at road  $n$ , i.e.  $\tau_k = \xi_{n,m}$ , and we have shown that  $x'_{n,i}(\xi_{n,m}^-) = x'_{n,i}(\eta_{n,m-1}^+) = 0$ . It thus follows that  $x'_{n,i}(\tau_k^-) = x'_{n,i}(\xi_{n,m}^-) = 0$ , so that

$$x'_{n,i}(\tau_k^+) = 0, \quad n, i = 1, 2 \quad (2.19)$$

3.  $S_n$  is induced by an  $e_6$  event. Event  $e_6$  corresponds to a switch from  $\alpha_n(t) - h_n(t) \leq 0$  to  $\alpha_n(t) - h_n(t) > 0$  while road  $n$  is undergoing a GREEN cycle, i.e.,  $z_n(t) > 0$ . Since this is an exogenous event,  $\tau'_{k,i} = 0$ ,  $i = 1, 2$ , and the subsequent analysis is similar to that of the previous case, so that (2.19) holds.

This completes the derivation of all state and event time derivatives required to apply IPA to the TLC problem setting contemplated in this chapter.

### 2.2.2 Cost Derivatives

It is clear from (2.13) that computing the IPA estimator of  $\frac{dJ}{ds_i}$ ,  $i = 1, 2$ , requires knowledge of: (i) the event times  $\xi_{n,m}$ ,  $\eta_{n,m}$ , and  $t_{n,m}^j$ , and (ii) the value of the state derivatives  $x'_{n,i}(t)$ , whose expressions were derived in the previous section, during each time interval. The quantities in (i) are easily observed using timers, and those

in (ii) ultimately depend on the values of the arrival and departure rates  $\alpha_n(t)$  and  $h_n(t)$  at event times *only*, which may be estimated through simple rate estimators. As a result, an algorithm for updating the value of  $\frac{dL(\mathbf{s})}{ds_i}$  after each observed event is straightforward to implement (and can be found in Appendix B). We also point out that our IPA estimator is linear in the number of events in the SFM, not in its states. Thus, our method could be readily extended to a network of intersections.

## 2.3 Simulation Results

With the intent of showing that performance improvements can be obtained when IPA is used to control the queue content thresholds, two sets of simulations were performed: one in which the thresholds were optimized considering a priori fixed values of cycle lengths  $\theta = [\theta_{1,\min}, \theta_{1,\max}, \theta_{2,\min}, \theta_{2,\max}]$  for each road, and another in which the cycle lengths and thresholds  $\mathbf{s} = [s_1, s_2]$  were optimized sequentially. Thus, first, the IPA algorithm from (Geng and Cassandras, 2013) was applied to determine optimal  $\theta$ ; then the values of  $s_1$  and  $s_2$  were optimized using the IPA algorithm described in this chapter.

In all our simulations, we assume that the vehicle arrival process is Poisson with rate  $\bar{\alpha}_n$ ,  $n = 1, 2$ , and approximate the departure rate by a constant value  $h_n(t) = H$  when road  $n$  is non-empty, which amounts to considering that the speed with which vehicles cross an intersection depends only on the behavior of the vehicles themselves. We emphasize, however, that our methodology applies independently of the distributions chosen to represent the arrival and departure processes. We

estimate the values of the arrival rate at event times as  $\alpha_n(\tau_k) = N_a/t_w$ , where  $N_a$  is the number of vehicle arrivals during a time window  $t_w$  around  $\tau_k$ . Simulations of the intersection modeled as a pure DES are thus run to generate sample paths to which the IPA estimator is applied. We also make use of a brute-force (BF) approach to generate a cost surface along which the convergence of the IPA-driven optimization algorithm is depicted. The BF method consists of discretizing the values of  $s_i$  and generating 10 sample paths for each pair of discretized threshold values  $(s_1, s_2) = (1, 1), (1, 2), \dots, (2, 1), \dots$ , from which the average total cost can then be obtained. In all results reported here, we set  $H = 1$ ,  $w_n = 1$ ,  $n = 1, 2$ , and measure the sample path length in terms of the number of observed light switches, which we choose to be  $N = 5000$ .

In our first set of simulations, the GREEN light cycles are fixed and equal on both roads by setting  $\theta_{n,\min} = 10$  sec and  $\theta_{n,\max} = 30$  sec,  $n = 1, 2$ . Two scenarios are considered: *Scenario A*, in which road 1 exhibits high traffic intensity while road 2 exhibits low traffic intensity (where we choose  $1/\bar{\alpha}_1 = 2$  and  $1/\bar{\alpha}_2 = 6$ ); *Scenario B*, in which both roads exhibit high but unequal traffic intensity (and we choose  $1/\bar{\alpha}_1 = 2$  and  $1/\bar{\alpha}_2 = 3$ ). We further consider two different initial threshold configurations for each scenario. Table 2.1 shows the optimal threshold values determined by both the BF method and the IPA-driven optimization algorithm, along with the cost reduction achieved by the latter (denoted as  $R$  and computed as a percentage of the initial cost). Sample convergence plots of the cost  $J$  and thresholds  $\mathbf{s}$  are presented in Figure 2-6,

while the cost surfaces of both scenarios, along with curves (black and yellow) that represent the trajectories corresponding to each initial configuration, are shown in Figures 2-7 and 2-8. Visual inspection of Figure 2-7 reveals that both trajectories converge to the same optimal point, namely  $s_{IPA}^* = [1.9, 3.7]$ , as presented in Table 2.1. Similarly for *Scenario B*, both trajectories depicted in Figure 2-8 converge to the optimal point shown in Table 2.1, i.e.  $s_{IPA}^* = [4.6, 5.1]$ .

**Table 2.1:** Optimization results for system with a priori fixed cycle lengths

	Initial Point		IPA			BF	
$1/\bar{\alpha}$	$s_0$	$J_0$	$s_{IPA}^*$	$J_{IPA}^*$	$R$	$s_{BF}^*$	$J_{BF}^*$
2, 6	10, 1	12.8	1.9, 3.7	4.3	66	1, 4	4.4
2, 6	9, 10	6.2	1.9, 3.7	4.3	31	1, 4	4.4
2, 3	15, 3	18.9	4.6, 5.1	7.9	58	5, 6	8.8
2, 3	15, 15	13.1	4.6, 5.1	7.9	40	5, 6	8.8

In our second set of simulations, we perform a sequential optimization of the cycle lengths and threshold values. We make use of the optimal light cycle lengths obtained through IPA (denoted by  $\theta_{IPA}^* = [\theta_{1,\min}^*, \theta_{1,\max}^*, \theta_{2,\min}^*, \theta_{2,\max}^*]$ ) in (Geng and Cassandras, 2013), and subsequently apply the IPA estimator derived in this chapter to optimize the queue content thresholds. The optimal light cycle lengths obtained in (Geng and Cassandras, 2013) for fixed and predetermined threshold values of  $\mathbf{s} = [8, 8]$  are reproduced in Table 2.2.

A comparison between IPA and BF results, including a quantitative assessment of the *additional* cost reduction achieved (computed as a percentage of the initial cost and labeled  $R$ ) is shown in Table 2.3.

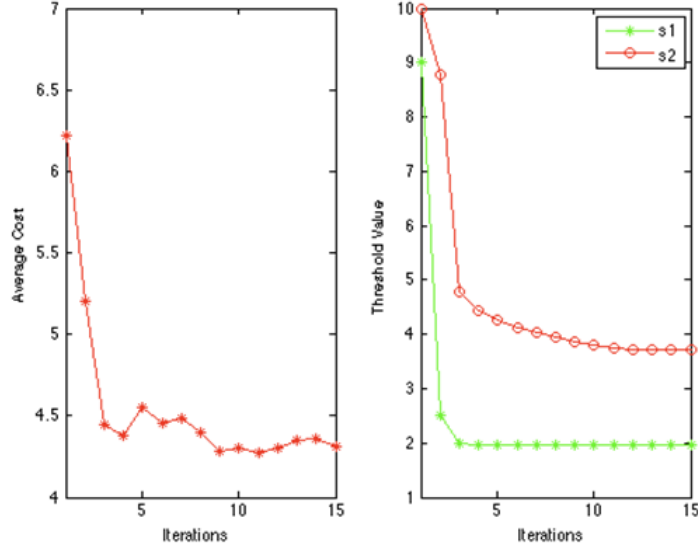


**Figure 2-6:** Sample cost and parameter trajectories for  $1/\bar{\alpha} = [2, 6], \theta = [10, 30, 10, 30]$ , and  $s_0 = [9, 10]$

**Table 2.2:** Optimal cycle lengths obtained in (Geng and Cassandras, 2013) for  $\mathbf{s} = [8, 8]$

$1/\bar{\alpha}$	$\theta_{IPA}^*$
[2, 3]	[10.2, 19.3, 10.1, 16.3]
[1.7, 3]	[10.1, 20.1, 10.6, 11.9]

In order to further illustrate the advantage of quasi-dynamically controlling the light cycle lengths and threshold values over a static IPA approach to the TLC problem, we include a comparison of the results generated by our methodology with those obtained when static control (as described in (Geng and Cassandras, 2012)) is applied to determine the optimal cycle lengths  $\theta_{static}^*$ . The static controller defined in (Geng and Cassandras, 2012) adjusts the green light cycles subject to some lower and upper bounds and determines  $\theta_{static}^* = [\theta_1^*, \theta_2^*]$ , where  $\theta_1^*$  ( $\theta_2^*$ , respectively) is the

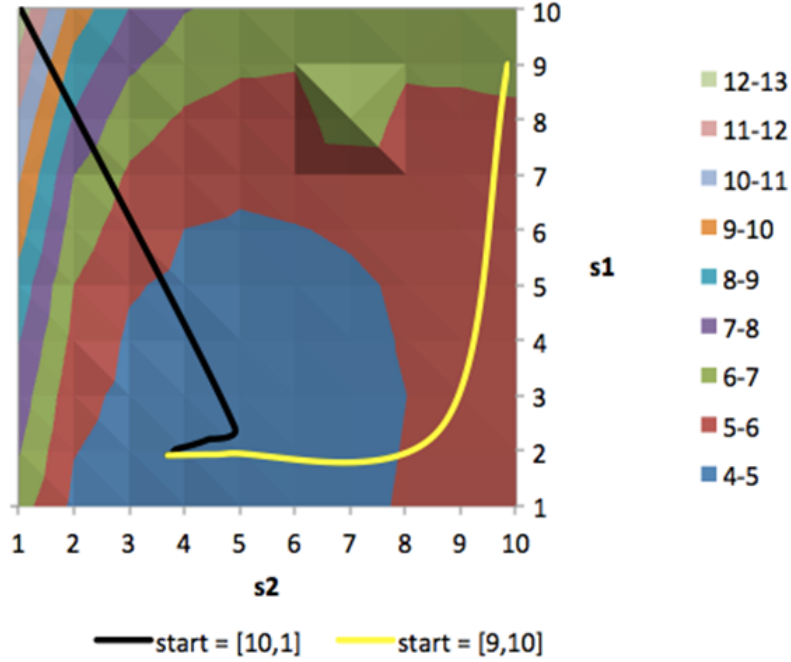


**Figure 2-7:** Cost surface and convergence trajectories for *Scenario A* (note: the color scale refers to the cost values)

green cycle length which should be allotted to road 1 (road 2, respectively) in order to minimize the average queue content on both roads. Table 2.4 summarizes the results obtained by each of the IPA approaches considered in this work: *Method 1*, in which a static controller is used to adjust the light cycles (results were obtained by using the same setting as in our second set of quasi-dynamic simulations and constraining  $\theta \in [10, 40]$ ); *Method 2*, in which only the light cycles are controlled quasi-dynamically (i.e. fixed and predetermined queue content thresholds are incorporated into the system model); *Method 3*, in which a sequential quasi-dynamic optimization of light cycle lengths and threshold values is performed in between two adjustment points. The columns labeled  $R_i$ ,  $i = 2, 3$ , present the cost reduction achieved by the quasi-

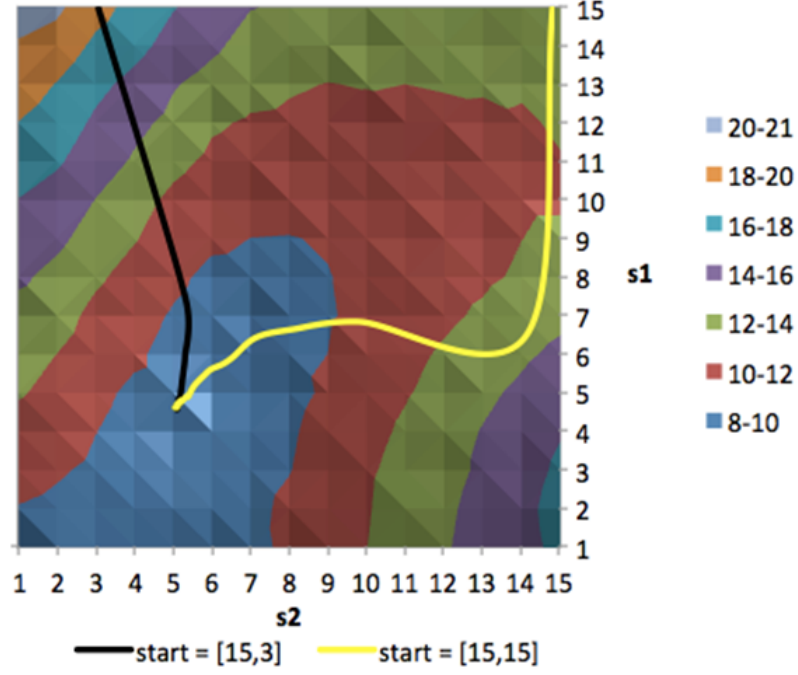


**Figure 2-8:** Cost surface and convergence trajectories for *Scenario B* (note: the color scale refers to the cost values)

dynamic methods with respect to the static approach, i.e.  $R_i = \frac{J_1^* - J_i^*}{J_1^*} * 100$ .

The numerical results presented thus far show that a considerable reduction in the mean queue content of both roads can be achieved by quasi-dynamically controlling the thresholds in systems with non-optimal cycle lengths. Moreover, determining optimal threshold values allows for additional improvements to the performance of systems running under optimal light cycle lengths. Such results indicate that a method in which the light cycle lengths and queue content thresholds are controlled *simultaneously* is likely to provide improved solutions to the TLC problem. We verify this in the following chapter, where we derive an IPA-based optimization algorithm that incorporates all such controllable parameters and ultimately determines the optimal

**Table 2.3:** Optimization results for system with optimal cycle lengths

	IPA			BF	
$1/\bar{\alpha}$	$s_{IPA}^*$	$J_{IPA}^*$	$R$ (%)	$s_{BF}^*$	$J_{BF}^*$
[2, 3]	[2.8, 4.3]	7.1	15	[2, 5]	7.2
[1.7, 3]	[4.8, 6.1]	14.9	11	[3, 8]	15.7

**Table 2.4:** Comparison between three IPA-based approaches to the TLC problem

	Method 1	Method 2		Method 3	
$1/\bar{\alpha}$	$J_1^*$	$J_2^*$	$R_2$ (%)	$J_3^*$	$R_3$ (%)
[2, 3]	14.4	8.4	42	7.1	51
[1.7, 3]	23.9	16.7	30	14.9	38

light cycle length/threshold configuration capable of minimizing traffic build-up at a given intersection.



## Chapter 3

# Traffic Light Control with Quasi-Dynamic Light Cycles and Thresholds

In this chapter, we extend our quasi-dynamic analysis of the TLC problem to parameterize the control policy by green and red cycle lengths *as well as* the road content thresholds. In what follows, we reintroduce the TLC problem formulation and derive an IPA estimator for the cost function gradient with respect to a controllable parameter vector defined by the light cycle lengths and threshold values. Results obtained by applying this methodology to a simulated urban setting are then presented.

### 3.1 TLC Problem Formulation

We continue to consider the system comprised of a single intersection, as shown in Figure 2.1, where, for simplicity, left-turn and right-turn traffic flows are not considered and yellow light cycles are implicitly accounted for within a red light cycle. In keeping with the notation defined in Chapter 2,  $x_i(t) \in \mathbb{R}^+$  denotes the content of queue  $i$ , and, for each queue  $i$ , we also define a “clock” state variable  $z_i(t)$ ,  $i = 1, 2$ , which measures the time since the last switch from RED to GREEN of the traffic light for queue  $i$ . Setting  $z(t) = [z_1(t), z_2(t)]$ , the complete system state vector is  $[x(t), z(t)]$ .

In contrast to the previous part of this work, we now define the controllable parameter vector of interest as  $v = [\theta_{1,\min}, \theta_{1,\max}, \theta_{2,\min}, \theta_{2,\max}, s_1, s_2]$ , where  $s_i \in \mathbb{R}^+$  is the queue content threshold value for road  $i = 1, 2$ , and  $\theta_{i,\min}$  ( $\theta_{i,\max}$ , respectively) denotes the minimum (maximum, respectively) GREEN cycle length allotted to road  $i$ . The notation  $x(v, t) = [x_1(v, t), x_2(v, t)]$  is used to stress the dependence of the state on these controllable parameters. However, for notational simplicity, we will henceforth write  $x(t)$  when no confusion arises; the same applies to  $z(t)$ .

We will continue to make use of the quasi-dynamic controller defined by (2.2)-(2.4), so that the hysteresis control rules presented in Section 2.1 still hold. Furthermore, we will maintain all assumptions regarding the underlying input stochastic processes, as well as consider the same feasible events and system dynamics that were introduced in Section 2.1. A simplified state transition diagram for the resulting SHA, in which the state variable dynamics have been omitted and the states  $x_n(t) = 0$  and  $x_n(t) > 0$  have been combined into a single one, is shown in Figure 3.1. In what follows, we derive the IPA state and event time derivatives for the events identified in Section 2.1.

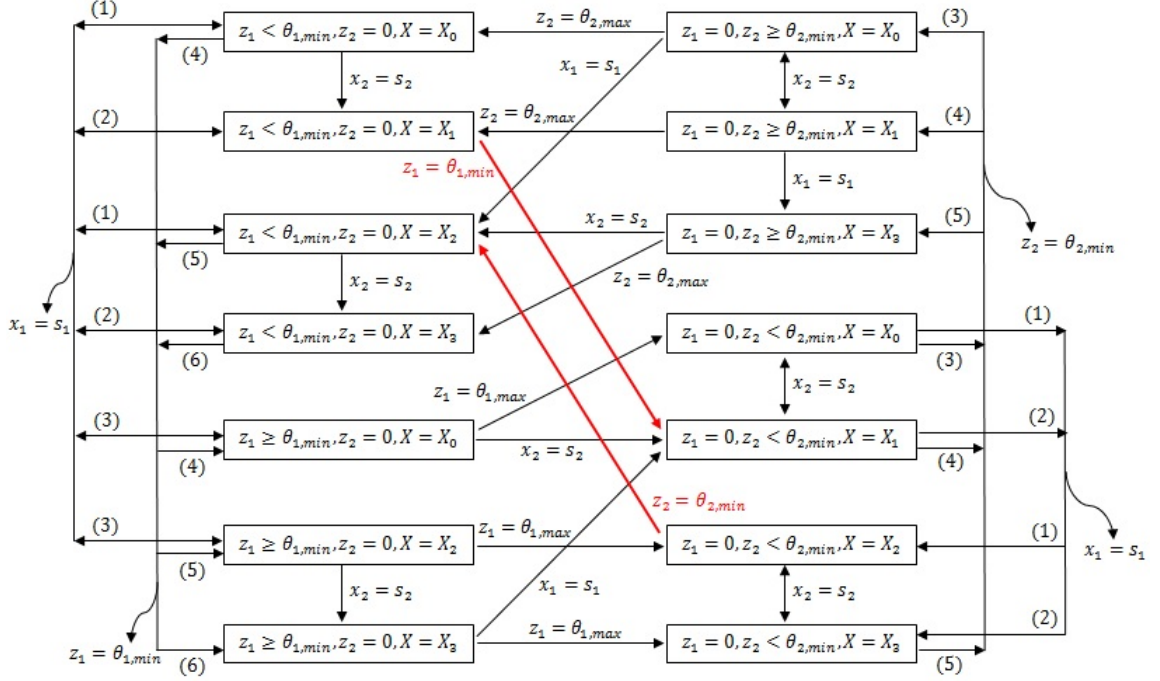


**Figure 3.1:** SHA under quasi-dynamic control

### 3.2 IPA for TLC with Quasi-Dynamic Light Cycles and Thresholds

For simplicity of notation, let us define the derivatives of the states  $x_n(v, t)$  and  $z_i(v, t)$  and event times  $\tau_k(v)$  with respect to  $v_i$ ,  $i = 1, \dots, 6$ , as follows:

$$x'_{n,i}(t) \equiv \frac{\partial x_n(v, t)}{\partial v_i}, \quad z'_{n,i}(t) \equiv \frac{\partial z_n(v, t)}{\partial v_i}, \quad \tau'_{k,i} \equiv \frac{\partial \tau_k(v)}{\partial v_i} \quad (3.1)$$

We have shown that  $\frac{\partial f_{n,k}(t)}{\partial x_n} = \frac{\partial f_{n,k}(t)}{\partial s_i} = 0$ ,  $n, i = 1, 2$ , so that in (A.7) we have  $\frac{d}{dt}x'(t) = 0$  for  $t \in [\tau_k, \tau_{k+1})$ . This means that the value of the state derivative of any road remains unaltered while the system is in a given discrete mode, so that (2.12)

holds. As a result, the IPA estimator here will also be given by (2.13). As in Chapter 2, we will proceed to revisit each of the event types  $(G2R_n, R2G_n, E_n, S_n)$  identified in Section 2.1 and derive the corresponding event time and state derivatives.

We will once again start by presenting a general result which applies to all light switching events  $G2R_n$  and  $R2G_n$ . Let us denote the time of occurrence of the  $j$ th light switching event by  $\sigma_j$  and define its derivative with respect to the control parameters as  $\sigma'_{j,i} \equiv \frac{\partial \sigma_j}{\partial v_i}$ ,  $i = 1, \dots, 6$ .

**Lemma 3.1** *The derivative  $\sigma'_{j,i}$ ,  $i = 1, \dots, 6$ , of light switching event times  $\sigma_j$ ,  $j = 1, 2, \dots$  with respect to the control parameters  $v_i$  satisfies:*

$$\sigma'_{j,i} = \begin{cases} \frac{1}{\alpha_n(\sigma_j)} \cdot \mathbf{1}[i = n + 4] - x'_{n,i}(\sigma_j^-) & \text{if } \zeta_n \text{ occurs at } \sigma_j \\ \frac{1}{\alpha_n(\sigma_j) - h_n(\sigma_j)} \cdot \mathbf{1}[i = n + 4] - x'_{n,i}(\sigma_j^-) & \text{if } \gamma_n \text{ occurs at } \sigma_j \\ \mathbf{1}[i = 2n - 1] + \sigma'_{j-1,i} & \text{if } \lambda_n \text{ occurs at } \sigma_j \\ \mathbf{1}[i = 2n] + \sigma'_{j-1,i} & \text{if } \mu_n \text{ occurs at } \sigma_j \\ \sigma'_{j-1,i} & \text{otherwise} \end{cases} \quad (3.2)$$

where  $\mathbf{1}[\cdot]$  is the usual indicator function.

*Proof:* See Appendix C.

Recall that, based on (A.8), the value of the state derivative at time  $\tau_k^+$  depends on the state dynamics  $f_{k-1}(\tau_k^-)$  and  $f_k(\tau_k^+)$ , as well as on the event time derivative  $\tau'_k$ . The analysis of the state dynamics at  $\tau_k^-$  and  $\tau_k^+$  in the present context is the same as the one presented in Section 2.2.1. As a result, the state derivative expressions corresponding to each event type  $(G2R_n, R2G_n, E_n, S_n)$  will again be given by (2.15)-(2.19), the only change being that now  $\tau'_k = \sigma'_{j,i}$  as given by (3.2). In a similar manner, the cost derivative expressions derived in Section 2.2.2 remain valid, so that the form of the IPA estimator is still given by (2.13). Once again, computing such

estimator requires knowledge of the time when events take place and of the value of the state derivatives, which ultimately depend on the values of the arrival and departure rates estimated at event times only. Hence, it is simple to implement an algorithm for updating the value of  $\frac{dL(v)}{dv_i}$  after each observed event. We will thus proceed to present results obtained by applying this methodology to a simulated urban setting.

### 3.3 Simulation Results

In what follows, we detail how an IPA-driven gradient based optimization technique can be used to simultaneously control the light cycle lengths and the queue content thresholds for an isolated traffic light intersection, which is modeled as a DES. Two sets of simulations were performed: one in which the same initial light cycle length/threshold setting was used for different traffic intensities, and another in which different starting points were used for certain values of traffic intensity.

In all our simulations, we assume that the vehicle arrival process is Poisson with rate  $\bar{\alpha}_n, n = 1, 2$ , and approximate the departure rate by a constant value  $h_n(t) = H$  when road  $n$  is non-empty, which amounts to considering that the speed with which vehicles cross an intersection depends only on the behavior of the vehicles themselves. We nevertheless note that our methodology applies independently of the distribution chosen to represent the arrival and departure processes. We estimate the values of the arrival rate at event times as  $\alpha_n(\tau_k) = N_a/t_w$ , where  $N_a$  corresponds to the number of vehicle arrivals during a time window of size  $t_w$  around  $\tau_k$ . Simulations of the intersection modeled as a pure DES are thus run to generate sample path data to

which the IPA estimator is applied. In all results reported here, we set  $H = 1$ ,  $w_n = 1$ ,  $n = 1, 2$ , and measure the sample path length in terms of the number of observed light switches, which we choose to be  $N = 5000$ .

In our first set of simulations, the initial configuration was chosen to be  $\theta_0 = [15, 30, 15, 30]$  and  $s_0 = [10, 10]$ . Table 3.1 presents the optimization results associated with different traffic intensities (denoted by  $1/\bar{\alpha}$ ), where  $\theta_{IPA}^*$  and  $\mathbf{s}_{IPA}^*$  denote the optimal light cycle lengths and threshold values, respectively, and  $J_{IPA}^*$  is the cost associated with the optimal configuration. We also include here a comparison of the results generated by our methodology with those obtained when static control, as defined in (Geng and Cassandras, 2012), is applied to determine the optimal cycle lengths. The cost reduction with respect to the static approach (labeled  $R$ ) for different traffic intensities is shown in Table 3.1, and sample convergence plots of the cost  $J$ , the light cycles  $\theta$ , and the queue content thresholds  $\mathbf{s}$  are presented in Figure 3.2. The left plot of Figure 3.2 shows the average cost, which in this work corresponds to the weighted mean of the queue length of both roads, while the middle and right plots display the convergence behavior of green phase lengths and threshold values, respectively.

**Table 3.1:** Optimization results for different traffic intensities

$1/\bar{\alpha}$	$\theta_{IPA}^*$	$\mathbf{s}_{IPA}^*$	$J_{IPA}^*$	$R(\%)$
[1.7, 3]	[12.3, 39.9, 12, 27.3]	[4.1, 8.2]	12.9	46
[1.8, 3]	[12.8, 30.8, 10, 29.9]	[3.6, 4.1]	10	47
[1.9, 3]	[14.4, 30, 11.2, 29.9]	[5.4, 6.6]	8.9	47
[2, 3]	[13.3, 29.9, 10, 30]	[3.8, 4.4]	7.7	47
[2.2, 2.7]	[14.5, 30, 12.8, 30]	[6.3, 6.9]	8.5	57
[2, 6]	[15, 31.5, 12.1, 29.9]	[5.7, 9.9]	5.6	48

The results presented in Chapter 2 served to establish the advantage of quasi-dynamically controlling the light cycle lengths and threshold values over a static IPA approach to the TLC problem. In fact, using the sequential optimization approach detailed in Section 2.3, it was possible to obtain a cost reduction of the order of 38 to 51%, i.e. the queue build-up for a system operating under sequential quasi-dynamic optimal light cycle lengths and thresholds was 38 to 51% lower than that of a system operating under static optimal light cycle lengths. As shown in Table 3.1, however, *simultaneously* optimizing both light cycle lengths and threshold values provides a cost reduction that is in most cases at least as high as the aforementioned sequential approach. Indeed, for  $1/\bar{\alpha} = [1.7, 3]$ , sequential optimization yielded a 38% cost reduction, while the simultaneous method described in this chapter allowed for a reduction of 46%, and for  $1/\bar{\alpha} = [2, 3]$  both approaches resulted in the same overall cost, which was 51% lower than the one obtained under static control. Most importantly, the present methodology *consistently* yields results in which the traffic build-up at the intersection is approximately half the size of the one under static control, unlike the sequential approach (recall, for instance, the cost reduction of 38% for the setting where  $1/\bar{\alpha} = [1.7, 3]$ ).

It is worthwhile to note that, in most of the analyzed scenarios, the value of the average cost converges much more slowly than the values of the controllable parameters. However, the purpose of this work is precisely to identify controllable parameters whereby an effective quasi-dynamic TLC may be imposed. As such, existing oscilla-

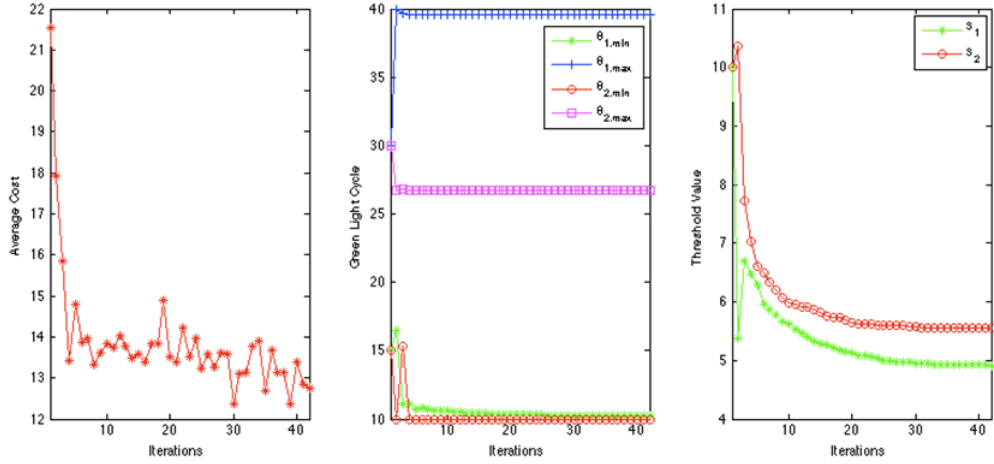


**Figure 3.2:** Sample cost and parameter trajectories for  $1/\bar{\alpha} = [1.7, 3]$

tions in the average cost value, albeit small once the green phase lengths and threshold values have converged, point to the robustness of the proposed approach. Another issue that warrants discussion is the difference in convergence time between the green phase length parameters and threshold parameters. It can be observed from Figure 3.2 that the real challenge in convergence lies with the threshold values, which represent the quasi-dynamic parameters introduced by our methodology, while the green phase lengths generally converge much faster to their optimal configuration.

In our second set of simulations, we analyze convergence results in light of the existence of local minima, and three different traffic intensity settings are contemplated. Table 3.2 summarizes the results obtained when different initial configurations ( $\theta_{init}$  and  $\mathbf{s}_{init}$  values) are used, and also displays information on the resulting cost reduction with respect to the static approach (labeled  $R$ ). It comes as no surprise that local minima exist throughout the six-dimensional cost surface of this system, imply-



ing that the optimal configuration to which the algorithm converges may depend on the starting point. More interestingly, however, is the fact that, for any given traffic intensity, this approach is able to consistently achieve a cost reduction of the order of 50% across different optimal configurations.

**Table 3.2:** Convergence results for different initial configurations

	Initial configuration		Optimal configuration			
$1/\bar{\alpha}$	$\theta_{init}$	$\mathbf{s}_{init}$	$\theta_{opt}^*$	$\mathbf{s}_{opt}^*$	$J_{opt}^*$	$R(\%)$
[1.7, 3]	[15, 30, 15, 30]	[10, 10]	[12.3, 39.9, 12, 27.3]	[4.1, 8.2]	12.9	46
	[10, 20, 10, 20]	[5, 5]	[10, 39.9, 10.9, 19.3]	[2.3, 6.1]	12.6	47
	[10, 20, 10, 30]	[10, 5]	[10, 39.9, 11.2, 28.9]	[5.7, 8.3]	12.7	47
[1.8, 3]	[15, 30, 15, 30]	[10, 10]	[12.8, 30.8, 10, 29.9]	[3.6, 4.1]	10	47
	[10, 20, 10, 20]	[5, 5]	[10, 23, 10, 18.8]	[4.6, 5.1]	10.2	49
	[10, 20, 10, 30]	[10, 5]	[10.5, 33.4, 10.5, 27.9]	[5.3, 7.0]	10.5	45
[1.9, 3]	[15, 30, 15, 30]	[10, 10]	[14.4, 30, 11.2, 29.9]	[5.4, 6.6]	8.9	47
	[10, 20, 10, 20]	[5, 5]	[10, 21.9, 10, 19.5]	[3.6, 4.7]	8.6	49
	[10, 20, 10, 30]	[10, 5]	[11, 26.3, 10, 28.3]	[4.6, 5.8]	8.7	48

An example of the simulated traffic flow variation is given in Figure 3-3, where the queue content on both roads is shown as a function of the simulation time. For ease of visualization, the entire sample path length in between updates of the controllable parameters is not shown in Figure 3-3. Nevertheless, it is possible to note that the queue lengths on both roads become increasingly bounded as the simulation progresses. This indicates that, as the algorithm converges to the optimal phase length and threshold settings, the number of vehicles on each road tends to oscillate within tighter bounds, whose values are directly related to the optimal threshold values determined for each road.

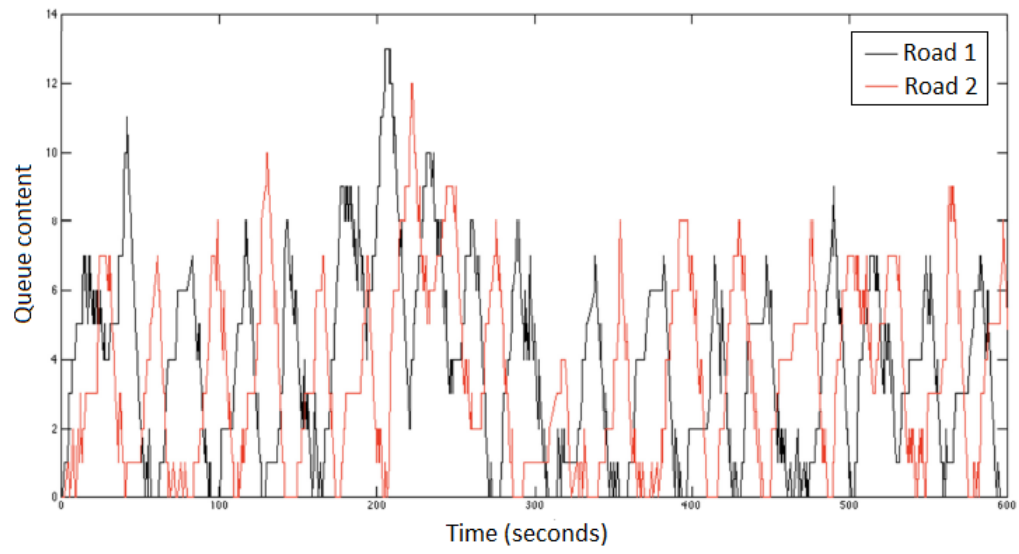


**Figure 3.3:** Simulated traffic flow variation for  $1/\bar{\alpha} = [2.2, 2.7]$

## Chapter 4

# Integrating Genomic Data to Infer Cancer Progression

In this chapter, we propose a novel formulation for integrating somatic mutation and gene expression data to infer the temporal sequence of events from cross-sectional data. Existing methods for identifying cancer specific markers and therapeutic targets typically analyze genetic, transcriptomics, proteomics or epigenetic data in search of common patterns. One of the biggest challenges in biomarker discovery is the heterogeneity of cancer data. Specific patterns discovered in one study often fail to validate in other studies or different data sets. The heterogeneity observed in clinical data may be due to

- (i) Limitations associated with the platforms used for generating molecular data (e.g., sequencing, microarray, etc.), since batch effects are commonly observed between different platforms or protocols;
- (ii) Limitations associated with existing cancer data sets, which are currently predominantly cross-sectional. This means that one time point measurements are generated for all patients, although such measurements may not necessarily be the most informative ones. In fact, certain genes dynamically change expres-

sion levels during the cell cycle, so that one time point measurements of gene expression may not capture the steady state expression level;

- (iii) Imperfections of clinical diagnosis and the ensuing difficulty in assessing the stage of each patient's tumor. As a result, clinical samples may not always be properly annotated;
- (iv) The reduced sample size with respect to the large number of measured features (genes or other molecules), which decreases the statistical power of the majority of commonly used approaches for biomarker discovery and patient stratification;
- (v) The heterogeneity of cancer mechanisms, which may also dynamically change during cancer progression.

In light of this, much of the research currently undertaken using cross-sectional data aims at determining whether the order in which genetic alterations occur within tumors follows common progression paths. Although not all patients with the same type of cancer harbor the exact same set of genetic abnormalities, there seems to be at least a subset of such changes that are consistent across a set of patients. This suggests that several combinations of mutations and gene expression patterns may lead to similar changes in cancer initiation and progression mechanisms such as apoptosis, differentiation, migration, and proliferation. In other words, different molecular patterns may contribute to cancer growth and proliferation in a similar way, i.e., through the deregulation of similar cellular mechanisms.

Much effort has recently been undertaken to collect, organize and make publicly available multiple data types obtained from genetic analysis of tumor samples. A case in point is the research developed by the The Cancer Genome Atlas (TCGA) Network, whereby different types of cancer have been profiled, such as breast invasive carcinoma (The Cancer Genome Atlas Research Network, 2012c), lung adenocarcinoma (The Cancer Genome Atlas Research Network, 2014), lung squamous carcinoma (The Cancer Genome Atlas Research Network, 2012a), colon cancer (The Cancer Genome Atlas Research Network, 2012b), among others.

Existing data sets of cross-sectional data have been extensively used to derive temporal models capable of inferring sequences of mutational events and/or sequences of affected pathways responsible for driving cancer progression. In (Gerstung et al., 2011), Bayesian networks constructed using mutation data were used to infer the temporal order of genetic mutations. The concept of probability raising was applied to copy number variation (CNV) data to infer causal models of cancer progression in (Loohuis et al., 2014). The model derived in (Michor et al., 2004) provided a quantitative understanding of the dynamics of tumorigenesis with respect to mutation, selection, genetic instability, and tissue architecture. The authors in (Beerenwinkel et al., 2007) developed a model of somatic evolution of colorectal cancer based on published data and used it to investigate the effect of different parameters on tumor evolution on a global scale, while those in (Dingli et al., 2007) suggested that stochastic dynamics alone might be responsible for either remission or rapid growth

of tumors in the hematopoietic system.

The importance of connecting different types of genomic alterations (as opposed to a single type of genomic data) was recognized in (Vaske et al., 2010) and (Ng et al., 2012), where probabilistic inference was used to predict the degree to which the activity of a pathway was altered in a given patient. For this purpose, each gene was modeled as a set of interconnected variables associated with expression, CNV and protein levels, and *a priori* information of molecular pathways was used to define the gene groups of interest and model the gene interactions.

Additional studies (Huzarski et al., 2014), (Nicolini et al., 2007), (Ahrendt et al., 2003) have established a correlation between certain mutations and survival rates, thus revealing the genetic heterogeneity of cancer and the existence of multiple subtypes. Another example is the prognostic role of BRCA1 mutation in patients with triple-negative breast cancer (Maksimenko et al., 2013).

Thus far, most attempts at reconstructing tumor progression at the pathway level have considered only known, *a priori* defined, pathways. The problem of simultaneously inferring the order of genetic mutation occurrence from somatic mutation cross-sectional data was formulated as an Integer Linear Program (ILP) in (Raphael and Vandin, 2015). Unlike existing work, our approach neither correlates a single type of cross-sectional data (e.g., mutation, gene expression, etc.) with cancer prognosis, nor analyzes these different types of data separately to combine the resulting analyses *post-factum*. Instead we combine the information from somatic mutations and gene

expression data using mathematical techniques and develop a model capable of inferring the chronological sequence of alterations at the genome as well as at the pathway level. Furthermore, our inference model is not restricted to *a priori* defined cellular pathways, but is also able to identify such pathways and the sequence in which these become altered during tumor evolution. Of note, our approach is general and easily applicable to various types of cancer; in what follows, we analyze breast cancer data as a case study.

#### 4.1 Problem Formulation

The problem of partitioning mutational events into a temporal sequence of events was formulated in (Raphael and Vandin, 2015) as an Integer Linear Program (ILP), in which an optimal partition must satisfy two biologically meaningful requirements. The first, termed *exclusivity of mutations*, derives from the common assumption that at most one driver mutation takes place during each step (or *phase*) of cancer progression. The second one establishes *progression across phases* by enforcing that, for any given patient, a mutation in some gene must take place in a given progression *phase* in order for another gene to become mutated in a subsequent *phase*. The existence of passenger mutations, false positives and false negatives in mutation detection, among other factors, may lead to the violation of these requirements. Therefore, in order to enforce both exclusivity and progression, changes may need to be made to the original mutation data set.

Our work extends the model in (Raphael and Vandin, 2015) by adding the in-

teraction between somatic mutations and gene expression. We propose a new Mixed Integer Linear Program (MILP) formulation which identifies the order in which mutations appear and produce changes of gene expression. In our approach, a *phase of cancer progression* is defined by both a group of *mutation genes* and a group of *expression genes*. We hypothesize that during a cancer progression *phase*, certain mutations lead to gene expression changes in multiple genes. Moreover, gene expression changes may cause mutations and expression changes in the downstream cancer progression *phases*.

Our formulation is based on the following assumptions:

- (A1) *Exclusivity of driver mutations within each cancer progression phase.* This implies that each sample can have only one mutated gene and each gene can only be assigned to one *phase*;
- (A2) *Progression of mutations across subsequent phases,* so that each sample must have one gene mutated in the previous *phase* in order to have a mutation in a subsequent *phase*;
- (A3) *Causality relationship between mutated genes and genes with abnormal expression.* Mutations in driver genes lead to changes in expression of certain genes. Hence, if a sample has no mutated genes in a given *phase*, all genes in the expression subset of that *phase* must have normal expression;
- (A4) *The strength of the connection between expression and mutation genes deter-*



*mines the assignment of the abnormal expression genes to the corresponding phases.* This means that each expression gene is assigned to a certain *phase* based on the strength of this gene's connection to the *mutation genes* that belong to that *phase*.

Our input data consists of an  $m \times n$  binary mutation matrix  $M$ , as well as an  $m \times r$  expression matrix  $E$ , where  $m$  is the number of samples (patients) in our database,  $n$  is the number of mutation genes considered in our study, and  $r$  is the number of expression genes considered in our study. The values of the entries  $M_{ij}$  of the mutation matrix are

$$M_{ij} = \begin{cases} 1 & \text{if mutation gene } j \text{ is mutated in sample } i \\ 0 & \text{otherwise} \end{cases}$$

while the entries  $E_{ih}$  of the expression matrix correspond to the measured expression level of expression gene  $h$  for sample  $i$ . We define the *connectivity* between mutation gene  $j$  and expression gene  $h$  to be the product between the mutation status of gene  $j$  and the expression level of gene  $h$ , compounded across all samples. Hence, we construct an  $r \times n$  real-valued connectivity matrix  $C \equiv E^T \cdot M$ .

The value of entry  $C_{hj}$  of the connectivity matrix can be interpreted as follows: values closer to zero indicate that most samples exhibit small absolute values of expression levels for gene  $h$  and/or have no mutation in gene  $j$ ; conversely, the further away the value of  $C_{hj}$  is from zero, the stronger is the connectivity between expression gene  $h$  and mutation gene  $j$  across the data set.

It is thus clear that a stronger connectivity is obtained when  $|E_{ih}| \gg \frac{1}{m} \sum_{i=1}^m E_{ih}$  and  $M_{ij} = 1$  for  $i = 1, \dots, m$  and  $\forall$  pair  $(h, j)$  of expression and mutation genes. Note that, in what concerns the expression levels, this condition implies that the most under/over expressed genes yield higher connectivity scores. This in turn points to the relevance of preprocessing matrix  $E$  so as to identify abnormally low/high  $E_{ih}$  values. Such task can be easily accomplished through outlier detection techniques. While outliers are typically associated with erroneous data, in this case values of  $E_{ih}$  that deviate markedly from the mean expression level are particularly relevant. Indeed, our ultimate goal is to infer sequences of abnormal cellular behavior that lead to cancer progression, which means that we are interested in analyzing genes that exhibit mutations and/or abnormal expression levels. As a result, we performed a percentile analysis for each expression gene  $h$ ,  $h = 1, \dots, r$  and considered entry  $E_{ih}$  to be over (under, respectively) expressed if it belonged to the 99<sup>th</sup> (1<sup>st</sup>, respectively) percentile of gene  $h$ . As a final preprocessing step, we modified the values of all entries  $E_{ih}$  so as to generate a binary expression matrix, where the value of 1 indicated that sample  $i$  belonged to either the 1<sup>st</sup> or 99<sup>th</sup> percentile of gene  $h$ , and the value of zero indicated otherwise.

In this context, the problem of inferring a model of cancer progression can be cast as that of finding a partition of the  $n$  columns of matrix  $M$  into  $K$  mutation *phases* and a partition of the  $r$  columns of matrix  $E$  into  $K$  expression *phases*. We address the role of the number of *phases*  $K$  in a subsequent discussion, but note that

the value of  $K$  is externally selected and varies depending on the desired number of *phases*. Intuitively,  $K$  reflects the level of abstraction of the model: a large (small, respectively) value of  $K$  corresponds to a microscopic (macroscopic, respectively) model. However, for the problem we consider here, it is not reasonable to assume that a microscopic model is necessarily superior to a macroscopic one, hence the need to vary the value of  $K$  and scrutinize the corresponding results. In this context, our problem can be formulated as the following MILP:

$$\min \left[ \frac{1-W}{m \cdot n} \sum_{i=1}^m \sum_{k=1}^K \left( \sum_{j=1}^n M_{i,j} p_{j,k}^M - a_{i,k}^M + 2f_{i,k}^M \right) - \frac{W}{K \cdot r} \sum_{k=1}^K \sum_{h=1}^r p_{h,k}^E \right] \quad (\text{P1})$$

$$s.t. \quad \sum_{k=1}^K p_{j,k}^M = 1 \quad \forall \text{ mutation gene } j \quad (C1)$$

$$\sum_{k=1}^K p_{h,k}^E \geq 0 \quad \forall \text{ expression gene } h \quad (C2)$$

$$\sum_{j=1}^n p_{j,k}^M \geq 1 \quad \forall \text{ phase } k \quad (C3)$$

$$\sum_{h=1}^r p_{h,k}^E \geq 0 \quad \forall \text{ phase } k \quad (C4)$$

$$a_{i,k}^M \geq a_{i,k+1}^M \quad \forall \text{ sample } i, \forall \text{ phase } k \quad (C5)$$

$$a_{i,k}^M \leq f_{i,k}^M + \sum_{j=1}^n M_{i,j} \cdot p_{j,k}^M \quad \forall \text{ sample } i, \forall \text{ phase } k \quad (C6)$$

$$p_{h,k}^E = \sum_{j=1}^n C_{h,j} \cdot p_{j,k}^M \quad \forall \text{ expression gene } h, \forall \text{ phase } k \quad (C7)$$

where the optimization is performed over variables  $p_{j,k}^M$ ,  $f_{i,k}^M$ , and  $a_{i,k}^M$ , which all take values in  $\{0, 1\}$  such that  $p_{j,k}^M = 1$  if mutation gene  $j$  is assigned to *phase*  $P_k$ ;  $f_{i,k}^M = 1$  if we need to flip one entry of columns in *phase*  $k$  in order for *phase*  $k$  to be mutated in sample  $i$ ;  $a_{i,k}^M = 1$  if sample  $i$  is considered mutated in *phase*  $k$  after any required flips. We also optimize over variable  $p_{h,k}^E \in [0, 1]$ , which is the probability of expression gene  $h$  being assigned to *phase*  $k$ .

The objective function in (P1) contains two terms, the first of which was proposed in (Raphael and Vandin, 2015). As mentioned previously, several factors may lead

to the violation of constraints (C1) – (C6), which means that it may be necessary to alter the mutation matrix  $M$  by flipping some of its entries from 0 to 1 (non-mutated to mutated) or 1 to 0 (mutated to non-mutated). In this context, the first term of the objective function corresponds to the number of entries of matrix  $M$  that need to be flipped, which should be minimized. This term can be interpreted as follows: for a given sample  $i$ ,  $i = 1, \dots, m$  and *phase*  $k$ ,  $k = 1, \dots, K$ , once the values of variables  $p_{j,k}^M$ ,  $f_{i,k}^M$ , and  $a_{i,k}^M$  have been fixed, the contribution of each sample  $i$  to the objective function corresponds to the number of entries in *phase*  $k$  that are flipped in sample  $i$ . Since two types of flips are possible (i.e.,  $f_{i,k}^M = 1$  if either a 0 to 1 flip or a 1 to 0 flip is performed), this number is given by  $\sum_{j=1}^n M_{i,j} p_{j,k}^M - a_{i,k}^M + 2f_{i,k}^M$ . The second term of the objective function, which we seek to maximize, compounds the probability of expression gene  $h$  being assigned to *phase*  $k$ , for  $h = 1, \dots, r$  and  $k = 1, \dots, K$ .

Note that because we define our objective function as a combination of objectives, it is necessary to ensure that each objective (i.e., each term of the objective function) is properly normalized. For each term, a normalization factor was defined as an upper bound on the corresponding objective component. It is simple to verify that, for the first term, the upper bound on the number of flips that could potentially need to be made corresponds to the total number of elements in matrix  $M$ , which is given by the product  $m \cdot n$ . In the case of the second term, since  $p_{h,k}^E$  is compounded across all expression genes and all *phases*, the natural normalization factor is simply given by the product  $r \cdot K$ . Recall that we define variable  $p_{h,k}^E$  as the probability of expression

gene  $h$  being assigned to *phase*  $k$ , so that it is also necessary to scale its value to the range  $[0, 1]$ . From (C7), it can be seen that variable  $p_{h,k}^E$  is a combination of matrix  $C$  and binary variable  $p_{j,k}^M$ . The latter is naturally normalized, and the entries  $C_{hj}$  of the former can be scaled as follows, for  $h = 1, \dots, r$ :

$$C_{hj} = \frac{C_{hj}}{\sum_{j=1}^n C_{h,j}}$$

Additionally, it can be seen that (P1) includes a weight  $W$  associated with the second objective component. In order to ensure that the objective function is a convex combination of objectives, we associate a weight  $1 - W$  with the first term. It is also important to mention that these weights are not necessary for the purposes of normalization, but that their values can be chosen so as to ultimately reflect a desired trade-off (e.g., more importance can be assigned to the mutation data by setting  $W < 0.5$ , and vice-versa for the gene expression data).

Finally, we briefly discuss the interpretation of constraints (C1) – (C7). The first constraint ensures that each mutation gene is assigned to exactly one cancer progression *phase*, while constraint (C2) enforces the assignment of each expression gene to at least one cancer progression *phase*. Moreover, any *phase* must consist of at least one mutated gene, but may have no expression genes assigned to it (constraints (C3) and (C4), respectively). Progression of mutational events is ensured in the fifth constraint, whereby sample  $i$  must have a certain mutated gene assigned to *phase*  $k$ , in order for this same sample to have another mutated gene assigned to *phase*

$k + 1$ . Constraint (C6) simply enforces the fact that, if sample  $i$  has a given mutated gene  $j$  assigned to *phase*  $k$ , then this gene is either already mutated in the original mutation matrix  $M$ , or its mutation status is a result of a  $0 \rightarrow 1$  mutation flip. The last constraint ensures that the assignment of each expression gene  $h$  to any *phase*  $k$  is determined in terms of the corresponding probability  $p_{h,k}^E$ .

We end by noting that, while exclusivity of driver mutations within each cancer progression *phase* is enforced in our formulation, exclusivity of changes in expression levels is not. As a result, for any given sample  $i$ , more than one expression gene  $h$  may be assigned to *phase*  $k$ . Nevertheless, our formulation enforces a temporal association between mutational events and changes in gene expression. In other words, for any given sample  $i$ , no expression genes may be assigned to *phase*  $k$ , unless a given mutation gene  $j$  has been assigned to this *phase*. For illustrative purposes, an example of a feasible solution for the proposed MILP is presented in Figure 4.1.

	Phase1					Phase2					Phase3			
	Mutation			Expression		Mutation		Expression			Mutation		Expression	
	Gene1	Gene2	Gene3	Gene8	Gene9	Gene4	Gene5	Gene10	Gene11	Gene12	Gene6	Gene7	Gene13	Gene14
Sample1	Red	White	White	Orange	White	Red	White	Orange	White	Orange	Red	White	White	White
Sample2	White	Red	White	Orange	Orange	White	White	White	White	White	White	White	White	White
Sample3	Red	White	White	White	Orange	White	Red	White	White	White	White	White	White	White
Sample4	White	White	Red	Orange	White	Red	White	Orange	Orange	White	White	Red	Orange	Orange

**Figure 4.1:** Example of a feasible solution of the MILP formulation proposed in this paper. Red boxes represent genes with mutation. Orange boxes mark genes with altered gene expression levels. White boxes correspond to those entries with no mutations or no expression changes.

## 4.2 Results

In what follows we present the results obtained by applying our methodology to both simulated data and real patient data from breast cancer studies. In all cases the MILP was solved using CPLEX v12.6 with default parameters.

### 4.2.1 Simulated data

We performed an experiment using simulated data to illustrate the desired behavior of our model. For such, we used an  $m \times n$  binary simulated mutation matrix  $M^S$  and an  $r \times n$  real-valued simulated connectivity matrix  $C^S$ , where  $m$  is the number of samples in our data set,  $n$  is the number of mutation genes, and  $r$  is the number of expression genes. For simplicity, and without loss of generality, we take  $M^S$  to be the mutation matrix obtained from the TCGA breast cancer data set, where  $m = 529$  samples and  $n = 72$  mutation genes. We defer a detailed description of this data set until Section 4.2.2., since complete details of the TCGA data are not necessary at this point. The purpose of our simulation experiments is to show that our MILP model is capable of correctly extracting the information contained in mutation and gene expression data regarding which expression genes are more strongly connected to which mutation genes. Hence, we arbitrarily assigned values to the entries  $c_{hj}^S$  of matrix  $C^S$  such that  $\sum_{j=1}^n c_{hj}^S = 1$ , for  $h = 1, \dots, r$ . This condition enforces an extreme scenario in which each expression gene is only connected to a single mutation gene. Thus, the expected outcome of applying our MILP model to such data is that each expression gene should

be uniquely assigned to the same *phase* as the mutation gene to which it is connected. For simplicity, and also without loss of generality, we took  $r = 319$  expression genes, so as to make the dimensions of the simulated data compatible with those of the real data we analyze.

Three simulation runs were performed by varying the number of *phases*  $K$  such that  $K \in \{2, 3, 4\}$ , and the corresponding results are shown in Tables 4.1 - 4.3. In all cases, our results showed that expression genes were partitioned in complete agreement with the connectivity data contained in  $C^S$ . In other words, each expression gene  $h$ ,  $h = 1, \dots, r$ , was assigned to *phase*  $k$ ,  $k = 1, \dots, K$ , iff  $c_{hj}^S = 1$  and mutation gene  $j$ ,  $j = 1, \dots, n$ , was also assigned to *phase*  $k$ . For example, by analyzing Table 4.3 and the data in matrix  $C^S$ , it is possible to verify that the 101 expression genes in *phase*  $k = 1$  are precisely the same ones that are connected to the mutation genes assigned to *phase* 1 (a similar analysis also holds for *phases*  $k = 2, 3, 4$ ).

**Table 4.1:** Number of mutation and expression genes assigned to each *phase* of cancer progression using simulated data for  $K=2$

Phase ( $k$ )	Number of mutation genes	Number of expression genes
1	39	175
2	33	144
<b>TOTAL</b>	<b>72</b>	<b>319</b>

**Table 4.2:** Number of mutation and expression genes assigned to each *phase* of cancer progression using simulated data for  $K=3$

Phase ( $k$ )	Number of mutation genes	Number of expression genes
1	26	117
2	25	111
3	21	91
<b>TOTAL</b>	<b>72</b>	<b>319</b>



**Table 4.3:** Number of mutation and expression genes assigned to each *phase* of cancer progression using simulated data for  $K=4$

Phase ( $k$ )	Number of mutation genes	Number of expression genes
1	22	101
2	22	99
3	19	82
4	9	37
<b>TOTAL</b>	<b>72</b>	<b>319</b>

#### 4.2.2 TCGA breast cancer data

Publicly available somatic mutation data (level 2) and gene expression data (level 3) from breast invasive carcinoma (BRCA) were downloaded from The Cancer Genome Atlas (TCGA) (Weinstein et al., 2013). The somatic mutation data was profiled for 993 subjects by Whole-Exome Sequencing on Illumina GA DNA Sequencing platform. Gene expression generated on UNC Agilent G4502A was profiled for 547 subjects (The Cancer Genome Atlas Research Network, 2012c). For our analysis, we consider 529 subjects with both types of data measurements (somatic mutations and gene expression). It is worthwhile to mention that the proposed MILP approach is general, and can thus be used to infer the sequence of events for any gene set. This thesis presents a case study in which we consider genes that are more relevant to breast cancer.

In order to determine the sequence of somatic mutation and gene expression changes, we first narrow down the mutation and expression gene sets to interesting breast cancer genes. In (Raphael and Vandin, 2015) the authors consider all present mutations. However, since many somatic mutations are passenger and do not impact cancer progression, we first select those genes that are more likely to be

drivers. Moreover, some genes are known to be involved in cancer associated cell processes, such as proliferation, migration and apoptosis. We are interested to see how the expression of these genes is affected by the driver mutation and which is the temporal order of changes that occur during cancer progression.

To select the relevant cancer driver genes based on their mutation frequency, we first classify genes into oncogenes or tumor suppressors by using the *20/20 rule* (Vogelstein et al., 2013). This method takes into account particular types of mutations and their frequencies. First, for a given gene, the total number of variants is computed across the data set. Then, each gene is assigned an oncogene (ONG) score and a tumor suppressor gene (TSG) score which are computed based on the frequency of gain-of-function or loss-of-function mutations, respectively. Gain-of-function mutations are defined as missense or in-frame indels that are recurrently mutated at the same aminoacid position, while loss-of-function mutations are nonstop, nonsense and frameshift indels (Vogelstein et al., 2013). For each gene, the ONG score is the frequency of gain-of-function mutations out of the total number of variants, while the TSG score is the frequency of all loss-of-function mutations out of the total number of variants. If the ONG score is greater than 20%, then the gene is classified as an oncogene. Similarly, if the TSG score is higher than 20%, then the gene is classified as a tumor suppressor.

We consider a gene to be a potential cancer driver if it presents mutations across the data set (a minimum number of 20) and has an ONG or a TSG score greater than

20%. Based on this criterion, 72 genes are selected. The list of 72 genes include genes that were previously found to be highly mutated in breast cancer, such as: PIK3CA, PTEN, TP53, GATA3, CDH1, RB1, MLL3, MAP3K1, TBX3, RUNX1, CBFB, NF1 (The Cancer Genome Atlas Research Network, 2012c) .

To infer the *cancer progression phases* of gene expression changes we consider the *Pathways in Cancer* set from the Kyoto Encyclopedia of Genes and Genomes database (KEGG) (Kanehisa et al., 2014), (Kanehisa and Goto, 2000). After overlapping this set with our data, we obtain 319 genes which are known to play a role in cancer initiation and progression. Therefore, we consider two sets of genes: genes that present driver mutations and genes implicated in cancer development.

In order to infer the stages in which mutations occur and the relations between mutational events and gene expression changes, we applied the proposed MILP formulation with a different number of predefined *phases*  $K = 2, 3, 4, 5$  and selected the most biologically meaningful one. For a number of 3 *phases*, the algorithm was able to stratify the mutation and expression genes in different proportions within each *phase*. For  $K = 2, 4, 5$ , most of the expression genes were placed in one *phase* and the results do not reflect a gradual progression. Figures 4.2(a),(b), 4.3(a),(b), 4.4(a),(b), and 4.5(a),(b) illustrate the number of genes assigned to each *phase* for the expression and mutation groups.

For a number of 3 *phases*, the mutation genes are more or less evenly distributed across the 3 *phases* (Figure 4.3(a)). The mutation genes of each *phase* are shown

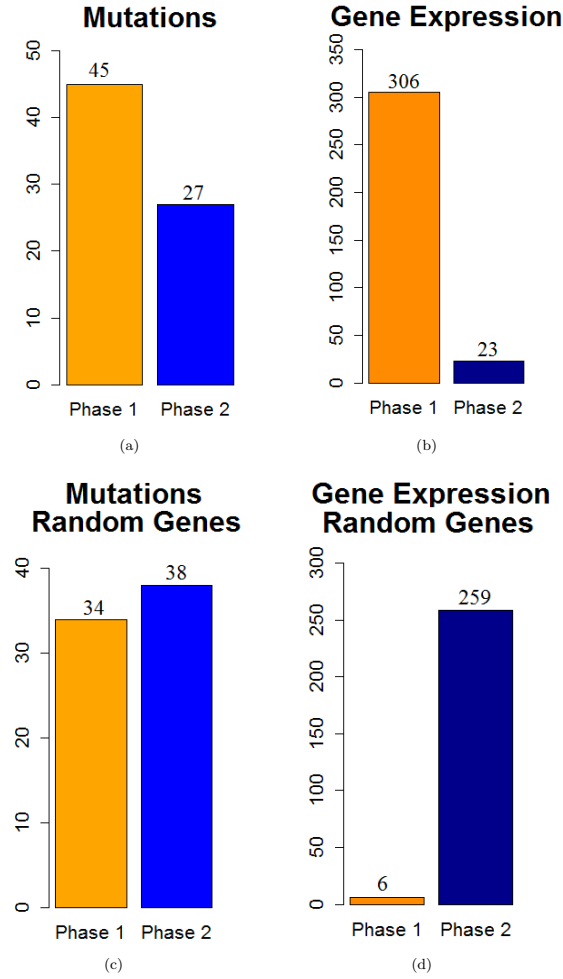


**Figure 4-2:** Number of genes assigned to each *phase of cancer progression* for  $K = 2$  (a) cancer mutation genes; (b) cancer expression genes; (c) random mutation genes; (d) random expression genes: 20% of genes were not assigned to any *phase*.

in Figure 4-6. In addition, one can notice that the number of gene expression modifications gradually decrease from *phase 1* to *phase 3* (Figure 4-3(b)). As expected, more cancer genes present abnormal expression under the influence of earlier stage mutations, such as PIK3CA and PTEN, since these genes are important in cancer

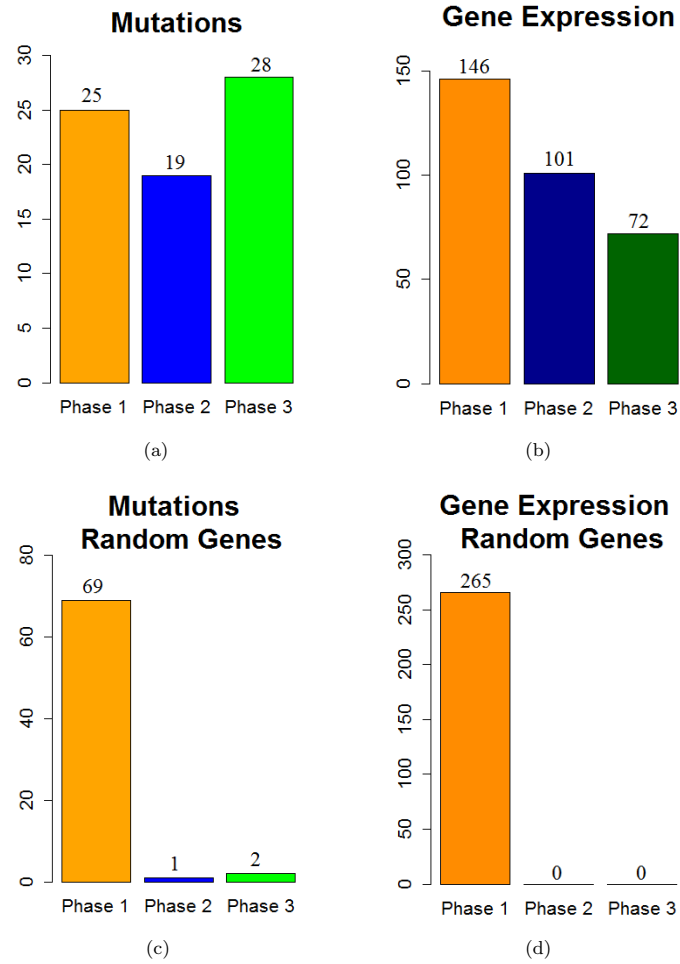


**Figure 4.3:** Number of genes assigned to each *phase of cancer progression* for  $K = 3$  (a) cancer mutation genes; (b) cancer expression genes; (c) random mutation genes; (d) random expression genes: 20% of genes were not assigned to any *phase*.

initiation.

In an additional set of simulations, we further validate our results by running similar experiments of different number of *phases*, on the same number of arbitrarily selected genes, both for mutation and expression sets (Figures 4.2(c),(d), 4.3(c),(d),

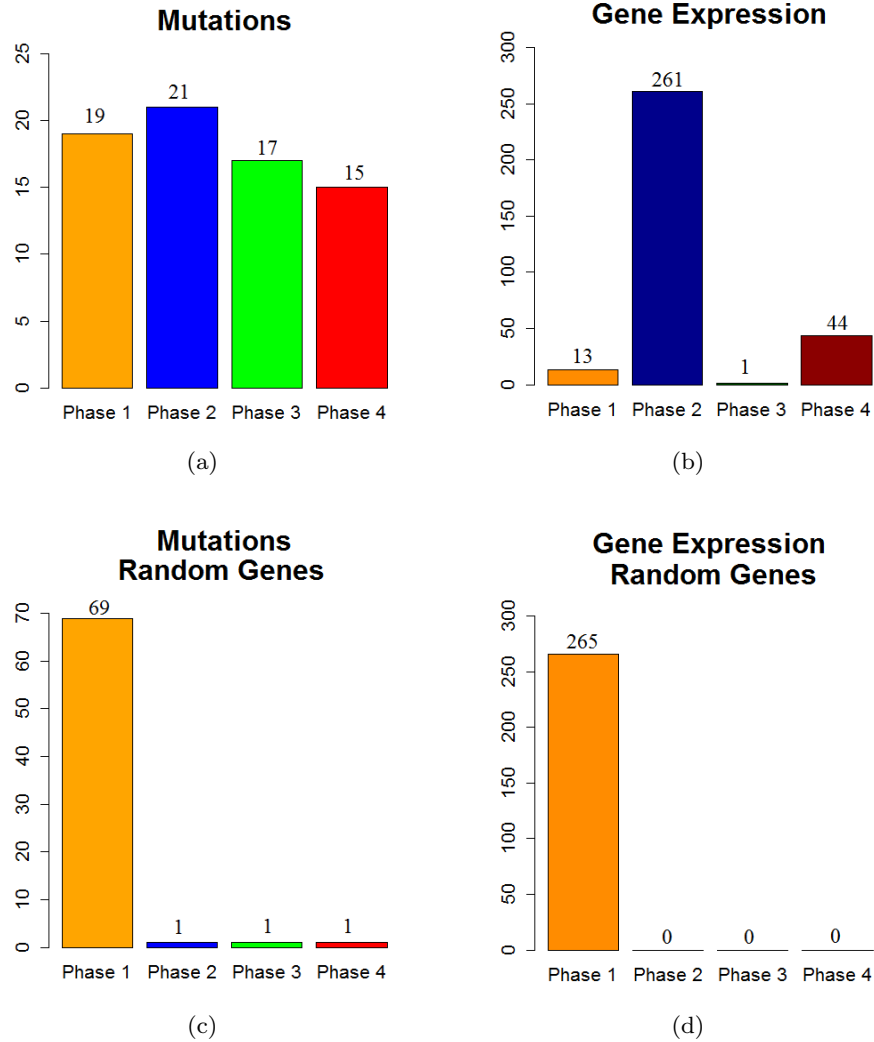


**Figure 4.4:** Number of genes assigned to each *phase of cancer progression* for  $K = 4$  (a) cancer mutation genes; (b) cancer expression genes; (c) random mutation genes; (d) random expression genes: 20% of genes were not assigned to any *phase*.

4.4(c),(d), and 4.5(c),(d)). To ensure that these experiments will serve as a negative control, we randomly select genes from the entire data set of 17814 mutation and expression genes. As expected, in this set of simulations the MILP assigns most

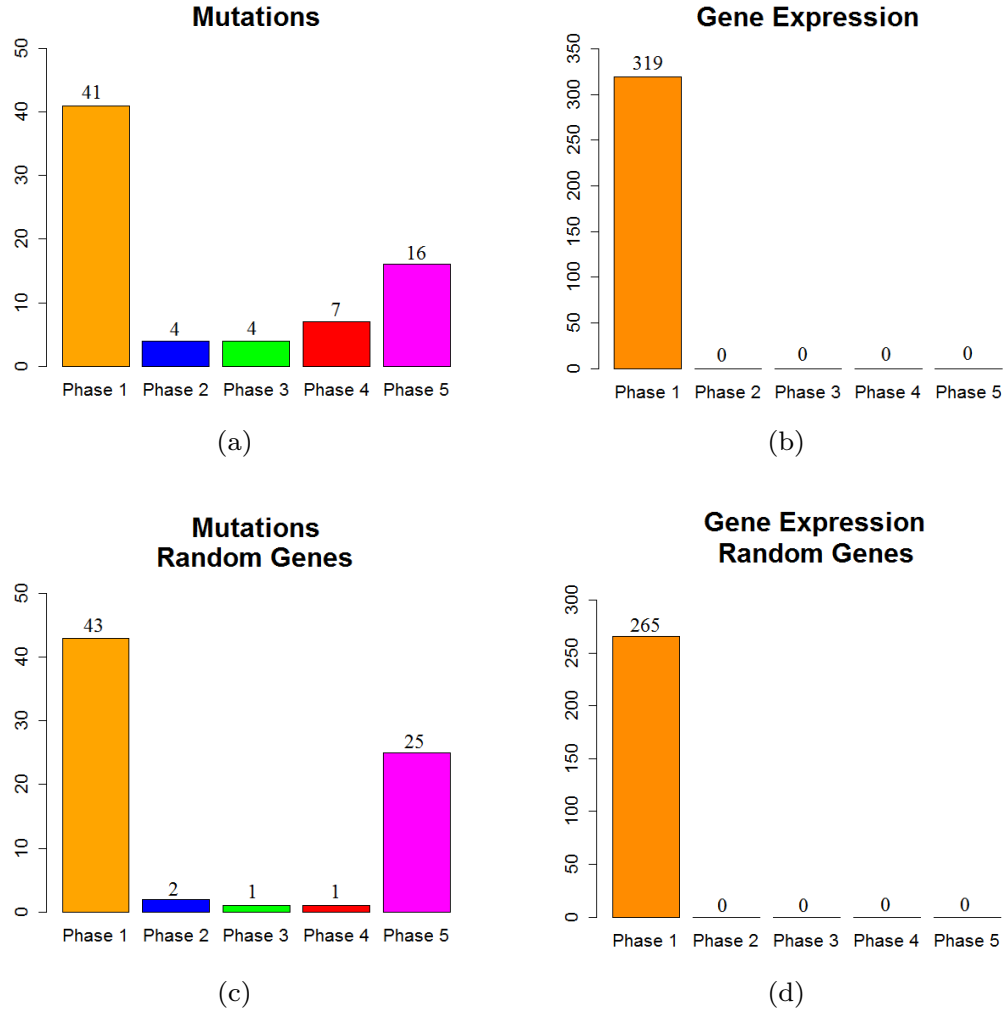


**Figure 4.5:** Number of genes assigned to each *phase of cancer progression* for  $K = 5$  (a) cancer mutation genes; (b) cancer expression genes; (c) random mutation genes; (d) random expression genes: 20% of genes were not assigned to any *phase*.

of the genes to one *phase*, not being able to find a temporal sequence of events. In addition, 20% of the expression genes are not assigned to any *phase*. Figures 4.3(c),(d) illustrate the random results for  $K=3$  *phases* using random gene sets. The difference

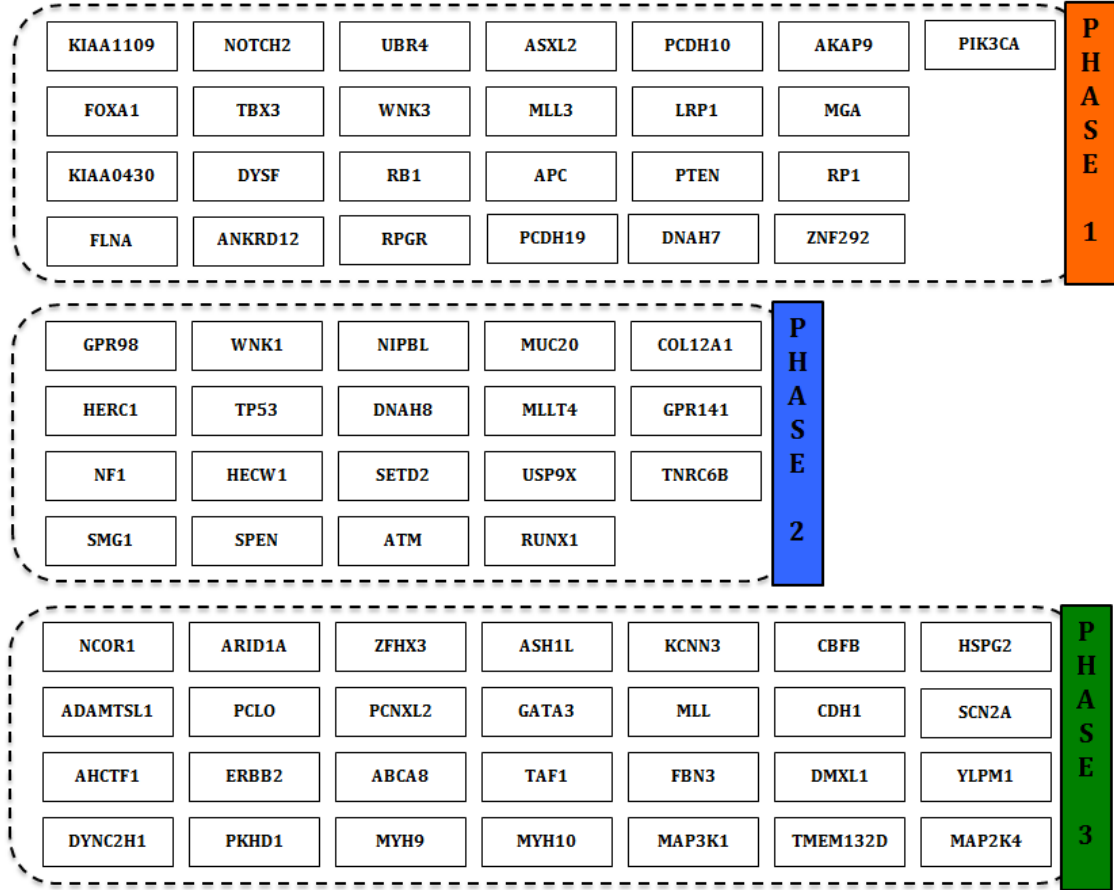


**Figure 4-6:** Optimal solution of the MILP algorithm for cancer mutation and expression genes ( $K=3$ ). Shown here is the assignment of mutation genes to each *phase of cancer progression*.

between the progression of cancer genes compared to random genes can be easily verified upon visual comparison of Figures 4-3(a),(b) and Figures 4-3(c),(d).

It is worthwhile to mention that the most adequate value for  $K$  will most likely change when different cancer data sets or gene sets are used. Hence, selection of the best configuration should take into account not only which configuration yields the most biologically meaningful results, but also how much this configuration differs from the negative control. In this context, comparing the results generated using the



genes of interest with those from a randomly selected set of genes could serve as a general approach for selecting  $K$ . This approach could be broadly applied to any cancer data set, provided it is used in combination with biological insight about the analyzed set of genes.

Additionally, for any given *phase* of mutation and expression genes, a patient has one and only one mutated gene during each *phase* which is associated to one or more genes with abnormal gene expression level, which clearly indicates that our method is able to stratify the heterogeneity of mutations and gene expression changes into a temporal order of events. This crucial observation points to the contribution of this work, but it also brings to light the issue of uniqueness of solution of the proposed MILP formulation, which we briefly address here. Note that the existence of a single optimal solution to our problem indicates that it is possible to find a unique configuration of *phases* that optimally satisfies our formulation. On the other hand, the lack of a unique optimum means that several equivalent solutions could potentially be identified, and that different configurations of *phases* could yield similar results. More importantly, either scenario (unique or multiple optimal solutions) may bring new insights for understanding the mechanisms of cancer development. In what follows, we discuss the insights provided by the results reported in this work.

We begin by evaluating the proposed partition so as to identify known causal gene relationships from cancer pathways, such as PI3K/AKT and TP53 from KEGG (Kanehisa and Goto, 2000). Figure 4.7(a) shows such interactions which occur in

*phase 1*. PIK3CA is an oncogenic driver which is highly mutated in breast cancer (the ONG score computed based on the method in (Vogelstein et al., 2013) is 90% compared to a TSG score of 0.5%). Also, PTEN gene presents significant loss-of-function mutations (the TSG score is 51% compared to an ONG score of 5%). We find PIK3CA and PTEN as being mutated in early stage during *phase 1*. Also, the events in *phase 1* produce abnormal gene expression changes of TP53. TP53 is a well known tumor suppressor (Hollstein and Hainaut, 2010), (Payne and Kemp, 2005), (Vassilev et al., 2004), situated downstream PIK3CA and PTEN in PI3K/AKT pathway. Mutations in PIK3CA or PTEN genes may decrease the gene expression level of TP53 tumor suppressor through AKT/MDM2 cascade. Consequently, low expression of TP53 may induce cell survival (Figure 4.7(a)).

Next, we evaluate the number of patients that present a potentially active PI3K/AKT pathway. We find 20% of patients to have mutations in PIK3CA, as well as decreased TP53 expression. In addition, about 2% of patients present PTEN mutations, as well as decreased TP53 expression (Figure 4.7(a)). In order to estimate if a gene is over- or under-expressed, we compare the log normalized gene expression to 0, where negative values indicate under-expression in respect to the normal level, while positive values indicate over-expression in respect to the normal level.

Moreover, we identify changes in TP53 pathway during *phase 2* of progression, as shown in Figure 4.7(b). Mutations in TP53 gene generally produce the loss-of-function of its tumor suppressor activity (Payne and Kemp, 2005). Loss-of-function

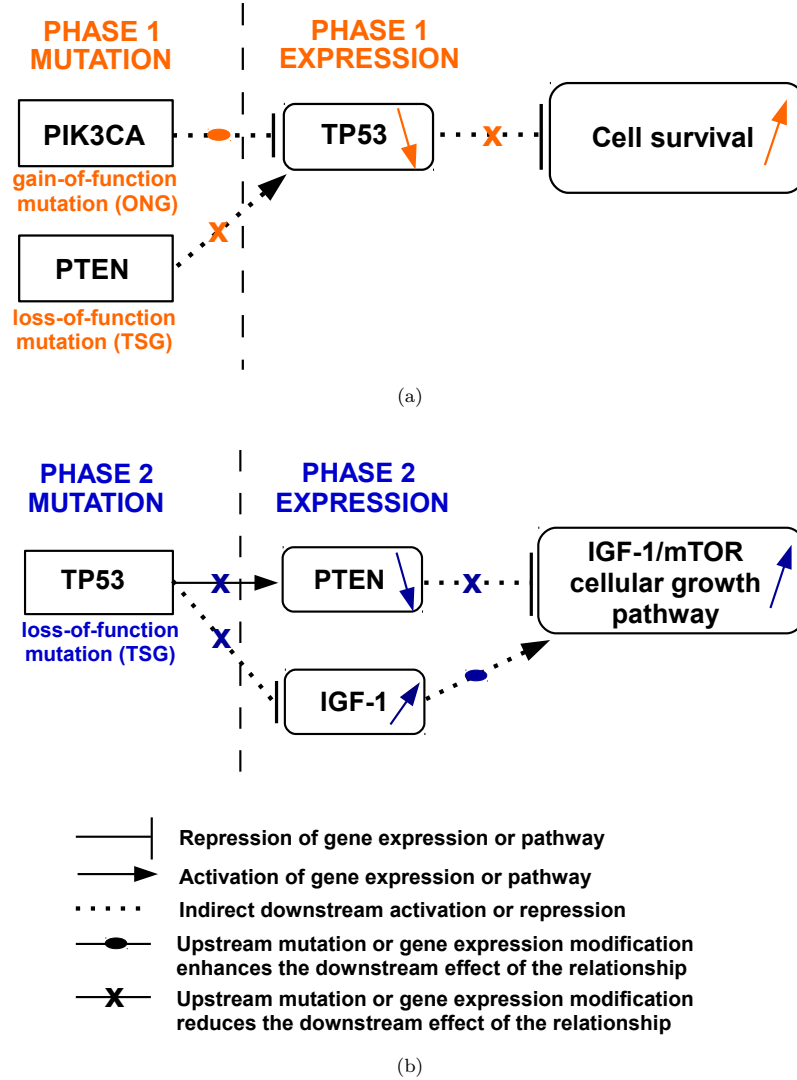


**Figure 4-7:** MILP model identifies causal relationships from PI3K/AKT and TP53 pathways (KEGG) (a) PI3K/AKT pathway is altered in *phase 1* of breast cancer progression; (b) TP53 pathway is altered in *phase 2* of breast cancer progression.

of TP53 gene may cause abnormal gene expression levels of the downstream genes, such as PTEN and IGF-1, which may activate the IGF1-mTOR cellular growth pathway and inhibit apoptosis. As expected, PTEN and IGF-1 are assigned to *phase 2*

*expression genes* of the proposed 3-*phase* partition. We find 29% of patients to have a mutation in TP53 gene and increased IGF-1 expression. Moreover, 6% of patients present a TP53 mutation, as well as both increased IGF-1 expression and decreased PTEN expression (Figure 4.7(b)).

Interestingly, about 5% of patients present mechanisms of both PI3K/AKT and TP53 pathways. They have a mutation in PIK3CA gene and decreased TP53 expression (Figure 4.7(a)). In addition, they present mutations in TP53 gene and increased IGF-1 expression (Figure 4.7(b)). Based on our approach, we are able to infer that mutations in PIK3CA (*phase 1*) precede the mutations in TP53 (*phase 2*).

## Chapter 5

# Personalized Cancer Therapy Design

In this chapter, we present a framework for Infinitesimal Perturbation Analysis (IPA) applications to personalized cancer therapy design which is illustrated with a case study of optimal prostate cancer therapy design. Prostate cancer is known to be a multistep process. For instance, a patient diagnosed with localized prostate cancer who has had all the tumor surgically removed is considered to remain in the state of “localized disease” until he progresses to a new state. At each state, distinct therapies can be prescribed, and the time spent by the patient in any given state is a measure of the efficacy of the corresponding intervention.

The primary treatments for patients with localized prostate cancer are surgery, radiation therapy, or active surveillance (Longo et al., 2012), which can be used alone or in combination. For patients who evolve into a state of metastatic disease, standard treatment is hormone therapy in the form of continuous androgen suppression (CAS) (Longo et al., 2012). The initial response to CAS is frequently positive, leading to a significant decrease in tumor size; unfortunately, most patients eventually develop resistance and relapse. A generally acceptable mechanism for explaining such relapse is the existence of an androgen-independent cancer cell phenotype that is resistant to

secondary endocrine therapy and whose outgrowth leads to tumor recurrence (Jackson, 2004a).

Intermittent androgen suppression (IAS) therapy is an alternative treatment strategy for delaying or even preventing time to relapse. The goal of IAS is to prevent the existing tumor from progressing into an androgen-independent state. In spite of extensive recent clinical experience with IAS, the design of an ideal protocol for any given patient remains one of the main challenges associated with effectively implementing this therapy (Hirata et al., 2010a). Although clinical trials (Bruchovsky et al., 2006), (Bruchovsky et al., 2007) revealed that the success of IAS ultimately depends on the ability to tailor on and off-treatment schemes to individual patients, defining optimal personalized IAS treatment schemes remains an unsolved problem.

A number of mathematical models have been proposed to explain the progression of prostate cancer in patients who are submitted to hormone therapy. (Jackson, 2004a) proposed a model in which prostate tumors are composed of two subpopulations of cancer cells, one that is sensitive to androgen suppression and another that is not, without directly addressing the issue of IAS therapy design. (Ideta et al., 2008) modeled the evolution of a prostate tumor under IAS using a hybrid dynamical system approach and applied numerical bifurcation analysis to study the effect of different therapy protocols on tumor growth and time to relapse. Various works that extend (Jackson, 2004a) and (Ideta et al., 2008) have recently been developed, and we briefly review some of them. (Shimada and Aihara, 2008) developed a nonlinear

model to explain the competition between different cancer cell subpopulations, while (Tao et al., 2010) proposed a model based on switched ordinary differential equations. (Suzuki et al., 2010) developed a piecewise affine system model and formulated the problem of personalized prostate cancer treatment as an optimal control problem. (Hirata et al., 2010a) performed patient classification using a feedback control system to model the prostate tumor under IAS, and (Hirata et al., 2010b) extended this work by deriving conditions for patient relapse.

Although the majority of existing models provide insights into the dynamics of prostate cancer evolution under androgen deprivation therapy, they fail to address the issue of therapy design. Moreover, previous works that suggest optimal treatment schemes by classifying patients into groups have been based on more manageable, albeit less accurate, approaches to nonlinear hybrid dynamical systems. Addressing this limitation, a nonlinear hybrid automaton model was recently developed and  $\delta$ -reachability analysis was performed to identify patient-specific treatment schemes in (Liu et al., 2015). In spite of being in good agreement with published clinical data, this model does not account for noise and fluctuations inherently associated with cell population dynamics and monitoring of clinical data. In contrast, a hybrid model of tumor growth under IAS therapy that incorporates stochastic effects is proposed in (Tanaka et al., 2010), but is not used for personalized therapy design.

In what follows, we propose a threshold-based policy for optimal IAS therapy design that is parameterized by lower and upper threshold values and is associated

with a cost metric that combines clinically relevant measures of therapy success. We use a Stochastic Hybrid Automaton (SHA) model of prostate cancer evolution under IAS and apply IPA to adaptively adjust threshold values so as to improve therapy outcomes. We also apply this methodology to clinical data from real patients, and obtain promising results and valuable insights for personalized IAS therapy design.

## 5.1 Problem Formulation

### 5.1.1 Stochastic Model of Prostate Cancer Evolution

The system we consider comprises a prostate tumor under IAS therapy, which is modeled as a Stochastic Hybrid Automaton (SHA). We adopt a standard SHA definition (Cassandras and Lafortune, 2008), as detailed in Appendix A. Within this framework, we define a SHA model of prostate cancer progression in terms of the following:

1. *Discrete state set  $Q$ .* Hormone therapy for prostate cancer consists of administering medical agents that cause androgen suppression in an effort to decrease the population of prostate cancer cells and hence the size of the tumor. A common biomarker used to monitor the efficacy of such treatment is the serum level of Prostate-Specific Antigen (PSA), whose value provides an estimate of the size of the prostate cancer population.

In IAS therapy, medication is suspended when a sufficient reduction in the size of the cancer cell populations is achieved. Since population sizes are not directly observable, this reduction is estimated in terms of the patient’s PSA level; hence, the patient goes off therapy once his PSA reaches a lower threshold value. Similarly,



medication is reinstated once the cancer cell populations have significantly recovered, which corresponds to when the patient's PSA level reaches an upper threshold value. Thus, we define  $Q = \{q^{ON}, q^{OFF}\}$ , where  $q^{ON}$  ( $q^{OFF}$ , respectively) is the on-treatment (off-treatment, respectively) operational mode of the system.

2. *State space  $X$ .* The continuous state space  $X$  is defined in terms of the biomarkers commonly monitored during IAS therapy, namely the PSA level and the androgen concentration in the patient's serum. We assume the coexistence of two subpopulations of cancer cells within the tumor: Hormone Sensitive Cells (HSCs) and Castration Resistant Cells (CRCs). The proliferation of the former is negatively affected by hormone therapy, while the survival rate of the latter decreases in androgen-rich environments.

We thus define a state vector  $x(t) = [x_1(t), x_2(t), x_3(t)]$  with  $x_i(t) \in \mathbb{R}^+$ , such that  $x_1(t)$  is the total population of HSCs,  $x_2(t)$  is the total population of CRCs, and  $x_3(t)$  is the concentration of androgen in the serum. Since prostate cancer cells secrete high levels of PSA, it is frequently assumed that the serum PSA concentration can be modeled as a linear combination of the cancer cell subpopulations, i.e.,  $c_1x_1(t) + c_2x_2(t)$ . Another common assumption is that both HSCs and CRCs secrete PSA equivalently, so that  $c_1 = c_2 = 1$  (Ideta et al., 2008). In this work, we adopt these assumptions. We also define a “clock” state variable  $z_i(t) \in \mathbb{R}^+$ ,  $i = 1, 2$ , where  $z_1(t)$  ( $z_2(t)$ , respectively) measures the time spent by the system in state  $q^{ON}$  ( $q^{OFF}$ , respectively). The clock is reset to zero once a state transition takes place. Setting

$z(t) = [z_1(t), z_2(t)]$ , the complete state vector is  $[x(t), z(t)]$ .

3. *Admissible control set  $U$ .* As described earlier, IAS therapy consists of cycles of androgen deprivation delivered intermittently with off-treatment periods. The cycles of androgen deprivation are suspended when the patient's PSA level reaches a lower threshold value, while therapy recommences once the PSA level reaches an upper threshold value. Hence, an IAS therapy can be viewed as a controlled process characterized by two parameters:  $\theta = [\theta_1, \theta_2] \in \Theta$ , where  $\theta_1 \in [\theta_1^{\min}, \theta_1^{\max}]$  is the lower threshold value of the patient's PSA level, and  $\theta_2 \in [\theta_2^{\min}, \theta_2^{\max}]$  is the upper threshold value of the patient's PSA level, with  $\theta_1^{\max} < \theta_2^{\min}$ . At any time  $t$ , the feasible control set for the IAS therapy controller is  $U = \{0, 1\}$  and the control is defined as:

$$u(x(t), z(t)) \equiv \begin{cases} 0 & \text{if } x_1(t) + x_2(t) < \theta_2, q(t) = q^{OFF} \\ 1 & \text{if } x_1(t) + x_2(t) > \theta_1, q(t) = q^{ON} \end{cases} \quad (5.1)$$

This is a simple form of hysteresis control to ensure that hormone therapy will be suspended whenever a patient's PSA level drops below a minimum threshold value, and that therapy will resume whenever a patient's PSA level reaches a maximum threshold value. An illustrative representation of such threshold-based IAS therapy scheme is depicted in Figure 5-1. Simulation driven by clinical data (Bruchovsky et al., 2006),(Bruchovsky et al., 2007) was performed to generate the plot in Figure 5-1, which shows a typical profile of PSA level variations along several treatment cycles.

4. *Event set  $E$ .* We define the SHA event set as  $E = \{e_1, e_2\}$ , where  $e_1$

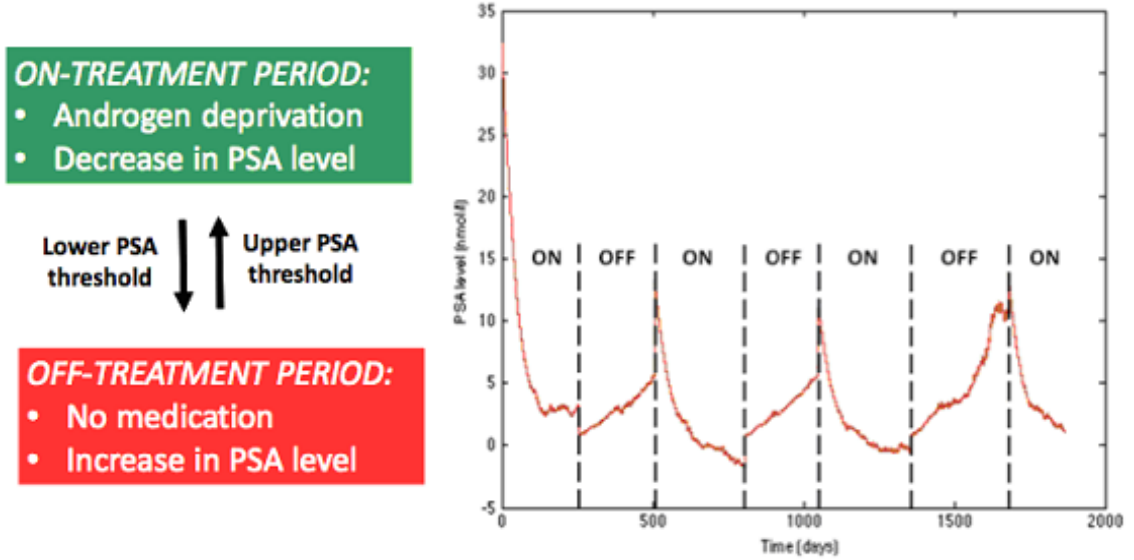


**Figure 5.1:** Schematic representation of Intermittent Androgen Suppression (IAS) therapy

corresponds to the condition  $[x_1(t) + x_2(t) = \theta_1 \text{ from above}]$  and  $e_2$  corresponds to  $[x_1(t) + x_2(t) = \theta_2 \text{ from below}]$ .

5. *System dynamics.* The SHA system dynamics describe the evolution of continuous state variables over time, as well as the rules for discrete state transitions. First, the *continuous (time-driven) dynamics* capture the prostate cancer cell population dynamics, which are defined in terms of their proliferation, apoptosis, and conversion rates. Existing studies commonly use Michaelis-Menten-like functions to model the rates of proliferation and apoptosis (Ideta et al., 2008),(Jackson, 2004a),(Jackson, 2004b). Recently (Liu et al., 2015) obtained greater consistency between clinical data and simulated population dynamics by modeling these rates using sigmoid functions. In what follows, we incorporate stochastic effects into the deterministic model from

(Liu et al., 2015) and obtain:

$$\begin{aligned}\dot{x}_1(t) &= \alpha_1 \left[1 + e^{-(x_3(t)-k_1)k_2}\right]^{-1} \cdot x_1(t) \\ &\quad - \beta_1 \left[1 + e^{-(x_3(t)-k_3)k_4}\right]^{-1} \cdot x_1(t) \\ &\quad - \left[m_1 \left(1 - \frac{x_3(t)}{x_{3,0}}\right) + \lambda_1\right] \cdot x_1(t) \\ &\quad + \mu_1 + \zeta_1(t)\end{aligned}\tag{5.2}$$

$$\begin{aligned}\dot{x}_2(t) &= \left[\alpha_2 \left(1 - d \frac{x_3(t)}{x_{3,0}}\right) - \beta_2\right] x_2(t) \\ &\quad + m_1 \left(1 - \frac{x_3(t)}{x_{3,0}}\right) x_1(t) + \zeta_2(t)\end{aligned}\tag{5.3}$$

$$\dot{x}_3(t) = \begin{cases} -\frac{x_3(t)}{\sigma} + \mu_3 + \zeta_3(t) & \text{if } x_1(t) + x_2(t) > \theta_1 \\ & \text{and } q(t) = q^{ON} \\ \frac{x_{3,0}-x_3(t)}{\sigma} + \mu_3 + \zeta_3(t) & \text{if } x_1(t) + x_2(t) < \theta_2 \\ & \text{and } q(t) = q^{OFF} \end{cases}\tag{5.4}$$

$$\dot{z}_1(t) = \begin{cases} 1 & \text{if } q(t) = q^{ON} \\ 0 & \text{otherwise} \end{cases}\tag{5.5}$$

$$z_1(t^+) = \begin{cases} 0 & \text{if } x_1(t) + x_2(t) = \theta_1 \\ & \text{and } q(t) = q^{ON} \end{cases}$$

$$\dot{z}_2(t) = \begin{cases} 1 & \text{if } q(t) = q^{OFF} \\ 0 & \text{otherwise} \end{cases}\tag{5.6}$$

$$z_2(t^+) = \begin{cases} 0 & \text{if } x_1(t) + x_2(t) = \theta_2 \\ & \text{and } q(t) = q^{OFF} \end{cases}$$

where  $\alpha_1$  and  $\alpha_2$  are the HSC proliferation constant and CRC proliferation constant, respectively;  $\beta_1$  and  $\beta_2$  are the HSC apoptosis constant and CRC apoptosis constant, respectively;  $k_1$  through  $k_4$  are HSC proliferation and apoptosis exponential constants;  $m_1$  is the HSC to CRC conversion constant;  $x_{3,0}$  corresponds to the patient-specific

androgen constant;  $\sigma$  is the androgen degradation constant;  $\lambda_1$  is the HSC basal degradation rate;  $\mu_1$  and  $\mu_3$  are the HSC basal production rate and androgen basal production rate, respectively. Finally,  $\{\zeta_i(t)\}$ ,  $i = 1, 2, 3$ , are stochastic processes which we allow to have arbitrary characteristics and only assume them to be piecewise continuous w.p. 1.

Observe that (5.2) and (5.3) seem to be independent of the discrete state (mode)  $q(t)$ ; however, their dependence on  $x_3(t)$ , whose dynamics are affected by mode transitions, implies that  $x_1(t)$ ,  $x_2(t)$  also change due to such transitions. To make this behavior explicit, we can solve (5.4) for  $x_3(t)$  and substitute this solution into (5.2) and (5.3), as detailed next.

Consider a sample path of the system over  $[0, T]$  and denote the time of occurrence of the  $k$ th event (of any type) by  $\tau_k(\theta)$ . Since our complete system state vector is  $[x(t), z(t)]$ , we shall denote the state dynamics over any interevent interval  $[\tau_k(\theta), \tau_{k+1}(\theta))$  as follows:

$$\dot{x}_n(t) = f_k^{x_n}(t), \dot{z}_i(t) = f_k^{z_i}(t), n = 1, \dots, 3, i = 1, 2$$

Although we include  $\theta$  as an argument in the expressions above to stress the dependence on the controllable parameter, we will subsequently drop this for ease of notation as long as no confusion arises.

We start our analysis by assuming  $q(t) = q^{ON}$  for  $t \in [\tau_k, \tau_{k+1})$ . It is clear from

(5.4) that  $\dot{x}_3(t) = -\frac{x_3(t)}{\sigma} + \mu_3 + \zeta_3(t)$ , which implies that, for  $t \in [\tau_k, \tau_{k+1})$ ,

$$\begin{aligned} x_3(t) &= x_3(\tau_k^+) e^{-(t-\tau_k)/\sigma} \\ &\quad + e^{-t/\sigma} \cdot \int_{\tau_k}^t e^{\varepsilon/\sigma} [\mu_3 + \zeta_3(\varepsilon)] d\varepsilon \end{aligned}$$

For notational simplicity, let

$$\tilde{\zeta}_3(t) = \int_{\tau_k}^t e^{-(t-\varepsilon)/\sigma} \zeta_3(\varepsilon) d\varepsilon \quad (5.7)$$

and define, for  $t \in [\tau_k, \tau_{k+1})$ ,

$$\begin{aligned} h^{ON} \left( t, \tilde{\zeta}_3(t) \right) &\equiv x_3(\tau_k^+) e^{-(t-\tau_k)/\sigma} \\ &\quad + \mu_3 \sigma [1 - e^{-(t-\tau_k)/\sigma}] + \tilde{\zeta}_3(t) \end{aligned} \quad (5.8)$$

Now let  $q(t) = q^{OFF}$  for  $t \in [\tau_k, \tau_{k+1})$ , so that (5.4) implies that, for  $t \in [\tau_k, \tau_{k+1})$ ,

$$\begin{aligned} x_3(t) &= x_3(\tau_k^+) e^{-(t-\tau_k)/\sigma} \\ &\quad + (\mu_3 \sigma + x_{3,0}) [1 - e^{-(t-\tau_k)/\sigma}] + \tilde{\zeta}_3(t) \end{aligned}$$

Similarly as above, we define, for  $t \in [\tau_k, \tau_{k+1})$ ,

$$\begin{aligned} h^{OFF} \left( t, \tilde{\zeta}_3(t) \right) &\equiv x_3(\tau_k^+) e^{-(t-\tau_k)/\sigma} \\ &\quad + (\mu_3 \sigma + x_{3,0}) [1 - e^{-(t-\tau_k)/\sigma}] + \tilde{\zeta}_3(t) \end{aligned} \quad (5.9)$$

It is thus clear that

$$x_3(t) = \begin{cases} h^{ON} \left( t, \tilde{\zeta}_3(t) \right) & \text{if } q(t) = q^{ON} \\ h^{OFF} \left( t, \tilde{\zeta}_3(t) \right) & \text{if } q(t) = q^{OFF} \end{cases}$$

Although we include  $\tilde{\zeta}_3(t)$  as an argument in (5.8)-(5.9) to stress the dependence on the stochastic process, we will subsequently drop this for ease of notation as long as no confusion arises. It is now clear that, by using (5.8)-(5.9) in (5.2)-(5.3), we may

rewrite the state variable dynamics as

$$\dot{x}_1(t) = \begin{cases} \left\{ \alpha_1 [1 + \phi_\alpha^{ON}(t)]^{-1} - \beta_1 [1 + \phi_\beta^{ON}(t)]^{-1} \right. \\ \left. + m_1 \left( \frac{h^{ON}(t)}{x_{3,0}} \right) - (m_1 + \lambda_1) \right\} \cdot x_1(t) \\ + \mu_1 + \zeta_1(t) & \text{if } q(t) = q^{ON} \\ \left\{ \alpha_1 [1 + \phi_\alpha^{OFF}(t)]^{-1} - \beta_1 [1 + \phi_\beta^{OFF}(t)]^{-1} \right. \\ \left. + m_1 \left( \frac{h^{OFF}(t)}{x_{3,0}} \right) - (m_1 + \lambda_1) \right\} \cdot x_1(t) \\ + \mu_1 + \zeta_1(t) & \text{if } q(t) = q^{OFF} \end{cases} \quad (5.10)$$

and

$$\dot{x}_2(t) = \begin{cases} \left[ \alpha_2 \left( 1 - d \frac{h^{ON}(t)}{x_{3,0}} \right) - \beta_2 \right] x_2(t) \\ + m_1 \left( 1 - \frac{h^{ON}(t)}{x_{3,0}} \right) x_1(t) + \zeta_2(t) & \text{if } q(t) = q^{ON} \\ \left[ \alpha_2 \left( 1 - d \frac{h^{OFF}(t)}{x_{3,0}} \right) - \beta_2 \right] x_2(t) \\ + m_1 \left( 1 - \frac{h^{OFF}(t)}{x_{3,0}} \right) x_1(t) + \zeta_2(t) & \text{if } q(t) = q^{OFF} \end{cases} \quad (5.11)$$

with

$$\phi_\alpha^{ON}(t) = e^{-(h^{ON}(t)-k_1)k_2}$$

$$\phi_\beta^{ON}(t) = e^{-(h^{ON}(t)-k_3)k_4}$$

$$\phi_\alpha^{OFF}(t) = e^{-(h^{OFF}(t)-k_1)k_2}$$

$$\phi_\beta^{OFF}(t) = e^{-(h^{OFF}(t)-k_3)k_4}$$

The *discrete (event-driven) dynamics* are dictated by the occurrence of events that cause state transitions. Based on the event set  $E = \{e_1, e_2\}$  we have defined, the occurrence of  $e_1$  results in a transition from  $q^{ON}$  to  $q^{OFF}$  and the occurrence of  $e_2$  results in a transition from  $q^{OFF}$  to  $q^{ON}$ . The corresponding SHA model of prostate

cancer evolution under IAS therapy is shown in Figure 5.2.

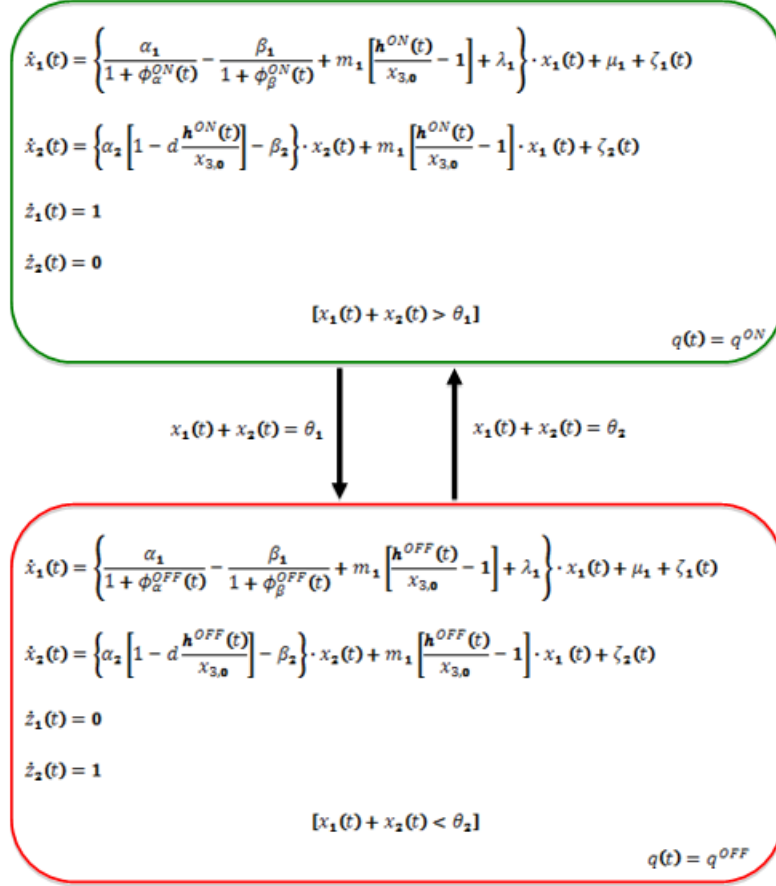


**Figure 5.2:** Stochastic Hybrid Automaton model of prostate cancer evolution under IAS therapy

### 5.1.2 IAS Therapy Evaluation and Optimization

Within the SHA framework we propose, the problem of personalizing an IAS treatment scheme can be cast as the search for the optimal IAS therapy that satisfies some performance criterion. In this sense, an IAS therapy can be viewed as a controlled process  $u(\theta, t)$  characterized by the parameter vector  $\theta$ , as in (5.1), whose effect can be quantified in terms of performance metrics of the form  $J[u(\theta, t)]$ . Although it is



clearly infeasible to evaluate  $J[u(\theta, t)]$  over all possible values of  $\theta$ , there exist very efficient ways to accomplish this goal for stochastic hybrid systems. In particular, Perturbation Analysis (PA) is a methodology to efficiently estimate the sensitivity of the system's performance with respect to  $\theta$  (note that when  $\theta$  is a real-valued scalar, this amounts to estimating the derivative  $dJ/d\theta$ ). This is accomplished by extracting data from a sample path (simulated or actual) of the observed system based on which an unbiased estimate of  $dJ/d\theta$  can indeed be obtained. The attractive feature of PA is that the resulting estimates are extracted from a *single* sample path in a non-intrusive manner and the computational cost of doing so is, in most cases of interest, minimal (Cassandras and Lafortune, 2008). This is in contrast to the conventional finite difference estimate of  $dJ/d\theta$  obtained through  $[J(\theta + \Delta) - J(\theta)]/\Delta$ . Thus, for a vector  $\theta$  of dimension  $N$ , estimating the gradient  $\nabla J(\theta)$  requires a single sample path (with some overhead) instead of  $N + 1$  sample paths. The simplest family of PA estimators is Infinitesimal Perturbation Analysis (IPA), which has been shown to provide *unbiased* gradient estimates (Cassandras et al., 2010) for virtually arbitrary stochastic hybrid systems. For the SHA model of prostate cancer evolution we consider here, our goal is to estimate the effects of different therapies  $u(\theta, t)$  by adapting IPA estimators of the form  $dJ[u(\theta, t)]/d\theta$ , and to ultimately design optimal therapy schemes by solving problems of the form  $\min_{\theta \in \Theta} J[u(\theta, t)]$ .

We define a sample function in terms of complementary measures of therapy success. In particular, we consider the most adequate IAS treatment schemes to be those

that (i) ensure PSA levels are kept as low as possible; (ii) reduce the frequency of on and off-treatment cycles. From a practical perspective, (i) translates into the ability to successfully keep the size of cancer cell populations under control, which is directly influenced by the duration of the on and off-treatment periods. On the other hand, (ii) aims at reducing the duration of on-treatment periods, thus decreasing the exposure of patients to medication and their side effects, and consequently improving the patients' quality of life throughout the treatment. Clearly there is a trade-off between keeping tumor growth under control and the cost associated with the corresponding IAS therapy. The latter is related to the duration of the therapy and could potentially include fixed set up costs incurred when therapy is reinstated. For simplicity, we disconsider fixed set up costs and take (ii) to be linearly proportional to the length of the on-treatment cycles. Hence, we define our sample function as the sum of the average PSA level and the average duration of an on-treatment cycle over a fixed time interval  $[0, T]$ . We also take into account that it may be desirable to design a therapy scheme which favors (i) over (ii) (or vice-versa) and thus associate weight  $W$  with (i) and  $1 - W$  with (ii), where  $0 \leq W \leq 1$ . Finally, to ensure that the trade-off between (i) and (ii) is captured appropriately, we normalize our sample function: we divide (i) by the value of the patient's PSA level at the start of the first on-treatment cycle ( $PSA_{init}$ ), and normalize (ii) by  $T$ .

Recall that the total population size of prostate cancer cells is assumed to reflect the serum PSA concentration, and that we have defined clock variables which measure

the time elapsed in each of the treatment modes, so that our sample function can be written as

$$L(\theta, x(0), z(0), T) = \frac{1}{T} \left[ W \int_0^T \left[ \frac{x_1(\theta, t) + x_2(\theta, t)}{PSA_{init}} \right] dt + (1 - W) \int_0^T \frac{z_1(t)}{T} dt \right] \quad (5.12)$$

where  $x(0)$  and  $z(0)$  are given initial conditions. We can then define the overall performance metric as

$$J(\theta, x(0), z(0), T) = E[L(\theta, x(0), z(0), T)] \quad (5.13)$$

Hence, the problem of determining the optimal IAS therapy can be formulated as

$$\min_{\theta \in \Theta} E[L(\theta, x(0), z(0), T)] \quad (5.14)$$

We note that it is not possible to derive a closed-form expression of  $J(\theta, x(0), z(0), T)$  without imposing limitations on the processes  $\{\zeta_i(t)\}$ ,  $i = 1, \dots, 3$ . Nevertheless, by assuming only that  $\zeta_i(t)$ ,  $i = 1, \dots, 3$ , are piecewise continuous w.p. 1, we can successfully apply the IPA methodology developed for general SHS in (Cassandras et al., 2010) and obtain an estimate of  $\nabla J(\theta)$  by evaluating the sample gradient  $\nabla L(\theta)$ . The knowledge of such gradient values can then be used to improve current operating conditions or to compute an optimal  $\theta^*$  through an iterative optimization algorithm of the form

$$\theta_{i,k+1} = \theta_{i,k} - \rho_k H_{i,k}(\theta_k, x(0), T, \omega_k) \quad (5.15)$$

where  $\rho_k$  is the step size at the  $k$ th iteration,  $k = 0, 1, \dots$ , and  $\omega_k$  denotes a sample path from which data are extracted and used to compute  $H_{i,k}(\theta_k, x(0), T, \omega_k)$ , which is an estimate of  $dJ(\theta)/d\theta_i$ . We will assume that the derivatives  $dL(\theta)/d\theta_i$  exist w.p. 1 for all  $\theta_i \in \mathbb{R}^+$ . It is also simple to verify that  $L(\theta)$  is Lipschitz continuous for  $\theta_i \in \mathbb{R}^+$ . We will further assume that  $\{\zeta_i(t)\}$ ,  $i = 1, \dots, 3$ , are stationary random processes over  $[0, T]$  and that no two events can occur at the same time w.p. 1. Under these conditions, it has been shown in (Cassandras et al., 2010) that  $dL(\theta)/d\theta_i$  is an *unbiased* estimator of  $dJ(\theta)/d\theta_i$ ,  $i = 1, 2$ . Hence, our goal is to compute the sample gradient  $\nabla L(\theta)$  using data extracted from a sample path of the system (e.g., by simulating a sample path of our SHA model using clinical data), and use this value as an estimate of  $\nabla J(\theta)$ .

## 5.2 IPA for the SHA Model of Prostate Cancer Evolution

For simplicity of notation, let us define the derivatives of the states  $x_n(\theta, t)$  and  $z_j(\theta, t)$  and event times  $\tau_k(\theta)$  with respect to  $\theta_i$ ,  $i = 1, 2$ ,  $n = 1, \dots, 3$ , as follows:

$$x'_{n,i}(t) \equiv \frac{\partial x_n(\theta, t)}{\partial \theta_i}, \quad z'_{j,i}(t) \equiv \frac{\partial z_j(\theta, t)}{\partial \theta_i}, \quad \tau'_{k,i} \equiv \frac{\partial \tau_k(\theta)}{\partial \theta_i} \quad (5.16)$$

In what follows, we derive the IPA state and event time derivatives for the events identified in our SHA model of prostate cancer progression.

### 5.2.1 State and Event Time Derivatives

For simplicity of notation, let us define the derivatives of the states  $x_n(\theta, t)$  and  $z_j(\theta, t)$  and event times  $\tau_k(\theta)$  with respect to  $\theta_i$ ,  $i = 1, 2$ ,  $n = 1, \dots, 3$ , as follows:

$$x'_{n,i}(t) \equiv \frac{\partial x_n(\theta, t)}{\partial \theta_i}, \quad z'_{j,i}(t) \equiv \frac{\partial z_j(\theta, t)}{\partial \theta_i}, \quad \tau'_{k,i} \equiv \frac{\partial \tau_k(\theta)}{\partial \theta_i} \quad (5.17)$$

We proceed by analyzing the state evolution of our SHA model of prostate cancer progression considering each of the states ( $q^{ON}$  and  $q^{OFF}$ ) and events ( $e_1$  and  $e_2$ ) therein defined.

1. *The system is in state  $q^{ON}$  over interevent time interval  $[\tau_k, \tau_{k+1})$ .* Using (A.7)

for  $x_1(t)$ , we obtain, for  $i = 1, 2$ ,

$$\begin{aligned} \frac{d}{dt} x'_{1,i}(t) &= \frac{\partial f_k^{x_1}(t)}{\partial x_1} x'_1(t) + \frac{\partial f_k^{x_1}(t)}{\partial x_2} x'_2(t) \\ &\quad + \frac{\partial f_k^{x_1}(t)}{\partial z_1} z'_1(t) + \frac{\partial f_k^{x_1}(t)}{\partial z_2} z'_2(t) + \frac{\partial f_k^{x_1}(t)}{\partial \theta_i} \end{aligned}$$

From (5.10), we have  $\frac{\partial f_k^{x_1}(t)}{\partial x_2} = \frac{\partial f_k^{x_1}(t)}{\partial z_i} = \frac{\partial f_k^{x_1}(t)}{\partial \theta_i} = 0$ ,  $i = 1, 2$ , and

$$\begin{aligned} \frac{\partial f_k^{x_1}(t)}{\partial x_1} &= \alpha_1 [1 + \phi_\alpha^{ON}(t)]^{-1} - \beta_1 [1 + \phi_\beta^{ON}(t)]^{-1} \\ &\quad - m_1 \left( 1 - \frac{h^{ON}(t)}{x_{3,0}} \right) - \lambda_1 \end{aligned}$$

It is thus simple to verify that solving (A.7) for  $x'_{1,i}(t)$  yields, for  $i = 1, 2$ ,

$$x'_{1,i}(t) = x'_{1,i}(\tau_k^+) e^{A(t)}, \quad t \in [\tau_k, \tau_{k+1}) \quad (5.18)$$

with

$$\begin{aligned} A(t) &\equiv \int_{\tau_k}^t \left[ \frac{\alpha_1}{1 + \phi_\alpha^{ON}(t)} - \frac{\beta_1}{1 + \phi_\beta^{ON}(t)} \right] dt \\ &\quad - \int_{\tau_k}^t \frac{m_1}{x_{3,0}} h^{ON}(t) dt - (m_1 + \lambda_1)(t - \tau_k) \end{aligned} \quad (5.19)$$

In particular, at  $\tau_{k+1}^-$ :

$$x'_{1,i}(\tau_{k+1}^-) = x'_{1,i}(\tau_k^+) e^{A(\tau_k)} \quad (5.20)$$

where  $A(\tau_k)$  is given from (6.5).

Similarly for  $x_2(t)$ , we have from (5.11) that  $\frac{\partial f_k^{x_2}(t)}{\partial z_i} = \frac{\partial f_k^{x_2}(t)}{\partial \theta_i} = 0$ ,  $i = 1, 2$ , and

$$\begin{aligned} \frac{\partial f_k^{x_2}(t)}{\partial x_1} &= m_1 \left( 1 - \frac{h^{ON}(t)}{x_{3,0}} \right) \\ \frac{\partial f_k^{x_2}(t)}{\partial x_2} &= \alpha_2 \left( 1 - d \frac{h^{ON}(t)}{x_{3,0}} \right) - \beta_2 \end{aligned}$$

Combining the last two equations and solving for  $x'_{2,i}(t)$  yields, for  $i = 1, 2$  and  $t \in [\tau_k, \tau_{k+1})$ ,

$$x'_{2,i}(t) = x'_{2,i}(\tau_k^+) e^{B_1(t)} + B_2(t, x'_{1,i}(\tau_k^+), A(t)) \quad (5.21)$$

with

$$\begin{aligned} B_1(t) &\equiv \int_{\tau_k}^t \left[ \alpha_2 \left( 1 - d \frac{h^{ON}(t)}{x_{3,0}} \right) - \beta_2 \right] dt \\ B_2(\cdot) &\equiv e^{B_1(t)} \int_{\tau_k}^t G_1(t, \tau_k) e^{-B_1(t)} dt \end{aligned} \quad (5.22)$$

where  $G_1(t, \tau_k) = m_1 \left( 1 - \frac{h^{ON}(t)}{x_{3,0}} \right) x'_{1,i}(\tau_k^+) e^{A(t)}$ ,  $t \in [\tau_k, \tau_{k+1})$ .

In particular, at  $\tau_{k+1}^-$ :

$$x'_{2,i}(\tau_{k+1}^-) = x'_{2,i}(\tau_k^+) e^{B_1(\tau_k)} + B_2(\tau_k, x'_{1,i}(\tau_k^+), A(\tau_k)) \quad (5.23)$$

where  $B_1(\tau_k)$  and  $B_2(\tau_k, x'_{1,i}(\tau_k^+), A(\tau_k))$  are given from (6.14).

Finally, for the “clock” state variable, from (5.5)-(5.6) we have  $\frac{\partial f_k^{z_i}(t)}{\partial x_n} = \frac{\partial f_k^{z_i}(t)}{\partial z_i} =$

$\frac{\partial f_k^{z_i}(t)}{\partial \theta_i} = 0$ ,  $n, i = 1, 2$ , so that  $\frac{d}{dt} z'_{j,i}(t) = 0$ ,  $j, i = 1, 2$ , for  $t \in [\tau_k, \tau_{k+1})$ . Hence,

$$z'_{j,i}(t) = z'_{j,i}(\tau_k^+), \quad j, i = 1, 2 \text{ and } t \in [\tau_k, \tau_{k+1}).$$

2. The system is in state  $q^{OFF}$  over interevent time interval  $[\tau_k, \tau_{k+1})$ . Starting

with  $x_1(t)$ , based on (5.10) we once again have  $\frac{\partial f_k^{x_1}(t)}{\partial x_2} = \frac{\partial f_k^{x_1}(t)}{\partial z_i} = \frac{\partial f_k^{x_1}(t)}{\partial \theta_i} = 0$ ,

$i = 1, 2$ , but now

$$\begin{aligned} \frac{\partial f_k^{x_1}(t)}{\partial x_1} &= \alpha_1 [1 + \phi_\alpha^{OFF}(t)]^{-1} - \beta_1 [1 + \phi_\beta^{OFF}(t)]^{-1} \\ &\quad - m_1 \left( 1 - \frac{h^{OFF}(t)}{x_{3,0}} \right) - \lambda_1 \end{aligned}$$

Therefore, (A.7) implies that, for  $i = 1, 2$ :

$$x'_{1,i}(t) = x'_{1,i}(\tau_k^+) e^{C(t)}, \quad t \in [\tau_k, \tau_{k+1}) \quad (5.24)$$

with

$$\begin{aligned} C(t) &\equiv \int_{\tau_k}^t \left[ \frac{\alpha_1}{1 + \phi_\alpha^{OFF}(t)} - \frac{\beta_1}{1 + \phi_\beta^{OFF}(t)} \right] dt \\ &\quad - \int_{\tau_k}^t \frac{m_1}{x_{3,0}} h^{OFF}(t) dt - (m_1 + \lambda_1)(t - \tau_k) \end{aligned} \quad (5.25)$$

In particular, at  $\tau_{k+1}^-$ :

$$x'_{1,i}(\tau_{k+1}^-) = x'_{1,i}(\tau_k^+) e^{C(\tau_k)} \quad (5.26)$$

where  $C(\tau_k)$  is given from (6.23).

Similarly for  $x_2(t)$ , we have

$$\begin{aligned} \frac{\partial f_k^{x_2}(t)}{\partial x_1} &= m_1 \left( 1 - \frac{h^{OFF}(t)}{x_{3,0}} \right) \\ \frac{\partial f_k^{x_2}(t)}{\partial x_2} &= \alpha_2 \left( 1 - d \frac{h^{OFF}(t)}{x_{3,0}} \right) - \beta_2 \end{aligned}$$

It is thus straightforward to verify that (A.7) yields, for  $i = 1, 2$  and  $t \in$

$[\tau_k, \tau_{k+1})$ ,

$$x'_{2,i}(t) = x'_{2,i}(\tau_k^+) e^{D_1(t)} + D_2(t, x'_{1,i}(\tau_k^+), C(t)) \quad (5.27)$$

with

$$D_1(t) \equiv \int_{\tau_k}^t \left[ \alpha_2 \left( 1 - d \frac{h^{OFF}(t)}{x_{3,0}} \right) - \beta_2 \right] dt \quad (5.28)$$

$$D_2(\cdot) \equiv e^{D_1(t)} \int_{\tau_k}^t G_2(t, \tau_k) e^{-D_1(t)} dt$$

where  $G_2(t, \tau_k) = m_1 \left( 1 - \frac{h^{OFF}(t)}{x_{3,0}} \right) x'_{1,i}(\tau_k^+) e^{C(t)}$ ,  $t \in [\tau_k, \tau_{k+1})$ .

In particular, at  $\tau_{k+1}^-$ :

$$x'_{2,i}(\tau_{k+1}^-) = x'_{2,i}(\tau_k^+) e^{D_1(\tau_k)} + D_2(\tau_k, x'_{1,i}(\tau_k^+), C(\tau_k)) \quad (5.29)$$

where  $D_1(\tau_k)$  and  $D_2(\tau_k, x'_{1,i}(\tau_k^+), C(\tau_k))$  are given from (6.32).

Finally, for the “clock” state variable, based on (5.5)-(5.6) we once again have

$$\frac{\partial f_k^{z_i}(t)}{\partial x_n} = \frac{\partial f_k^{z_i}(t)}{\partial z_i} = \frac{\partial f_k^{z_i}(t)}{\partial \theta_i} = 0, \quad n, i = 1, 2, \text{ so that } \frac{d}{dt} z'_{j,i}(t) = 0, \quad j, i = 1, 2, \text{ for}$$

$t \in [\tau_k, \tau_{k+1})$ . As a result,  $z'_{j,i}(t) = z'_{j,i}(\tau_k^+)$ ,  $j, i = 1, 2$  and  $t \in [\tau_k, \tau_{k+1})$ .

3. A state transition from  $q^{ON}$  to  $q^{OFF}$  occurs at time  $\tau_k$ . This necessarily implies that event  $e_1$  took place at time  $\tau_k$ , i.e.,  $q(t) = q^{ON}$ ,  $t \in [\tau_{k-1}, \tau_k)$  and  $q(t) = q^{OFF}$ ,  $t \in [\tau_k, \tau_{k+1})$ . From (A.8) we have, for  $i = 1, 2$ ,

$$x'_{1,i}(\tau_k^+) = x'_{1,i}(\tau_k^-) + [f_k^{x_1}(\tau_k^-) - f_{k+1}^{x_1}(\tau_k^+)] \cdot \tau'_{k,i} \quad (5.30)$$



and

$$x'_{2,i}(\tau_k^+) = x'_{2,i}(\tau_k^-) + [f_k^{x_2}(\tau_k^-) - f_{k+1}^{x_2}(\tau_k^+)] \cdot \tau'_{k,i} \quad (5.31)$$

where  $f_k^{x_1}(\tau_k^-) - f_{k+1}^{x_1}(\tau_k^+)$  and  $f_k^{x_2}(\tau_k^-) - f_{k+1}^{x_2}(\tau_k^+)$  ultimately depend on  $h^{ON}(\tau_k^-)$  and  $h^{OFF}(\tau_k^+)$ . Evaluating  $h^{ON}(\tau_k^-)$  from (5.8) over the appropriate time interval results in

$$\begin{aligned} h^{ON}(\tau_k^-) &= x_3(\tau_{k-1}^+) e^{-(\tau_k - \tau_{k-1})/\sigma} \\ &\quad + \mu_3 \sigma [1 - e^{-(\tau_k - \tau_{k-1})/\sigma}] + \tilde{\zeta}_3(\tau_k) \end{aligned}$$

and it follows directly from (5.9) that  $h^{OFF}(\tau_k^+) = x_3(\tau_k^+)$ . Moreover, by continuity of  $x_n(t)$  (due to conservation of mass),  $x_n(\tau_k^+) = x_n(\tau_k^-)$ ,  $n = 1, 2$ . Also, since we have assumed that  $\{\zeta_i(t)\}$ ,  $i = 1, \dots, 3$ , is piecewise continuous w.p.1 and that no two events can occur at the same time w.p.1,  $\zeta_i(\tau_k^-) = \zeta_i(\tau_k^+)$ ,  $i = 1, \dots, 3$ . Hence, for  $x_1(t)$ , evaluating  $\Delta_f^1(\tau_k) \equiv f_k^{x_1}(\tau_k^-) - f_{k+1}^{x_1}(\tau_k^+)$  yields

$$\begin{aligned} \Delta_f^1(\tau_k, \zeta_3(\tau_k)) &= \left\{ \alpha_1 [1 + \phi_\alpha^{ON}(\tau_k^-)]^{-1} \right. \\ &\quad - \alpha_1 [1 + \phi_\alpha^{OFF}(\tau_k^+)]^{-1} - \beta_1 [1 + \phi_\beta^{ON}(\tau_k^-)]^{-1} \\ &\quad + \beta_1 [1 + \phi_\beta^{OFF}(\tau_k^+)]^{-1} \\ &\quad \left. + \frac{m_1}{x_{3,0}} [h^{ON}(\tau_k^-) - x_3(\tau_k)] \right\} \cdot x_1(\tau_k) \end{aligned} \quad (5.32)$$

Finally, the term  $\tau'_{k,i}$ , which corresponds to the event time derivative with respect to  $\theta_i$  at event time  $\tau_k$ , is determined using (A.12), as detailed in (6.48) later.

A similar analysis applies to  $x_2(t)$ , so that  $f_k^{x_2}(\tau_k^-)$  and  $f_{k+1}^{x_2}(\tau_k^+)$  ultimately depend on  $h^{ON}(\tau_k^-)$  and  $h^{OFF}(\tau_k^+)$ , respectively. Hence, evaluating  $\Delta_f^2(\tau_k) \equiv$

$f_k^{x_2}(\tau_k^-) - f_{k+1}^{x_2}(\tau_k^+)$  from (5.11) yields

$$\begin{aligned} \Delta_f^2(\tau_k, \zeta_3(\tau_k)) &= \frac{\alpha_2 d}{x_{3,0}} [x_3(\tau_k) - h^{ON}(\tau_k^-)] \cdot x_2(\tau_k) \\ &\quad - \frac{m_1}{x_{3,0}} [h^{ON}(\tau_k^-) - x_3(\tau_k)] \cdot x_1(\tau_k) \end{aligned} \quad (5.33)$$

In the case of the “clock” state variable,  $z_1(t)$  is discontinuous in  $t$  at  $t = \tau_k$ , while  $z_2(t)$  is continuous. Hence, based on (A.9) and (5.5), we have that  $z'_{1,i}(\tau_k^+) = 0$ . From (A.8) and (5.6), it is straightforward to verify that  $z'_{2,i}(\tau_k^+) = z'_{2,i}(\tau_k^-) - \tau'_{k,i}$ ,  $i = 1, 2$ .

4. *A state transition from  $q^{OFF}$  to  $q^{ON}$  occurs at time  $\tau_k$ .* This necessarily implies that event  $e_2$  took place at time  $\tau_k$ , i.e.,  $q(t) = q^{OFF}$ ,  $t \in [\tau_{k-1}, \tau_k)$  and  $q(t) = q^{ON}$ ,  $t \in [\tau_k, \tau_{k+1})$ . The same reasoning as above holds, so that (6.41)-(6.42) also apply. For  $x_1(t)$ ,  $f_k^{x_1}(\tau_k^-) - f_{k+1}^{x_1}(\tau_k^+)$  can be evaluated from (5.10) and ultimately depends on  $h^{OFF}(\tau_k^-)$  and  $h^{ON}(\tau_k^+)$ . Evaluating  $h^{OFF}(\tau_k^-)$  from (5.9) over the appropriate time interval results in

$$\begin{aligned} h^{OFF}(\tau_k^-) &= x_3(\tau_{k-1}^+) e^{-(\tau_k - \tau_{k-1})/\sigma} \\ &\quad + (\mu_3 \sigma + x_{3,0}) [1 - e^{-(\tau_k - \tau_{k-1})/\sigma}] + \tilde{\zeta}_3(\tau_k) \end{aligned}$$

and it follows directly from (5.8) that  $h^{ON}(\tau_k^+) = x_3(\tau_k^+)$ .

As in the previous case, continuity due to conservation of mass applies, so that evaluating  $\Delta_f^1(\tau_k) \equiv f_k^{x_1}(\tau_k^-) - f_{k+1}^{x_1}(\tau_k^+)$  yields

$$\begin{aligned} \Delta_f^1(\tau_k, \zeta_3(\tau_k)) &= \left\{ \alpha_1 [1 + \phi_\alpha^{OFF}(\tau_k^-)]^{-1} \right. \\ &\quad - \alpha_1 [1 + \phi_\alpha^{ON}(\tau_k^+)]^{-1} - \beta_1 [1 + \phi_\beta^{OFF}(\tau_k^-)]^{-1} \\ &\quad + \beta_1 [1 + \phi_\beta^{ON}(\tau_k^+)]^{-1} \\ &\quad \left. + \frac{m_1}{x_{3,0}} [h^{OFF}(\tau_k^-) - x_3(\tau_k)] \right\} \cdot x_1(\tau_k) \end{aligned} \quad (5.34)$$

Similarly for  $x_2(t)$ , by evaluating  $\Delta_f^2(\tau_k) \equiv f_k^{x_2}(\tau_k^-) - f_{k+1}^{x_2}(\tau_k^+)$  from (5.11), and making the appropriate simplifications due to continuity, we obtain

$$\begin{aligned} \Delta_f^2(\tau_k, \zeta_3(\tau_k)) &= \frac{\alpha_2 d}{x_{3,0}} [x_3(\tau_k) - h^{OFF}(\tau_k^-)] \cdot x_2(\tau_k) \\ &\quad - \frac{m_1}{x_{3,0}} [h^{OFF}(\tau_k^-) - x_3(\tau_k)] \cdot x_1(\tau_k) \end{aligned} \quad (5.35)$$

In the case of the “clock” state variable,  $z_1(t)$  is continuous in  $t$  at  $t = \tau_k$ , while  $z_2(t)$  is discontinuous. As a result, based on (A.8) and (5.5), we have that  $z'_{1,i}(\tau_k^+) = z'_{1,i}(\tau_k^-) - \tau'_{k,i}$ . From (A.9) and (5.6), it is simple to verify that  $z'_{2,i}(\tau_k^+) = 0$ ,  $i = 1, 2$ .

Note that, since  $z'_{j,i}(t) = z'_{j,i}(\tau_k^+)$ ,  $t \in [\tau_k, \tau_{k+1})$ , we will have that  $z'_{j,i}(\tau_k^-) = z'_{j,i}(\tau_{k-1}^+)$ ,  $j, i = 1, 2$ . Moreover, the sample path of our SHA consists of a sequence of alternating  $e_1$  and  $e_2$  events, which implies that  $z'_{1,i}(\tau_k^-) = 0$  if event  $e_1$  occurred at  $\tau_{k-1}$ , while  $z'_{2,i}(\tau_k^-) = 0$  if event  $e_2$  occurred at  $\tau_{k-1}$ . Then, adopting the notation  $p, \bar{p} = \{1, 2\}$  such that  $p + \bar{p} = 3$ , we have:

$$z'_{p,i}(\tau_k^+) = \begin{cases} -\tau'_{k,i} & \text{if event } e_{\bar{p}} \text{ occurs at } \tau_k \\ 0 & \text{otherwise} \end{cases} \quad (5.36)$$

We now proceed with a general result which applies to all events defined for our SHA model. We denote the time of occurrence of the  $j$ th state transition by  $\tau_j$ , define its derivative with respect to the control parameters as  $\tau'_{j,i} \equiv \frac{\partial \tau_j}{\partial \theta_i}$ ,  $i = 1, 2$ , and also define  $f_j^{x_n}(\tau_j) \equiv \dot{x}_n(\tau_j)$ ,  $n = 1, 2$ .

**Lemma 5.1** *When an event  $e_p$ ,  $p = 1, 2$ , occurs, the derivative  $\tau'_{j,i}$ ,  $i = 1, 2$ , of state transition times  $\tau_j$ ,  $j = 1, 2, \dots$  with respect to the control parameters  $\theta_i$ ,  $i = 1, 2$ ,*

satisfies:

$$\tau'_{j,i} = \begin{cases} \frac{1-x'_{1,i}(\tau_j^-)-x'_{2,i}(\tau_j^-)}{f_{j-1}^{x_1}(\tau_j^-)+f_{j-1}^{x_2}(\tau_j^-)} & \text{if event } e_1 \text{ occurs and } i = 1 \\ & \text{or event } e_2 \text{ occurs and } i = 2 \\ \frac{-x'_{1,i}(\tau_j^-)-x'_{2,i}(\tau_j^-)}{f_{j-1}^{x_1}(\tau_j^-)+f_{j-1}^{x_2}(\tau_j^-)} & \text{if event } e_1 \text{ occurs and } i = 2 \\ & \text{or event } e_2 \text{ occurs and } i = 1 \end{cases} \quad (5.37)$$

**Proof.** See Appendix C. ■

We note that the numerator in (6.48) is determined using (6.8) and (6.17) if  $q(\tau_j^-) = q^{ON}$ , or (6.26) and (6.38) if  $q(\tau_j^-) = q^{OFF}$ . Moreover, the denominator in (6.48) is computed using (5.10)-(5.11) and it is simple to verify that, if event  $e_1$  takes place at time  $\tau_j$ ,

$$\begin{aligned} f_{j-1}^{x_1}(\tau_j^-) + f_{j-1}^{x_2}(\tau_j^-) &= \alpha_1 [1 + \phi_\alpha^{ON}(\tau_j^-)]^{-1} \cdot x_1(\tau_j) \\ &\quad - \left\{ \beta_1 [1 + \phi_\beta^{ON}(\tau_j^-)]^{-1} + \lambda_1 \right\} \cdot x_1(\tau_j) + \mu_1 \\ &\quad + \left[ \alpha_2 \left( 1 - d \frac{h^{ON}(\tau_j^-)}{x_{3,0}} \right) - \beta_2 \right] \cdot x_2(\tau_j) \\ &\quad + \zeta_1(\tau_j) + \zeta_2(\tau_j) \end{aligned} \quad (5.38)$$

and, if event  $e_2$  takes place at time  $\tau_j$ ,

$$\begin{aligned} f_{j-1}^{x_1}(\tau_j^-) + f_{j-1}^{x_2}(\tau_j^-) &= \alpha_1 [1 + \phi_\alpha^{OFF}(\tau_j^-)]^{-1} \cdot x_1(\tau_j) \\ &\quad - \left\{ \beta_1 [1 + \phi_\beta^{OFF}(\tau_j^-)]^{-1} + \lambda_1 \right\} \cdot x_1(\tau_j) + \mu_1 \\ &\quad + \left[ \alpha_2 \left( 1 - d \frac{h^{OFF}(\tau_j^-)}{x_{3,0}} \right) - \beta_2 \right] \cdot x_2(\tau_j) \\ &\quad + \zeta_1(\tau_j) + \zeta_2(\tau_j) \end{aligned} \quad (5.39)$$

We now proceed to present the expression of the cost derivative corresponding to the performance metric defined in (5.12).

### 5.2.2 Cost Derivative

Let us denote the total number of on and off-treatment periods (complete or incomplete) in  $[0, T]$  by  $K_T$ . Also let  $\xi_k$  denote the start of the  $k^{th}$  period and  $\eta_k$  denote the end of the  $k^{th}$  period (of either type). Finally, let  $M_T = \lfloor \frac{K_T}{2} \rfloor$  be the total number of complete on-treatment periods, and  $\Delta_m^{ON}$  denote the duration of the  $m^{th}$  complete on-treatment period, where clearly

$$\Delta_m^{ON} \equiv \eta_m - \xi_m, \quad m = 1, 2, \dots$$

**Theorem 5.1** *The derivative of the sample function  $L(\theta)$  with respect to the control parameters satisfies:*

$$\begin{aligned} \frac{dL(\theta)}{d\theta_i} = & \frac{W}{T} \sum_{k=1}^{K_T} \int_{\xi_k}^{\eta_k} \left[ \frac{x'_{1,i}(\theta, t) + x'_{2,i}(\theta, t)}{PSA_{init}} \right] dt \\ & + \frac{(1-W)}{T} \sum_{m=1}^{M_T} \frac{\Delta_m^{ON}}{T} \cdot (\eta'_{m,i} - \xi'_{m,i}) \\ & - \frac{(1-W)}{T} \mathbf{1}[K_T \text{ is odd}] \cdot \xi'_{M_T+1,i} \cdot \left( \frac{T - \xi_{M_T+1}}{T} \right) \end{aligned} \quad (5.40)$$

where  $\mathbf{1}[\cdot]$  is the usual indicator function and  $PSA_{init}$  is the value of the patient's PSA level at the start of the first on-treatment cycle.

**Proof.** See Appendix C. ■

It is clear that evaluating (6.51) requires knowledge of: (i) the event times  $\xi_{n,m}$  and  $\eta_{n,m}$ , and (ii) the value of the state derivatives  $x'_{1,i}(\theta, t)$  and  $x'_{2,i}(\theta, t)$  over all on and off-treatment periods. The quantities in (i) are easily observed using timers whose start and end times are observable events; eventually knowledge of the noise processes  $\zeta_1(t)$  and  $\zeta_2(t)$  evaluated at event times *only* is also needed to compute (6.49)-(6.50). Information on the noise processes can be extracted from the observed

sample path, as explained in Section 5.3. The state derivatives in (ii) are obtained from (6.2) and (6.11) over on-treatment periods, and from (6.20) and (6.29) over off-treatment periods. Ultimately, these expressions depend on (5.8) and (5.9), so that it is necessary to evaluate the integral of the noise process  $\zeta_3(t)$ , which can also be accomplished using data extracted from the observed sample path.

As a result, it is straightforward to implement an algorithm for updating the value of  $dL(\theta)/d\theta_i$  after each observed event, as outlined in Algorithm 1.

---

**Algorithm 1** IPA Algorithm for Optimal IAS Therapy Design

---

**Whenever an event occurs at time  $\tau_k$ ,  $k = 1, 2, \dots$**

*Step 1*      Update event time derivatives using (6.48)

*Step 2*      Update state derivatives using (6.41)-(6.42) and (6.47)

*Step 3*      Update cost derivatives using (6.51)

**End**

**Repeat**

---

Note that *Step 1* requires knowledge of the noise processes  $\zeta_1(t)$  and  $\zeta_2(t)$  in order to evaluate (6.49) whenever an event  $e_1$  takes place, and (6.50) whenever an event  $e_2$  occurs. In what follows, details are given on how to include this type of information using data from the observed sample path.

### 5.3 Simulation Results

The results shown here represent a first attempt at incorporating randomness into a SHA model of prostate cancer evolution in which we consider only noise and fluctuations associated with cell population dynamics, and do not account for noise in the patient's androgen level. Representing randomness as Gaussian white noise, the

authors in (Tanaka et al., 2010) verified that variable time courses of the PSA levels were produced without losing the tendency of the deterministic system, thus yielding simulation results that were comparable to the statistics of clinical data. For this reason, in this work we take  $\{\zeta_i(t)\}$ ,  $i = 1, 2$ , to be Gaussian white noise with zero mean and standard deviation of 0.001, similarly to (Tanaka et al., 2010), although we remind the reader that our methodology applies independently of the distribution chosen to represent  $\{\zeta_i(t)\}$ ,  $i = 1, 2$ . We estimate the noise associated with cell population dynamics at event times by randomly sampling from a uniform distribution with zero mean and standard deviation of 0.001. Simulations of the prostate cancer model as a pure DES are thus run to generate sample path data to which the IPA estimator is applied. In all results reported here, we measure the sample path length in between updates of the controllable parameter vector  $\theta$  in terms of the number of days elapsed since the onset of IAS therapy, which we choose to be  $T = 2500$  days. We also adopt the notation "Patient # $k$ ", as in (Liu et al., 2015), in reference to the system dynamics model of patient  $k$  (complete details on how such models were generated using clinical data from the corresponding patients can be found in (Liu et al., 2015)).

Two sets of simulations were performed: one in which we set  $W = 0.5$  and determine personalized treatment schemes for two different patients, and another in which we analyze the effect of  $W$  on the design of a given patient's optimal therapy. For the former, we make use of the clinical models of Patient #15 and Patient #1 (Liu

et al., 2015).

Figures 5.3-5.5 present the convergence plots of the average cost and control parameters considering different initial configurations for Patient #15.

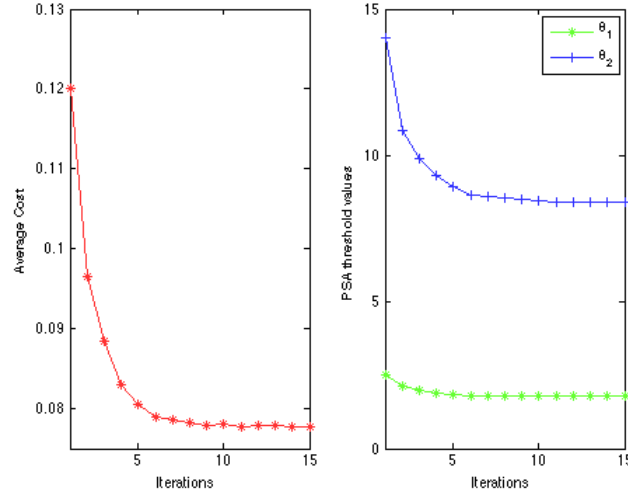


**Figure 5.3:** Convergence plots of average cost and PSA threshold values for initial configuration  $[\theta_1^{init}, \theta_2^{init}] = [2.5, 14.0]$  (Patient #15)

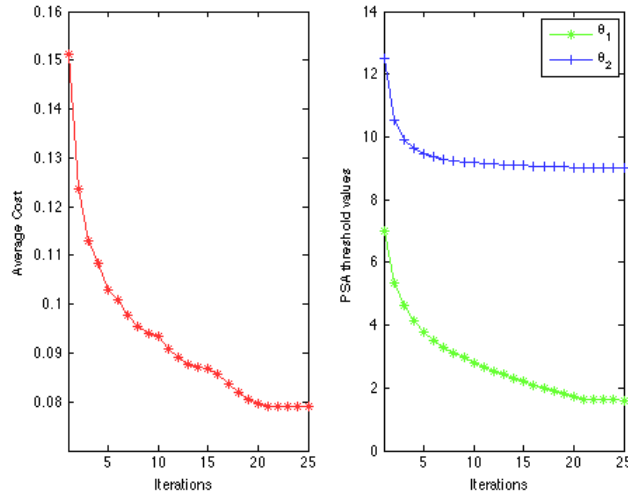


**Figure 5.4:** Convergence plots of average cost and PSA threshold values for initial configuration  $[\theta_1^{init}, \theta_2^{init}] = [7.0, 12.5]$  (Patient #15)



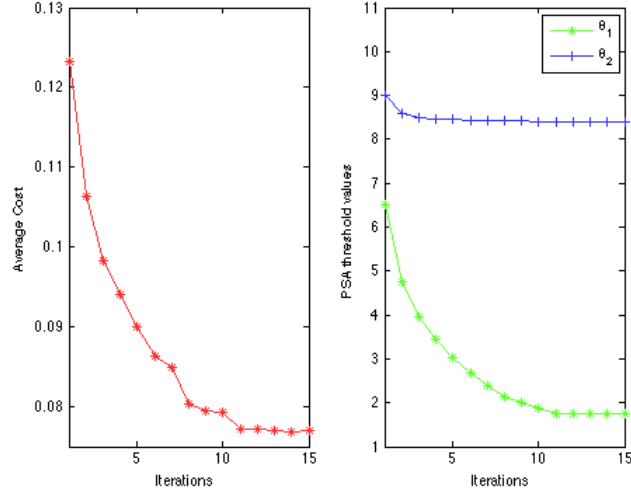


**Figure 5-5:** Convergence plots of average cost and PSA threshold values for initial configuration  $[\theta_1^{init}, \theta_2^{init}] = [6.5, 9.0]$  (Patient #15)

Figures 5-6-5-8 present the convergence plots of the average cost and control parameters considering different initial configurations for Patient #1.

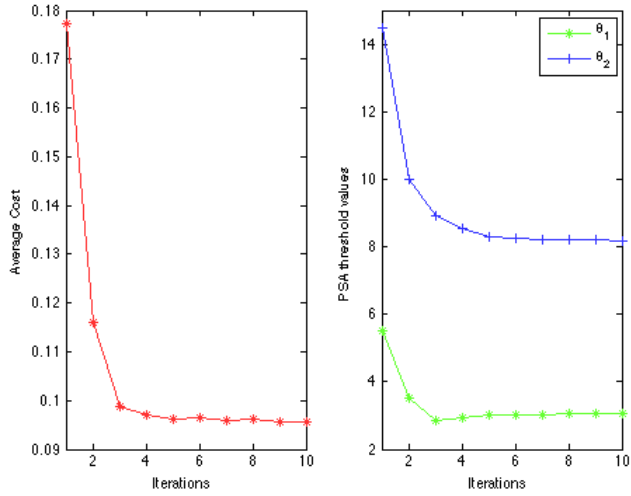


**Figure 5-6:** Convergence plots of average cost and PSA threshold values for initial configuration  $[\theta_1^{init}, \theta_2^{init}] = [5.5, 14.5]$  (Patient #1)

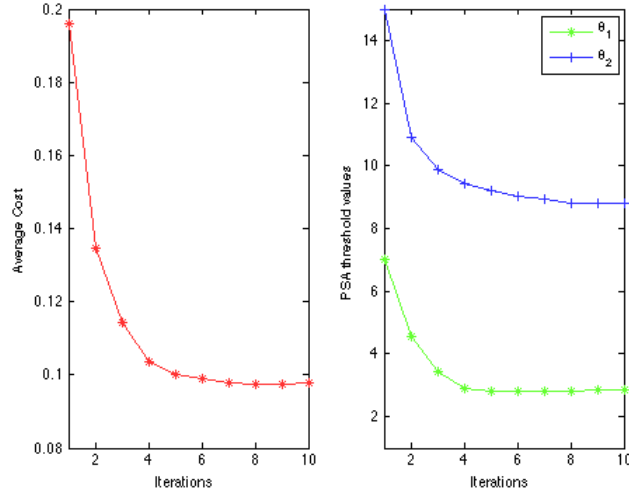


**Figure 5.7:** Convergence plots of average cost and PSA threshold values for initial configuration  $[\theta_1^{init}, \theta_2^{init}] = [7.0, 15.0]$  (Patient #1)

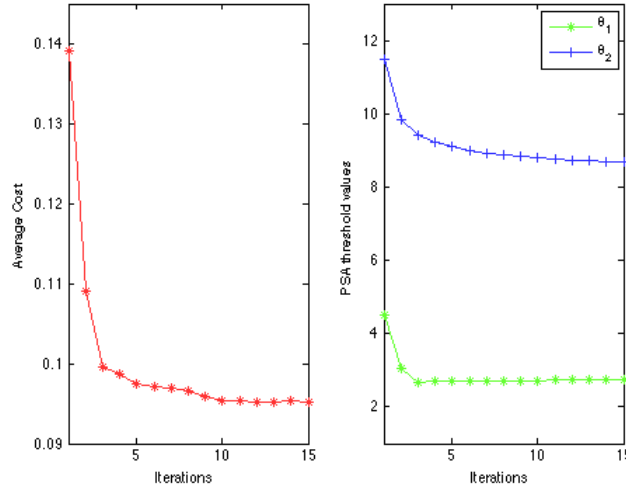


**Figure 5.8:** Convergence plots of average cost and PSA threshold values for initial configuration  $[\theta_1^{init}, \theta_2^{init}] = [4.5, 11.5]$  (Patient #1)

Using a brute force approach, the response surface corresponding to our cost function was generated. In Figure 5.9, the convergence trajectories from Figures 5.3-5.5 are plotted against the response surface of Patient #15, and it can be seen that

all configurations converge to the region of minimum cost.

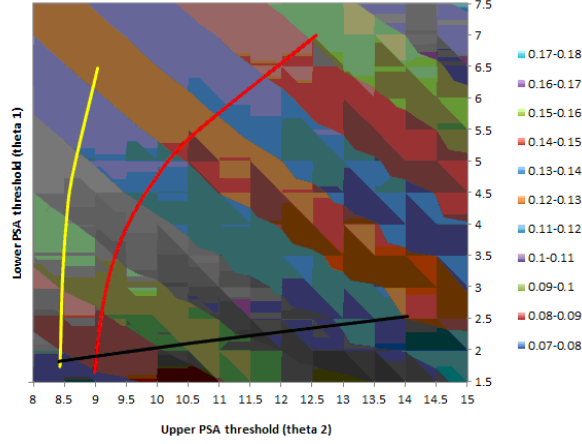


**Figure 5-9:** Response surface and convergence trajectories (Patient #15)

In Figure 5-10, the convergence trajectories from Figures 5-6-5-8 are plotted against the response surface of Patient #1, and again it can be seen that all configurations converge to the region of minimum cost.

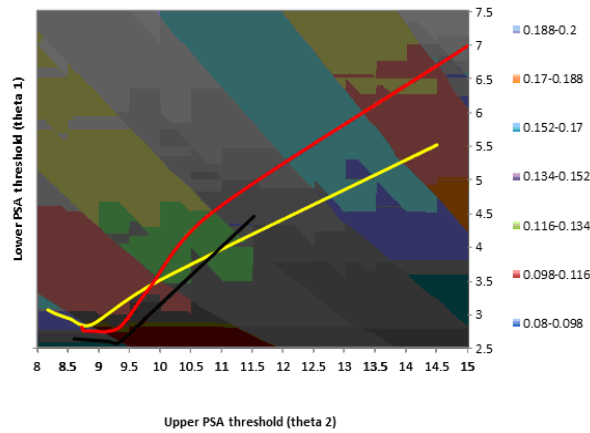


**Figure 5-10:** Response surface and convergence trajectories (Patient #1)

In our second set of simulations, we use the clinical model of Patient #1 (Liu et al., 2015) and take  $W \in \{0.1, 0.5, 0.9\}$ . Recall that our sample function contains two terms, each of which represents complementary measures of therapy success. We take into account the fact that it may be desirable to design a therapy scheme that favors one of these terms over the other by associating weight  $W$  with the first term and  $1 - W$  with the second term, as detailed in Section 5.1.2. Table 5.1 presents the values of optimal lower and upper PSA threshold values ( $\theta_1^*$  and  $\theta_2^*$ , respectively) and the corresponding cost of treatment ( $J^*$ ) using the clinical model Patient #1 for different values of  $W$ . In what follows, we adopt the notation  $x \approx y$  to indicate that  $x$  takes values *approximately equal* to  $y$ , and  $x \gtrsim y$  to indicate that  $x$  takes values *approximately equal or slightly greater* than  $y$ .

**Table 5.1:** Optimization results for different values of  $W$  using the clinical model of Patient 1

$W$	$\theta_1^*$	$\theta_2^*$	$J^*$
0.1	$\approx 2.5$	$\approx 8.0$	0.017
0.5	$\approx 2.5$	$\approx 8.0$	0.086
0.9	$\approx 2.5$	$\approx 8.0$	0.154

It can be seen from Table 5.1 that the ranges of optimal lower and upper PSA threshold values are equivalent for  $W \in \{0.1, 0.5, 0.9\}$ , i.e.,  $\theta_1^* \gtrsim \theta_1^{\min}$  and  $\theta_2^* \gtrsim \theta_2^{\min}$  for all values of  $W$  considered here. In other words, the value of  $J^*$  changes with the value of  $W$ , but the regions of minimum and maximum cost remain essentially unchanged. This means that a common optimal treatment scheme exists irrespective of the chosen value of  $W$ . Hence, it is possible to consistently achieve therapy personalization, as detailed next.

### 5.3.1 Achieving Therapy Personalization

Recall that solving problem (5.14) is equivalent to searching for the IAS treatment scheme that not only keeps PSA levels as low as possible, but that also reduces the frequency of on and off-treatment cycles. In this context, the resulting optimal IAS therapy is one in which both the low and high PSA thresholds take values as small as possible, i.e.,  $\theta_1^* \gtrsim \theta_1^{\min}$  and  $\theta_2^* \gtrsim \theta_2^{\min}$ . This tendency is verified in Figures 5-9 and 5-10, where it can be seen that the regions of minimum cost are those immediately surrounding  $[\theta_1^{\min}, \theta_2^{\min}]$ .

Moreover, it is interesting to note that although this tendency is consistent across different patients, successful IAS therapy schemes are only obtained when  $\theta_1 \geq 1.5$  for Patient #15 and  $\theta_1 \geq 2.5$  for Patient #1. This means that, for Patient #15, a therapy in which the low PSA threshold takes values smaller than 1.5 will eventually lead to uncontrolled cancer cell growth and disease relapse. The same analysis holds for Patient #1, except that in this case, there is a higher lower bound on the value of  $\theta_1$ . Clearly this variation across patients is associated with the fact that each patient responds differently to IAS therapy; hence the underlying need for designing *personalized* treatment schemes.

Finally, personalizing IAS therapy based on the cost metric proposed in this work involves, among other things, assessing the smallest value that the low PSA threshold can be allowed to reach, which varies across patients. This can be done using clinical data from patients, when available. In cases where no model exists to predict a pa-

tient's response to therapy (e.g., for patients who have never been submitted to IAS therapy), a possible course of action would be to devise an optimal therapy scheme using another patient's model, which could be selected based on clinical indicators of patient similarity and/or insights from the physician. After recording the new patient's response to the first cycle(s) of treatment, it would be possible to iteratively adjust his initial treatment until an improved scheme is found. Such iterative search for an optimal IAS therapy scheme could be successfully performed using the methodology outlined in this chapter.

## Chapter 6

# Issues in Cancer Therapy Personalization: Robustness vs. Optimality

In this chapter we focus on the importance of accurate modeling in conjunction with optimal therapy design. In particular, by evaluating sensitivity estimates with respect to several model parameters, we identify critical parameters and verify the extent to which the SHA model of prostate cancer evolution is robust to them. In what follows, we reintroduce the SHA model of prostate cancer evolution and apply IPA to derive estimators of the cost metric gradient with respect to various model and therapy parameters. These estimators are subsequently used for system analysis. Simulation results demonstrate that relaxing the optimality condition in favor of increased robustness to modeling errors provides an alternative objective to therapy design for at least some patients.

## 6.1 Problem Formulation

We continue to consider the system comprised of a prostate tumor under IAS therapy, which is modeled as a Stochastic Hybrid Automaton (SHA), as detailed in Chapter 5. In contrast to the previous part of this work, here we use IPA to explore the tradeoff

between system optimality and robustness (or, equivalently, fragility), thus providing valuable insights on modeling and control of cancer progression. Of note, several potentially critical parameters exist in the SHA model of prostate cancer evolution. The results shown here reflect a first step towards analyzing their relative importance, in which we select a subset of all model parameters in order to illustrate the applicability of our IPA-based methodology. The parameters we consider here are  $\alpha_1$  and  $\alpha_2$  (HSC proliferation constant and CRC proliferation constant, respectively), as well as  $\beta_1$  and  $\beta_2$  (HSC apoptosis constant and CRC apoptosis constant, respectively). These constants are intrinsically related to the cancer cell subpopulations' net growth rate, whose value dictates how fast the PSA threshold values will be reached, and ultimately how soon treatment will be suspended or reinstated. As a result, correctly estimating the values of  $\alpha_i$  and  $\beta_i$ ,  $i = 1, 2$ , is presumably crucial for the purposes of personalized IAS therapy design.

In this context, we define an extended parameter vector  $\theta = [\theta_1, \dots, \theta_6]$ , where  $\theta_1$  ( $\theta_2$ , respectively) corresponds to the lower (upper, respectively) threshold value of the patient's PSA level,  $\theta_3$  ( $\theta_4$ , respectively) corresponds to the HSC (CRC, respectively) proliferation constant, and  $\theta_5$  ( $\theta_6$ , respectively) corresponds to the HSC (CRC, respectively) apoptosis constant.

We will continue to make use of the sample function defined by (5.12) and will maintain all assumptions regarding the underlying stochastic processes, as well as consider the same feasible events and system dynamics that were introduced in Section



5.1. In what follows, we derive the IPA state and event time derivatives for the events identified in Section 5.1.

## 6.2 IPA for the SHA Model of Prostate Cancer Evolution

For simplicity of notation, let us define the derivatives of the states  $x_n(\theta, t)$  and  $z_j(\theta, t)$  and event times  $\tau_k(\theta)$  with respect to  $\theta_i$ ,  $i = 1, \dots, 6$ ,  $n = 1, \dots, 3$ , as follows:

$$x'_{n,i}(t) \equiv \frac{\partial x_n(\theta, t)}{\partial \theta_i}, \quad z'_{j,i}(t) \equiv \frac{\partial z_j(\theta, t)}{\partial \theta_i}, \quad \tau'_{k,i} \equiv \frac{\partial \tau_k(\theta)}{\partial \theta_i} \quad (6.1)$$

In what follows, we derive the IPA state and event time derivatives for the events identified in our SHA model of prostate cancer progression.

### 6.2.1 State and Event Time Derivatives

We proceed by analyzing the state evolution of our SHA model of prostate cancer progression considering each of the states ( $q^{ON}$  and  $q^{OFF}$ ) and events ( $e_1$  and  $e_2$ ) therein defined.

1. *The system is in state  $q^{ON}$  over interevent time interval  $[\tau_k, \tau_{k+1})$ .* Using (A.7)

for  $x_1(t)$ , we obtain, for  $i = 1, \dots, 6$ ,

$$\begin{aligned} \frac{d}{dt} x'_{1,i}(t) &= \frac{\partial f_k^{x_1}(t)}{\partial x_1} x'_1(t) + \frac{\partial f_k^{x_1}(t)}{\partial x_2} x'_2(t) \\ &\quad + \frac{\partial f_k^{x_1}(t)}{\partial z_1} z'_1(t) + \frac{\partial f_k^{x_1}(t)}{\partial z_2} z'_2(t) + \frac{\partial f_k^{x_1}(t)}{\partial \theta_i} \end{aligned}$$

From (5.10), we have  $\frac{\partial f_k^{x_1}(t)}{\partial x_2} = \frac{\partial f_k^{x_1}(t)}{\partial z_j} = \frac{\partial f_k^{x_1}(t)}{\partial \theta_i} = 0$ ,  $i = 1, 2, 4, 6$ ,  $j = 1, 2$ , and

$$\begin{aligned}\frac{\partial f_k^{x_1}(t)}{\partial x_1} &= \alpha_1 [1 + \phi_\alpha^{ON}(t)]^{-1} - \beta_1 [1 + \phi_\beta^{ON}(t)]^{-1} \\ &\quad - m_1 \left(1 - \frac{h^{ON}(t)}{x_{3,0}}\right) - \lambda_1 \\ \frac{\partial f_k^{x_1}(t)}{\partial \theta_3} &= x_1 [1 + \phi_\alpha^{ON}(t)]^{-1} \\ \frac{\partial f_k^{x_1}(t)}{\partial \theta_5} &= -x_1 [1 + \phi_\beta^{ON}(t)]^{-1}\end{aligned}$$

It is thus simple to verify that solving (A.7) for  $x'_{1,i}(t)$  yields, for  $t \in [\tau_k, \tau_{k+1})$ ,

$$x'_{1,i}(t) = x'_{1,i}(\tau_k^+) e^{A_1(t)}, \quad i = 1, 2, 4, 6 \quad (6.2)$$

$$x'_{1,3}(t) = x'_{1,3}(\tau_k^+) e^{A_1(t)} + A_2(t) \quad (6.3)$$

$$x'_{1,5}(t) = x'_{1,5}(\tau_k^+) e^{A_1(t)} + A_3(t) \quad (6.4)$$

with

$$\begin{aligned}A_1(t) &\equiv \int_{\tau_k}^t \left[ \frac{\alpha_1}{1 + \phi_\alpha^{ON}(t)} - \frac{\beta_1}{1 + \phi_\beta^{ON}(t)} \right] dt \\ &\quad - \int_{\tau_k}^t \frac{m_1}{x_{3,0}} h^{ON}(t) dt - (m_1 + \lambda_1)(t - \tau_k)\end{aligned} \quad (6.5)$$

$$A_2(t) \equiv e^{A_1(t)} \int_{\tau_k}^t \left[ \frac{x_1(t)}{1 + \phi_\alpha^{ON}(t)} e^{-A_1(t)} \right] dt \quad (6.6)$$

$$A_3(t) \equiv e^{A_1(t)} \int_{\tau_k}^t \left[ -\frac{x_1(t)}{1 + \phi_\beta^{ON}(t)} e^{A_1(t)} \right] dt \quad (6.7)$$

In particular, at  $\tau_{k+1}^-$ :

$$x'_{1,i}(\tau_{k+1}^-) = x'_{1,i}(\tau_k^+) e^{A(\tau_k)} \quad (6.8)$$

$$x'_{1,3}(\tau_{k+1}^-) = x'_{1,3}(\tau_k^+) e^{A(\tau_k)} + A_2(\tau_k) \quad (6.9)$$

$$x'_{1,5}(\tau_{k+1}^-) = x'_{1,5}(\tau_k^+)e^{A(\tau_k)} + A_3(\tau_k) \quad (6.10)$$

where  $A_1(\tau_k)$ ,  $A_2(\tau_k)$ , and  $A_3(\tau_k)$  are given from (6.5).

Similarly for  $x_2(t)$ , we have from (5.11) that  $\frac{\partial f_k^{x_2}(t)}{\partial z_j} = \frac{\partial f_k^{x_2}(t)}{\partial \theta_i} = 0$ ,  $i = 1, 2, 3, 5$ ,  $j = 1, 2$ , and

$$\begin{aligned} \frac{\partial f_k^{x_2}(t)}{\partial x_1} &= m_1 \left( 1 - \frac{h^{ON}(t)}{x_{3,0}} \right) \\ \frac{\partial f_k^{x_2}(t)}{\partial x_2} &= \alpha_2 \left( 1 - d \frac{h^{ON}(t)}{x_{3,0}} \right) - \beta_2 \\ \frac{\partial f_k^{x_2}(t)}{\partial \theta_4} &= \left( 1 - d \frac{h^{ON}(t)}{x_{3,0}} \right) x_2(t) \\ \frac{\partial f_k^{x_2}(t)}{\partial \theta_6} &= -x_2(t) \end{aligned}$$

Combining the last four equations and solving for  $x'_{2,i}(t)$  yields, for  $t \in [\tau_k, \tau_{k+1})$ ,

$$x'_{2,i}(t) = x'_{2,i}(\tau_k^+)e^{B_1(t)} + B_2(t, x'_{1,i}(\tau_k^+), A_1(t)), \quad i = 1, 2, 3, 5 \quad (6.11)$$

$$x'_{2,4}(t) = x'_{2,4}(\tau_k^+)e^{B_1(t)} + B_3(t, x'_{1,4}(\tau_k^+), B_1(t)) \quad (6.12)$$

$$x'_{2,6}(t) = x'_{2,6}(\tau_k^+)e^{B_1(t)} + B_4(t, x'_{1,6}(\tau_k^+), B_1(t)) \quad (6.13)$$

with

$$B_1(t) \equiv \int_{\tau_k}^t \left[ \alpha_2 \left( 1 - d \frac{h^{ON}(t)}{x_{3,0}} \right) - \beta_2 \right] dt \quad (6.14)$$

$$\begin{aligned} B_2(\cdot) &\equiv e^{B_1(t)} \int_{\tau_k}^t G_1(t, \tau_k) e^{-B_1(t)} dt \\ B_3(\cdot) &\equiv e^{B_1(t)} \int_{\tau_k}^t G_2(t, \tau_k) e^{-B_1(t)} dt \end{aligned} \quad (6.15)$$

$$B_4(\cdot) \equiv e^{B_1(t)} \int_{\tau_k}^t G_3(t, \tau_k) e^{-B_1(t)} dt \quad (6.16)$$

where, for  $t \in [\tau_k, \tau_{k+1})$ ,  $G_1(t, \tau_k) = m_1 \left( 1 - \frac{h^{ON}(t)}{x_{3,0}} \right) x'_{1,i}(\tau_k^+)e^{A_1(t)}$ ,

$$G_2(t, \tau_k) = e^{-B_1(t)} x_2(t) \left(1 - d \frac{h^{ON}(t)}{x_{3,0}}\right) + e^{-B_1(t)} x'_{1,4}(t) \cdot m_1 \left(1 - d \frac{h^{ON}(t)}{x_{3,0}}\right),$$

$$G_3(t, \tau_k) = e^{-B_1(t)} \left[ x'_{1,6}(t) \cdot m_1 \left(1 - d \frac{h^{ON}(t)}{x_{3,0}}\right) - x_2(t) \right].$$

In particular, at  $\tau_{k+1}^-$ :

$$x'_{2,i}(\tau_{k+1}^-) = x'_{2,i}(\tau_k^+) e^{B_1(\tau_k)} + B_2(\tau_k, x'_{1,i}(\tau_k^+), A(\tau_k)) \quad (6.17)$$

$$x'_{2,4}(\tau_{k+1}^-) = x'_{2,4}(\tau_k^+) e^{B_1(\tau_k)} + B_3(t, x'_{1,4}(\tau_k^+), B_1(\tau_k)) \quad (6.18)$$

$$x'_{2,6}(\tau_{k+1}^-) = x'_{2,6}(\tau_k^+) e^{B_1(\tau_k)} + B_4(t, x'_{1,6}(\tau_k^+), B_1(\tau_k)) \quad (6.19)$$

where  $B_1(\tau_k)$ ,  $B_2(\tau_k, x'_{1,i}(\tau_k^+), A(\tau_k))$ ,  $B_3(t, x'_{1,4}(\tau_k^+), B_1(\tau_k))$ ,

and  $B_4(t, x'_{1,6}(\tau_k^+), B_1(\tau_k))$  are given from (6.14).

Finally, for the “clock” state variable, from (5.5)-(5.6) we have  $\frac{\partial f_k^{z_i}(t)}{\partial x_n} = \frac{\partial f_k^{z_i}(t)}{\partial z_j} = \frac{\partial f_k^{z_i}(t)}{\partial \theta_i} = 0$ ,  $n, j = 1, 2$ ,  $i = 1, \dots, 6$ , so that  $\frac{d}{dt} z'_{j,i}(t) = 0$ ,  $j = 1, 2$ ,  $i = 1, \dots, 6$ , for  $t \in [\tau_k, \tau_{k+1})$ . Hence,  $z'_{j,i}(t) = z'_{j,i}(\tau_k^+)$ ,  $j = 1, 2$ ,  $i = 1, \dots, 6$ , and  $t \in [\tau_k, \tau_{k+1})$ .

2. *The system is in state  $q^{OFF}$  over interevent time interval  $[\tau_k, \tau_{k+1})$ .* Starting with  $x_1(t)$ , based on (5.10) we once again have  $\frac{\partial f_k^{x_1}(t)}{\partial x_2} = \frac{\partial f_k^{x_1}(t)}{\partial z_j} = \frac{\partial f_k^{x_1}(t)}{\partial \theta_i} = 0$ ,  $j = 1, 2$ ,  $i = 1, 2, 4, 6$ , but now

$$\begin{aligned} \frac{\partial f_k^{x_1}(t)}{\partial x_1} &= \alpha_1 [1 + \phi_\alpha^{OFF}(t)]^{-1} - \beta_1 [1 + \phi_\beta^{OFF}(t)]^{-1} \\ &\quad - m_1 \left(1 - \frac{h^{OFF}(t)}{x_{3,0}}\right) - \lambda_1 \\ \frac{\partial f_k^{x_1}(t)}{\partial \theta_3} &= x_1 [1 + \phi_\alpha^{ON}(t)]^{-1} \\ \frac{\partial f_k^{x_1}(t)}{\partial \theta_5} &= -x_1 [1 + \phi_\beta^{ON}(t)]^{-1} \end{aligned}$$

Therefore, (A.7) implies that, for  $t \in [\tau_k, \tau_{k+1})$ :

$$x'_{1,i}(t) = x'_{1,i}(\tau_k^+)e^{C_1(t)}, \quad i = 1, 2, 4, 6 \quad (6.20)$$

$$x'_{1,3}(t) = x'_{1,3}(\tau_k^+)e^{C_1(t)} + C_2(t) \quad (6.21)$$

$$x'_{1,5}(\tau_{k+1}^-) = x'_{1,5}(\tau_k^+)e^{C_1(\tau_k)} + C_3(t) \quad (6.22)$$

with

$$C_1(t) \equiv \int_{\tau_k}^t \left[ \frac{\alpha_1}{1+\phi_\alpha^{OFF}(t)} - \frac{\beta_1}{1+\phi_\beta^{OFF}(t)} \right] dt - \int_{\tau_k}^t \frac{m_1}{x_{3,0}} h^{OFF}(t) dt - (m_1 + \lambda_1)(t - \tau_k) \quad (6.23)$$

$$C_2(t) \equiv e^{C_1(t)} \int_{\tau_k}^t \left[ \frac{x_1(t)}{1 + \phi_\alpha^{OFF}(t)} e^{-C_1(t)} \right] dt \quad (6.24)$$

$$C_3(t) \equiv e^{C_1(\tau_k)} \int_{\tau_k}^{\tau_{k+1}} \left[ -\frac{x_1(t)}{1 + \phi_\beta^{OFF}(t)} e^{C_1(t)} \right] dt \quad (6.25)$$

In particular, at  $\tau_{k+1}^-$ :

$$x'_{1,i}(\tau_{k+1}^-) = x'_{1,i}(\tau_k^+)e^{C_1(\tau_k)} \quad (6.26)$$

$$x'_{1,3}(\tau_{k+1}^-) = x'_{1,3}(\tau_k^+)e^{C_1(\tau_k)} + C_2(\tau_k) \quad (6.27)$$

$$x'_{1,5}(\tau_{k+1}^-) = x'_{1,5}(\tau_k^+)e^{C_1(\tau_k)} + C_3(\tau_k) \quad (6.28)$$

where  $C_1(\tau_k)$ ,  $C_2(\tau_k)$ , and  $C_3(\tau_k)$  are given from (6.23).

Similarly for  $x_2(t)$ , we have

$$\begin{aligned}\frac{\partial f_k^{x_2}(t)}{\partial x_1} &= m_1 \left(1 - \frac{h^{OFF}(t)}{x_{3,0}}\right) \\ \frac{\partial f_k^{x_2}(t)}{\partial x_2} &= \alpha_2 \left(1 - d \frac{h^{OFF}(t)}{x_{3,0}}\right) - \beta_2 \\ \frac{\partial f_k^{x_2}(t)}{\partial \theta_4} &= \left(1 - d \frac{h^{OFF}(t)}{x_{3,0}}\right) x_2(t) \\ \frac{\partial f_k^{x_2}(t)}{\partial \theta_6} &= -x_2(t)\end{aligned}$$

It is thus straightforward to verify that (A.7) yields, for  $t \in [\tau_k, \tau_{k+1})$ ,

$$x'_{2,i}(t) = x'_{2,i}(\tau_k^+) e^{D_1(t)} + D_2(t, x'_{1,i}(\tau_k^+), C_1(t)), \quad i = 1, 2, 4, 6 \quad (6.29)$$

$$x'_{2,4}(t) = x'_{2,4}(\tau_k^+) e^{D_1(t)} + D_3(t, x'_{1,4}(\tau_k^+), D_1(t)) \quad (6.30)$$

$$x'_{2,6}(t) = x'_{2,6}(\tau_k^+) e^{D_1(t)} + D_4(t, x'_{1,6}(\tau_k^+), D_1(t)) \quad (6.31)$$

with

$$D_1(t) \equiv \int_{\tau_k}^t \left[ \alpha_2 \left(1 - d \frac{h^{OFF}(t)}{x_{3,0}}\right) - \beta_2 \right] dt \quad (6.32)$$

$$\begin{aligned}D_2(\cdot) &\equiv e^{D_1(t)} \int_{\tau_k}^t G_2(t, \tau_k) e^{-D_1(t)} dt \\ D_3(\cdot) &\equiv e^{D_1(t)} \int_{\tau_k}^t G_3(t, \tau_k) e^{-D_1(t)} dt\end{aligned} \quad (6.33)$$

$$D_4(\cdot) \equiv e^{D_1(t)} \int_{\tau_k}^t G_4(t, \tau_k) e^{-D_1(t)} dt \quad (6.34)$$

where, for  $t \in [\tau_k, \tau_{k+1})$ ,

$$G_2(t, \tau_k) = m_1 \left( 1 - \frac{h^{OFF}(t)}{x_{3,0}} \right) x'_{1,i}(\tau_k^+) e^{C_1(t)} \quad (6.35)$$

$$G_3(t, \tau_k) = x_2(t) \left( 1 - d \frac{h^{OFF}(t)}{x_{3,0}} \right) + x'_{1,4}(t) \cdot m_1 \left( 1 - d \frac{h^{OFF}(t)}{x_{3,0}} \right) \quad (6.36)$$

$$G_4(t, \tau_k) = x'_{1,6}(t) \cdot m_1 \left( 1 - d \frac{h^{OFF}(t)}{x_{3,0}} \right) - x_2(t) \quad (6.37)$$

In particular, at  $\tau_{k+1}^-$ :

$$x'_{2,i}(\tau_{k+1}^-) = x'_{2,i}(\tau_k^+) e^{D_1(\tau_k)} + D_2(\tau_k, x'_{1,i}(\tau_k^+), C(\tau_k)) \quad (6.38)$$

$$x'_{2,4}(t) = x'_{2,4}(\tau_k^+) e^{D_1(t)} + D_3(t, x'_{1,4}(\tau_k^+), D_1(\tau_k)) \quad (6.39)$$

$$x'_{2,6}(t) = x'_{2,6}(\tau_k^+) e^{D_1(t)} + D_4(t, x'_{1,6}(\tau_k^+), D_1(\tau_k)) \quad (6.40)$$

where  $D_1(\tau_k)$ ,  $D_2(\cdot)$ ,  $D_3(\cdot)$ , and  $D_4(\cdot)$  are given from (6.32).

Finally, for the “clock” state variable, based on (5.5)-(5.6) we once again have

$$\frac{\partial f_k^{z_i}(t)}{\partial x_n} = \frac{\partial f_k^{z_i}(t)}{\partial z_j} = \frac{\partial f_k^{z_i}(t)}{\partial \theta_i} = 0, \quad n, j = 1, 2, \quad i = 1, \dots, 6, \quad \text{so that } \frac{d}{dt} z'_{j,i}(t) = 0, \quad j = 1, 2,$$

$i = 1, \dots, 6$ , for  $t \in [\tau_k, \tau_{k+1})$ . As a result,  $z'_{j,i}(t) = z'_{j,i}(\tau_k^+)$ ,  $j = 1, 2$ ,  $i = 1, \dots, 6$ , and

$t \in [\tau_k, \tau_{k+1})$ .

3. A state transition from  $q^{ON}$  to  $q^{OFF}$  occurs at time  $\tau_k$ . This necessarily implies that event  $e_1$  took place at time  $\tau_k$ , i.e.,  $q(t) = q^{ON}$ ,  $t \in [\tau_{k-1}, \tau_k)$  and  $q(t) = q^{OFF}$ ,  $t \in [\tau_k, \tau_{k+1})$ . From (A.8) we have, for  $i = 1, \dots, 6$ ,

$$x'_{1,i}(\tau_k^+) = x'_{1,i}(\tau_k^-) + [f_k^{x_1}(\tau_k^-) - f_{k+1}^{x_1}(\tau_k^+)] \cdot \tau'_{k,i} \quad (6.41)$$

and

$$x'_{2,i}(\tau_k^+) = x'_{2,i}(\tau_k^-) + [f_k^{x_2}(\tau_k^-) - f_{k+1}^{x_2}(\tau_k^+)] \cdot \tau'_{k,i} \quad (6.42)$$

where  $f_k^{x_1}(\tau_k^-) - f_{k+1}^{x_1}(\tau_k^+)$  and  $f_k^{x_2}(\tau_k^-) - f_{k+1}^{x_2}(\tau_k^+)$  ultimately depend on  $h^{ON}(\tau_k^-)$  and  $h^{OFF}(\tau_k^+)$ . Evaluating  $h^{ON}(\tau_k^-)$  from (5.8) over the appropriate time interval results in

$$\begin{aligned} h^{ON}(\tau_k^-) &= x_3(\tau_{k-1}^+) e^{-(\tau_k - \tau_{k-1})/\sigma} \\ &\quad + \mu_3 \sigma [1 - e^{-(\tau_k - \tau_{k-1})/\sigma}] + \tilde{\zeta}_3(\tau_k) \end{aligned}$$

and it follows directly from (5.9) that  $h^{OFF}(\tau_k^+) = x_3(\tau_k^+)$ . Moreover, by continuity of  $x_n(t)$  (due to conservation of mass),  $x_n(\tau_k^+) = x_n(\tau_k^-)$ ,  $n = 1, 2$ . Also, since we have assumed that  $\{\zeta_i(t)\}$ ,  $i = 1, \dots, 3$ , is piecewise continuous w.p.1 and that no two events can occur at the same time w.p.1,  $\zeta_i(\tau_k^-) = \zeta_i(\tau_k^+)$ ,  $i = 1, \dots, 3$ . Hence, for  $x_1(t)$ , evaluating  $\Delta_f^1(\tau_k) \equiv f_k^{x_1}(\tau_k^-) - f_{k+1}^{x_1}(\tau_k^+)$  yields

$$\begin{aligned} \Delta_f^1(\tau_k, \zeta_3(\tau_k)) &= \left\{ \alpha_1 [1 + \phi_\alpha^{ON}(\tau_k^-)]^{-1} \right. \\ &\quad - \alpha_1 [1 + \phi_\alpha^{OFF}(\tau_k^+)]^{-1} - \beta_1 [1 + \phi_\beta^{ON}(\tau_k^-)]^{-1} \\ &\quad + \beta_1 [1 + \phi_\beta^{OFF}(\tau_k^+)]^{-1} \\ &\quad \left. + \frac{m_1}{x_{3,0}} [h^{ON}(\tau_k^-) - x_3(\tau_k)] \right\} \cdot x_1(\tau_k) \end{aligned} \quad (6.43)$$

Finally, the term  $\tau'_{k,i}$ , which corresponds to the event time derivative with respect to  $\theta_i$  at event time  $\tau_k$ , is determined using (A.12), as detailed in (6.48) later.

A similar analysis applies to  $x_2(t)$ , so that  $f_k^{x_2}(\tau_k^-)$  and  $f_{k+1}^{x_2}(\tau_k^+)$  ultimately depend on  $h^{ON}(\tau_k^-)$  and  $h^{OFF}(\tau_k^+)$ , respectively. Hence, evaluating  $\Delta_f^2(\tau_k) \equiv f_k^{x_2}(\tau_k^-) - f_{k+1}^{x_2}(\tau_k^+)$  from (5.11) yields

$$\begin{aligned} \Delta_f^2(\tau_k, \zeta_3(\tau_k)) &= \frac{\alpha_2 d}{x_{3,0}} [x_3(\tau_k) - h^{ON}(\tau_k^-)] \cdot x_2(\tau_k) \\ &\quad - \frac{m_1}{x_{3,0}} [h^{ON}(\tau_k^-) - x_3(\tau_k)] \cdot x_1(\tau_k) \end{aligned} \quad (6.44)$$



In the case of the “clock” state variable,  $z_1(t)$  is discontinuous in  $t$  at  $t = \tau_k$ , while  $z_2(t)$  is continuous. Hence, based on (A.9) and (5.5), we have that  $z'_{1,i}(\tau_k^+) = 0$ . From (A.8) and (5.6), it is straightforward to verify that  $z'_{2,i}(\tau_k^+) = z'_{2,i}(\tau_k^-) - \tau'_{k,i}$ ,  $i = 1, \dots, 6$ .

4. A state transition from  $q^{OFF}$  to  $q^{ON}$  occurs at time  $\tau_k$ . This necessarily implies that event  $e_2$  took place at time  $\tau_k$ , i.e.,  $q(t) = q^{OFF}$ ,  $t \in [\tau_{k-1}, \tau_k)$  and  $q(t) = q^{ON}$ ,  $t \in [\tau_k, \tau_{k+1})$ . The same reasoning as above holds, so that (6.41)-(6.42) also apply. For  $x_1(t)$ ,  $f_k^{x_1}(\tau_k^-) - f_{k+1}^{x_1}(\tau_k^+)$  can be evaluated from (5.10) and ultimately depends on  $h^{OFF}(\tau_k^-)$  and  $h^{ON}(\tau_k^+)$ . Evaluating  $h^{OFF}(\tau_k^-)$  from (5.9) over the appropriate time interval results in

$$\begin{aligned} h^{OFF}(\tau_k^-) &= x_3(\tau_{k-1}^+) e^{-(\tau_k - \tau_{k-1})/\sigma} \\ &\quad + (\mu_3 \sigma + x_{3,0}) [1 - e^{-(\tau_k - \tau_{k-1})/\sigma}] + \tilde{\zeta}_3(\tau_k) \end{aligned}$$

and it follows directly from (5.8) that  $h^{ON}(\tau_k^+) = x_3(\tau_k^+)$ .

As in the previous case, continuity due to conservation of mass applies, so that evaluating  $\Delta_f^1(\tau_k) \equiv f_k^{x_1}(\tau_k^-) - f_{k+1}^{x_1}(\tau_k^+)$  yields

$$\begin{aligned} \Delta_f^1(\tau_k, \zeta_3(\tau_k)) &= \left\{ \alpha_1 [1 + \phi_\alpha^{OFF}(\tau_k^-)]^{-1} \right. \\ &\quad - \alpha_1 [1 + \phi_\alpha^{ON}(\tau_k^+)]^{-1} - \beta_1 [1 + \phi_\beta^{OFF}(\tau_k^-)]^{-1} \\ &\quad + \beta_1 [1 + \phi_\beta^{ON}(\tau_k^+)]^{-1} \\ &\quad \left. + \frac{m_1}{x_{3,0}} [h^{OFF}(\tau_k^-) - x_3(\tau_k)] \right\} \cdot x_1(\tau_k) \end{aligned} \tag{6.45}$$

Similarly for  $x_2(t)$ , by evaluating  $\Delta_f^2(\tau_k) \equiv f_k^{x_2}(\tau_k^-) - f_{k+1}^{x_2}(\tau_k^+)$  from (5.11), and

making the appropriate simplifications due to continuity, we obtain

$$\begin{aligned}\Delta_f^2(\tau_k, \zeta_3(\tau_k)) &= \frac{\alpha_2 d}{x_{3,0}} [x_3(\tau_k) - h^{OFF}(\tau_k^-)] \cdot x_2(\tau_k) \\ &\quad - \frac{m_1}{x_{3,0}} [h^{OFF}(\tau_k^-) - x_3(\tau_k)] \cdot x_1(\tau_k)\end{aligned}\tag{6.46}$$

In the case of the “clock” state variable,  $z_1(t)$  is continuous in  $t$  at  $t = \tau_k$ , while  $z_2(t)$  is discontinuous. As a result, based on (A.8) and (5.5), we have that  $z'_{1,i}(\tau_k^+) = z'_{1,i}(\tau_k^-) - \tau'_{k,i}$ . From (A.9) and (5.6), it is simple to verify that  $z'_{2,i}(\tau_k^+) = 0$ ,  $i = 1, \dots, 6$ .

Note that, since  $z'_{j,i}(t) = z'_{j,i}(\tau_k^+)$ ,  $t \in [\tau_k, \tau_{k+1})$ , we will have that  $z'_{j,i}(\tau_k^-) = z'_{j,i}(\tau_{k-1}^+)$ ,  $j = 1, 2$ ,  $i = 1, \dots, 6$ . Moreover, the sample path of our SHA consists of a sequence of alternating  $e_1$  and  $e_2$  events, which implies that  $z'_{1,i}(\tau_k^-) = 0$  if event  $e_1$  occurred at  $\tau_{k-1}$ , while  $z'_{2,i}(\tau_k^-) = 0$  if event  $e_2$  occurred at  $\tau_{k-1}$ . Then, adopting the notation  $p, \bar{p} = \{1, 2\}$  such that  $p + \bar{p} = 3$ , we have:

$$z'_{p,i}(\tau_k^+) = \begin{cases} -\tau'_{k,i} & \text{if event } e_{\bar{p}} \text{ occurs at } \tau_k \\ 0 & \text{otherwise} \end{cases}\tag{6.47}$$

We now proceed with a general result which applies to all events defined for our SHA model. We denote the time of occurrence of the  $j$ th state transition by  $\tau_j$ , define its derivative with respect to the control parameters as  $\tau'_{j,i} \equiv \frac{\partial \tau_j}{\partial \theta_i}$ ,  $i = 1, \dots, 6$ , and also define  $f_j^{x_n}(\tau_j) \equiv \dot{x}_n(\tau_j)$ ,  $n = 1, 2$ .

**Lemma 6.1** *When an event  $e_p$ ,  $p = 1, 2$ , occurs, the derivative  $\tau'_{j,i}$ ,  $i = 1, \dots, 6$ , of state transition times  $\tau_j$ ,  $j = 1, 2, \dots$  with respect to the control parameters  $\theta_i$ ,*

$i = 1, \dots, 6$ , satisfies:

$$\tau'_{j,i} = \begin{cases} \frac{1-x'_{1,i}(\tau_j^-)-x'_{2,i}(\tau_j^-)}{f_{j-1}^{x_1}(\tau_j^-)+f_{j-1}^{x_2}(\tau_j^-)} & \text{if } e_1 \text{ occurs and } i = 1 \\ & \text{or } e_2 \text{ occurs and } i = 2 \\ \frac{-x'_{1,i}(\tau_j^-)-x'_{2,i}(\tau_j^-)}{f_{j-1}^{x_1}(\tau_j^-)+f_{j-1}^{x_2}(\tau_j^-)} & \text{if } e_1 \text{ occurs and } i \neq 1 \\ & \text{or } e_2 \text{ occurs and } i \neq 2 \end{cases} \quad (6.48)$$

**Proof.** The proof is analogous to that of Lemma 5.1, which can be found in Appendix C. ■

We note that the numerator in (6.48) is determined using (6.8) and (6.17) if  $q(\tau_j^-) = q^{ON}$ , or (6.26) and (6.38) if  $q(\tau_j^-) = q^{OFF}$ . Moreover, the denominator in (6.48) is computed using (5.10)-(5.11) and it is simple to verify that, if event  $e_1$  takes place at time  $\tau_j$ ,

$$\begin{aligned} f_{j-1}^{x_1}(\tau_j^-) + f_{j-1}^{x_2}(\tau_j^-) &= \alpha_1 [1 + \phi_\alpha^{ON}(\tau_j^-)]^{-1} \cdot x_1(\tau_j) \\ &\quad - \left\{ \beta_1 [1 + \phi_\beta^{ON}(\tau_j^-)]^{-1} + \lambda_1 \right\} \cdot x_1(\tau_j) + \mu_1 \\ &\quad + \left[ \alpha_2 \left( 1 - d \frac{h^{ON}(\tau_j^-)}{x_{3,0}} \right) - \beta_2 \right] \cdot x_2(\tau_j) \\ &\quad + \zeta_1(\tau_j) + \zeta_2(\tau_j) \end{aligned} \quad (6.49)$$

and, if event  $e_2$  takes place at time  $\tau_j$ ,

$$\begin{aligned} f_{j-1}^{x_1}(\tau_j^-) + f_{j-1}^{x_2}(\tau_j^-) &= \alpha_1 [1 + \phi_\alpha^{OFF}(\tau_j^-)]^{-1} \cdot x_1(\tau_j) \\ &\quad - \left\{ \beta_1 [1 + \phi_\beta^{OFF}(\tau_j^-)]^{-1} + \lambda_1 \right\} \cdot x_1(\tau_j) + \mu_1 \\ &\quad + \left[ \alpha_2 \left( 1 - d \frac{h^{OFF}(\tau_j^-)}{x_{3,0}} \right) - \beta_2 \right] \cdot x_2(\tau_j) \\ &\quad + \zeta_1(\tau_j) + \zeta_2(\tau_j) \end{aligned} \quad (6.50)$$

## 6.2.2 Cost Derivative

Let us denote the total number of on and off-treatment periods (complete or incomplete) in  $[0, T]$  by  $K_T$ . Also let  $\xi_k$  denote the start of the  $k^{th}$  period and  $\eta_k$  denote the end of the  $k^{th}$  period (of either type). Finally, let  $M_T = \lfloor \frac{K_T}{2} \rfloor$  be the total number

of complete on-treatment periods, and  $\Delta_m^{ON}$  denote the duration of the  $m^{th}$  complete on-treatment period, where clearly

$$\Delta_m^{ON} \equiv \eta_m - \xi_m, \quad m = 1, 2, \dots$$

It was shown in Section 5.2.2 that the derivative of the sample function  $L(\theta)$  with respect to the control parameters satisfies:

$$\begin{aligned} \frac{dL(\theta)}{d\theta_i} &= \frac{W}{T} \sum_{k=1}^{K_T} \int_{\xi_k}^{\eta_k} \left[ \frac{x'_{1,i}(\theta, t) + x'_{2,i}(\theta, t)}{PSA_{init}} \right] dt \\ &\quad + \frac{(1-W)}{T} \sum_{m=1}^{M_T} \frac{\Delta_m^{ON}}{T} \cdot (\eta'_{m,i} - \xi'_{m,i}) \\ &\quad - \frac{(1-W)}{T} \mathbf{1}[K_T \text{ is odd}] \cdot \xi'_{M_T+1,i} \cdot \left( \frac{T - \xi_{M_T+1}}{T} \right) \end{aligned} \quad (6.51)$$

where  $\mathbf{1}[\cdot]$  is the usual indicator function and  $PSA_{init}$  is the value of the patient's PSA level at the start of the first on-treatment cycle.

The derivation of (6.51) is detailed in Section 5.2.2. We now proceed to present the results obtained from our IPA-driven sensitivity analysis.

### 6.3 Simulation Results

We continue to consider only noise and fluctuations associated with cell population dynamics, and take  $\{\zeta_i(t)\}$ ,  $i = 1, 2$ , to be Gaussian white noise with zero mean and standard deviation of 0.001, similarly to (Tanaka et al., 2010), although we remind the reader that our methodology applies independently of the distribution chosen to represent  $\{\zeta_i(t)\}$ ,  $i = 1, 2$ . We estimate the noise associated with cell population dynamics at event times by randomly sampling from a uniform distribution with zero

mean and standard deviation of 0.001. Simulations of the prostate cancer model as a pure DES are thus run to generate sample path data to which the IPA estimator is applied. In all results reported here, we measure the sample path length in terms of the number of days elapsed since the onset of IAS therapy, which we choose to be  $T = 2500$  days. We also adopt the notation "Patient  $\#k$ ", as in (Liu et al., 2015), in reference to the system dynamics model of patient  $k$  (complete details on how such models were generated using clinical data from the corresponding patients can be found in (Liu et al., 2015)).

Three sets of simulations were performed: in the first one we consider the optimal therapy configuration determined for Patient  $\#15$  in Section 5.3 and vary the values of  $\theta_i$ ,  $i = 3, \dots, 6$  (one at a time). For the second, we use PSA threshold values that yield a therapy of maximum cost and once again vary the values of  $\theta_i$ ,  $i = 3, \dots, 6$  (one at a time). Finally, in our third set of simulations, we let  $\theta_i$ ,  $i = 3, \dots, 6$ , take the nominal values from (Liu et al., 2015) and vary the values of  $\theta_1$  and  $\theta_2$  along their allowable ranges.

Table 6.1 presents the sensitivity of the model parameters,  $\frac{dL}{d\theta_i}$ ,  $i = 3, \dots, 6$ , around the optimal configuration  $[\theta_1^*, \theta_2^*] = [1.5, 8.0]$  for the values of  $\theta_i$ ,  $i = 3, \dots, 6$ , fitted to the model of Patient  $\#15$  in (Liu et al., 2015). We note that the results from the first two sets of simulations are representative of the phenomena that may be uncovered by this type of analysis, and were hence generated using the model of a single patient. Moreover, while the use of different patient models may potentially reveal additional

phenomena, the insights presented below are interesting in their own right and thus set the stage for extending this analysis to other patients.

**Table 6.1:** Sensitivity of model parameters around the optimal therapy configuration

$\frac{dL}{d\theta_3}$	$\frac{dL}{d\theta_4}$	$\frac{dL}{d\theta_5}$	$\frac{dL}{d\theta_6}$
5.44	-0.25	-5.95	0.28

Recall that  $\theta_3$  and  $\theta_4$  correspond to the HSC proliferation constant and CRC proliferation constant, respectively, while  $\theta_5$  and  $\theta_6$  are the HSC apoptosis constant and CRC apoptosis constant, respectively. Several interesting remarks can be made based on the above results; in what follows, we adopt the notation  $x \approx y$  to indicate that  $x$  takes values *approximately equal* to  $y$ .

From Table 6.1, it can be seen that  $\frac{dL}{d\theta_3} \approx -\frac{dL}{d\theta_5}$  and  $\frac{dL}{d\theta_4} \approx -\frac{dL}{d\theta_6}$ , which indicates that the sensitivities of proliferation and apoptosis constants are of the same order of magnitude (in absolute value) for any given cancer cell subpopulation. It is also possible to verify a large difference in the values of the sensitivities across different subpopulations; in fact the sensitivities of HSC proliferation and apoptosis constants are approximately 21 times higher than those of CRC constants. In other words, the system is more sensitive to changes in the HSC constants than changes in the CRC constants, i.e.,  $\theta_3$  and  $\theta_5$  are more critical model parameters than  $\theta_4$  and  $\theta_6$ . Additionally,  $\frac{dL}{d\theta_3} > 0$  and  $\frac{dL}{d\theta_6} > 0$ , while  $\frac{dL}{d\theta_4} < 0$  and  $\frac{dL}{d\theta_5} < 0$ . A possible explanation for this has to do with the fact that HSCs are the dominant subpopulation in a prostate tumor under IAS therapy, which means that the size of this subpopulation

has a greater impact on the overall size of the tumor, and consequently, on the value of the PSA level. As a result, increasing  $\theta_3$  (or decreasing  $\theta_5$ ) leads to an increase in the size of the HSC population, reflected in the PSA level, thus increasing the overall cost. On the other hand, increasing  $\theta_4$  (or decreasing  $\theta_6$ ) directly increases the size of the CRC population; however, since the conditions under which CRCs thrive are those under which HSCs perish, an increase in the size of the CRC population implies that the size of the HSC population will decrease. Given that HSCs are the dominant subpopulation, the PSA level would ultimately decrease, thus decreasing the overall cost.

The effect of changes in  $\theta_i$ ,  $i = 3, \dots, 6$ , on the sensitivity of model parameters was analyzed next. As the values of  $\theta_i$ ,  $i = 3, \dots, 6$ , were progressively altered, two scenarios emerged: *Scenario A* - a set of model parameter values was found for which the evolution of the prostate tumor is permanently halted after one or two cycles of treatment, i.e., the simulated IAS therapy scheme is curative; *Scenario B* - a set of model parameter values was found for which the prostate tumor grows in an uncontrollable manner, i.e., the simulated IAS therapy scheme is ineffective. *Scenario A* occurred when  $\theta_3$  took on values that were at least 15% smaller than the nominal value given in (Liu et al., 2015), or when  $\theta_5$  took on values that were at least 30% smaller than the nominal value given in (Liu et al., 2015); no variations in either  $\theta_4$  or  $\theta_6$  lead to such scenario. On the other hand, *Scenario B* occurred when  $\theta_3$  took on values that were at least 15% higher than the nominal value given in (Liu et al.,

2015), or when  $\theta_4$  took on values that were at least 10% higher than the nominal value given in (Liu et al., 2015), or when  $\theta_5$  took on values that were at least 30% higher than the nominal value given in (Liu et al., 2015), or when  $\theta_6$  took on values that were at least 10% smaller than the nominal value given in (Liu et al., 2015).

In practical terms, the above results reinforce the importance of *customizing* treatment schemes to individual patients. In fact, if the optimal IAS therapy (designed using the model of Patient #15) were applied to a new patient whose HSC population dynamics are slower than those of Patient #15 (i.e., the new patient's HSC proliferation constant is at least 15% smaller than that of Patient #15; or the new patient's HSC apoptosis constant is at least 30% smaller than that of Patient #15), then the size of the new patient's tumor would remain stable and under control after at most two treatment cycles. On the other hand, if the optimal IAS therapy (designed using the model of Patient #15) were applied to a new patient whose HSC population dynamics are faster than those of Patient #15, then the size of the new patient's tumor would grow uncontrollably.

In our second set of simulations, we let  $\theta_1$  and  $\theta_2$  take suboptimal values and once again vary the values of  $\theta_i$ ,  $i = 3, \dots, 6$  (one at a time). Table 6.2 presents the sensitivity of the model parameters,  $\frac{dL}{d\theta_i}$ ,  $i = 3, \dots, 6$ , around the suboptimal configuration  $[\theta_1, \theta_2] = [7.5, 15.0]$  for the values of  $\theta_1$ ,  $i = 3, \dots, 6$ , fitted to the model of Patient #15 in (Liu et al., 2015).

Once again, the effect of changes in  $\theta_i$ ,  $i = 3, \dots, 6$ , on the sensitivity of model



**Table 6.2:** Sensitivity of model parameters around a suboptimal therapy configuration

$\frac{dL}{d\theta_3}$	$\frac{dL}{d\theta_4}$	$\frac{dL}{d\theta_5}$	$\frac{dL}{d\theta_6}$
17.78	0.014	-17.15	-0.016

parameters was analyzed. *Scenario A* occurred when  $\theta_3$  took on values that were at least 10% smaller than the nominal value given in (Liu et al., 2015), or when  $\theta_5$  took on values that were at least 20% larger than the nominal value given in (Liu et al., 2015); no variations in either  $\theta_4$  or  $\theta_6$  lead to such scenario. Moreover, *Scenario B* did not emerge in any of the simulations performed under this suboptimal configuration.

In our third set of simulations, we investigate the behavior of the model parameter sensitivities,  $\frac{dL}{d\theta_i}$ ,  $i = 3, \dots, 6$ , across different PSA threshold settings. In particular, we study how the sensitivity values change as we move from an optimal therapy setting towards various suboptimal settings. For such, we let  $\theta_i$ ,  $i = 3, \dots, 6$ , take the nominal values given in (Liu et al., 2015) and vary the values of the lower and upper PSA thresholds along  $[\theta_1^{\min}, \theta_1^{\max}]$  and  $[\theta_2^{\min}, \theta_2^{\max}]$ , respectively.

Figures 6·1-6·4 show how the values of the sensitivities  $\frac{dL}{d\theta_i}$ ,  $i = 3, \dots, 6$ , vary as a function of the values of the lower and upper PSA thresholds ( $\theta_1$  and  $\theta_2$ , respectively) for the model of Patient #15.

Figures 6·5-6·8 show how the values of the sensitivities  $\frac{dL}{d\theta_i}$ ,  $i = 3, \dots, 6$ , vary as a function of the values of the lower and upper PSA thresholds ( $\theta_1$  and  $\theta_2$ , respectively) for the model of Patient #1.

The above results lend themselves to the following discussion: first, the values

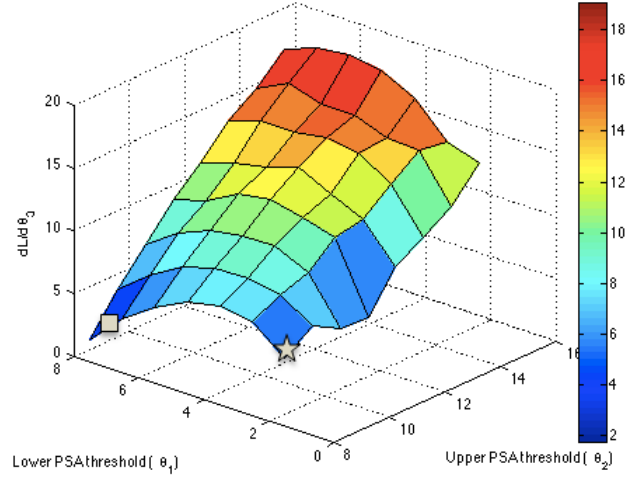


**Figure 6.1:** Sensitivity of  $\theta_3$  as a function of the values of  $\theta_1$  and  $\theta_2$  (Patient #15)

of the model parameter sensitivities,  $\frac{dL}{d\theta_i}$ ,  $i = 3, \dots, 6$ , are neither monotonically increasing nor monotonically decreasing along the allowable ranges of  $\theta_1$  and  $\theta_2$ ; this is verified for both patients. Second, the system is more sensitive to parameters  $\theta_3$  and  $\theta_5$  (HSC proliferation and apoptosis constants, respectively), and more robust to  $\theta_4$  and  $\theta_6$  (CRC proliferation and apoptosis constants, respectively); again this is verified across different patients. A possible explanation for this has to do with the fact that HSCs are commonly assumed to be the dominant subpopulation in a prostate tumor undergoing IAS therapy, which means that the size of this subpopulation has a greater impact on the overall size of the tumor and, consequently, on the value of the PSA level.

Additionally, note that two points are marked in Figures 6.1-6.5: a star marks the optimal therapy configuration and a square marks the values of  $\theta_1$  and  $\theta_2$  for

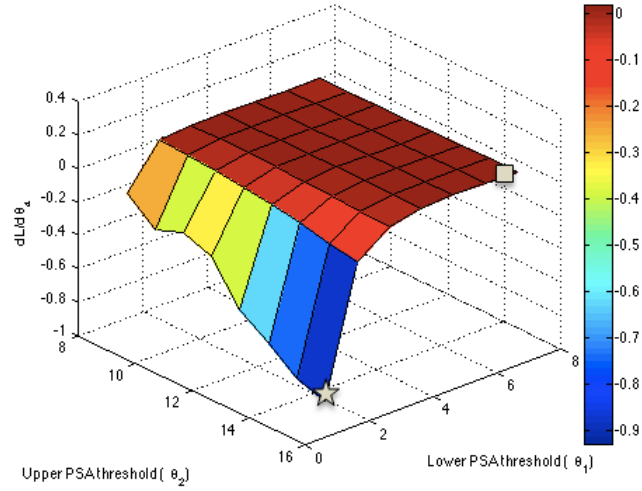


**Figure 6.2:** Sensitivity of  $\theta_4$  as a function of the values of  $\theta_1$  and  $\theta_2$  (Patient #15)

which the sensitivities  $\frac{dL}{d\theta_i}$ ,  $i = 3, \dots, 6$ , are minimal. In Section 5.3, the optimal therapy configurations were found to be  $[\theta_1^*, \theta_2^*] = [1.5, 8.0]$  for Patient #15 and  $[\theta_1^*, \theta_2^*] = [2.5, 8.0]$  for Patient #1. As it can be seen in Figures 6.1-6.5, these settings are not located in the regions of minimum sensitivities. Of note, the sensitivities  $\frac{dL}{d\theta_i}$ ,  $i = 3, \dots, 6$ , take their minimum value at the same suboptimal configuration (namely  $[\theta_1, \theta_2] = [7.5, 8.0]$ ) across different patients. This could potentially point to the existence of an underlying, and most likely as of yet poorly understood, equilibrium of cancer cell subpopulation dynamics at this suboptimal setting.

Moreover, the tradeoff between system fragility and optimality seems more strongly applicable to  $\theta_1$ , and less so to  $\theta_2$ ; interestingly, the value of  $\theta_1^*$  differed across patients, while  $\theta_2^*$  did not. In this sense, relaxing the optimality condition in favor of increased system robustness could potentially be worthwhile in at least some cases. In fact, for

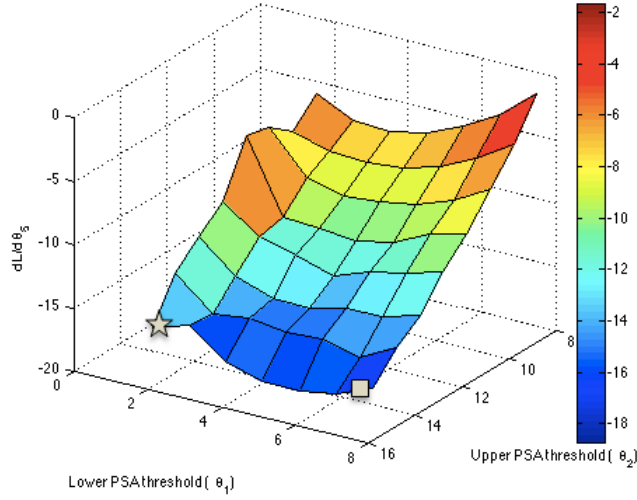


**Figure 6.3:** Sensitivity of  $\theta_5$  as a function of the values of  $\theta_1$  and  $\theta_2$  (Patient #15)

Patient #1, moving from an optimal therapy setting to a slightly suboptimal setting along  $\theta_2$  (namely  $[\theta_1, \theta_2] = [2.5, 9.0]$ ) leads to a 9% increase in the cost of treatment. However, the model parameter sensitivities at this setting decrease by approximately 30% for  $\theta_3$  and  $\theta_5$  and by approximately 70% for  $\theta_4$  and  $\theta_6$ . If we move to a suboptimal setting along  $\theta_1$  (namely  $[\theta_1, \theta_2] = [3.5, 8.0]$ ), the cost increases by 16%, while the sensitivities decrease by approximately 50% for  $\theta_3$  and  $\theta_5$  and by approximately 90% for  $\theta_4$  and  $\theta_6$ . In this case, it seems advantageous to tradeoff optimality for increased robustness.

It is interesting to note that the above analysis is not consistently verified across different patients. In fact, for Patient #15, a marked decrease in system fragility only occurs when we move to a suboptimal setting along  $\theta_1$  (namely  $[\theta_1, \theta_2] = [7.5, 8.0]$ ), at which point the sensitivities decrease by approximately 70% for  $\theta_3$  and  $\theta_5$  and by

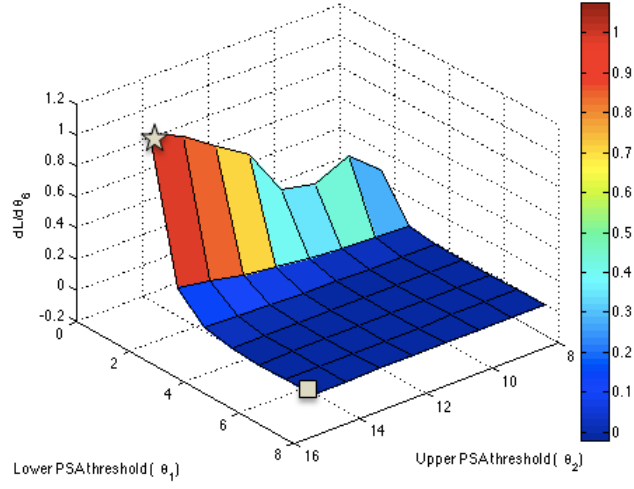


**Figure 6.4:** Sensitivity of  $\theta_6$  as a function of the values of  $\theta_1$  and  $\theta_2$  (Patient #15)

approximately 99% for  $\theta_4$  and  $\theta_6$ . However, there is an increase in the cost value of the order of 70%, which indicates that system optimality is significantly compromised. These results highlight the importance of applying our methodology on a patient-by-patient basis. More generally, they validate recent efforts favoring the development of *personalized* cancer therapies, as opposed to traditional treatment schemes that are typically generated over a cohort of patients and thus effective only on average.

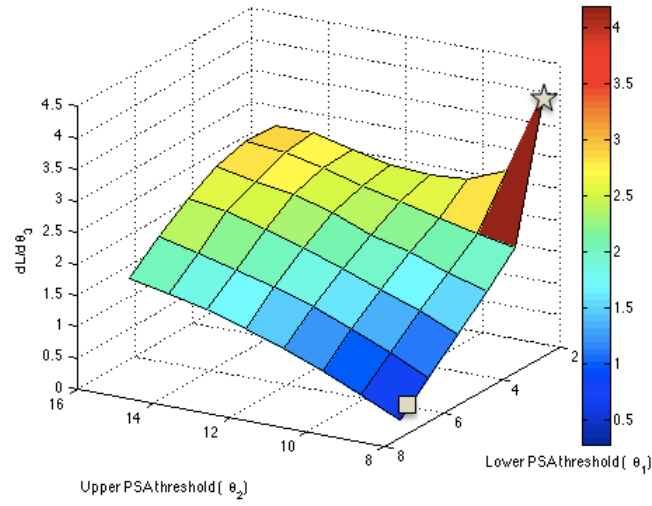


**Figure 6·5:** Sensitivity of  $\theta_3$  as a function of the values of  $\theta_1$  and  $\theta_2$  (Patient #1)

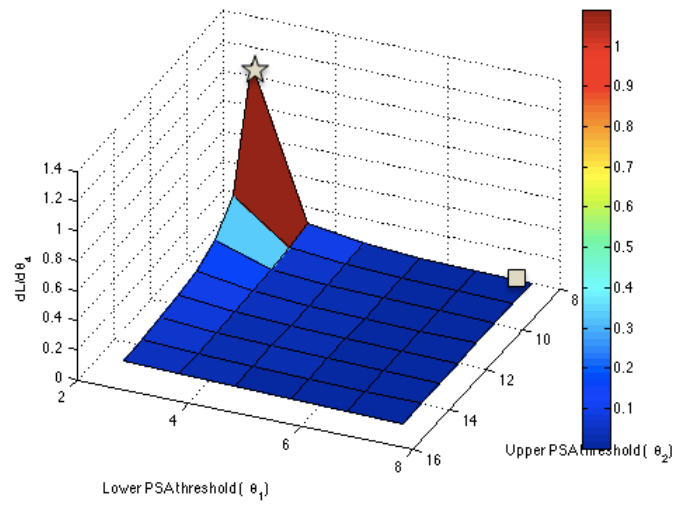


**Figure 6·6:** Sensitivity of  $\theta_4$  as a function of the values of  $\theta_1$  and  $\theta_2$  (Patient #1)

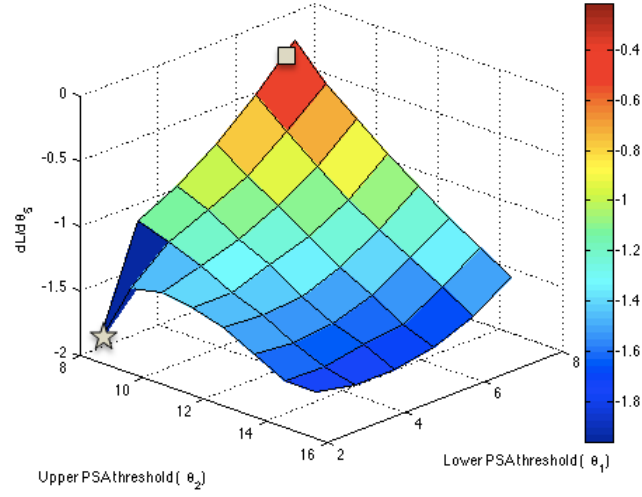


**Figure 6.7:** Sensitivity of  $\theta_5$  as a function of the values of  $\theta_1$  and  $\theta_2$  (Patient #1)

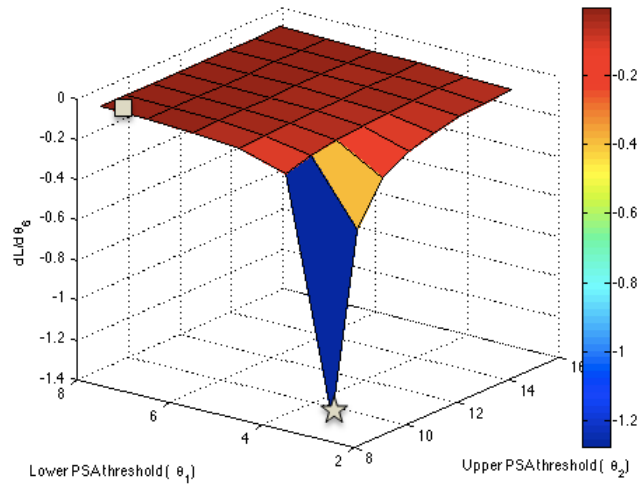


**Figure 6.8:** Sensitivity of  $\theta_6$  as a function of the values of  $\theta_1$  and  $\theta_2$  (Patient #1)

## Chapter 7

# Conclusion

In the first part of this work, we modeled a single traffic light intersection as a Stochastic Flow Model (SFM) and formulated the corresponding Traffic Light Control (TLC) problem within a quasi-dynamic control setting to which Infinitesimal Perturbation Analysis (IPA) techniques were applied in order to derive gradient estimates of a cost metric with respect to controllable parameters of interest. We initially defined the controllable parameters to be the queue content threshold values and, by incorporating the corresponding IPA estimators into a gradient-based optimization algorithm, obtained a considerable reduction in the mean queue content of both roads with respect to a static IPA-based control approach. We subsequently derived IPA estimators necessary for simultaneously controlling the light cycle lengths and queue content thresholds. By applying this methodology to a simulated urban setting consisting of an isolated intersection, we were able to consistently reduce traffic build-up by approximately half of that under static control.

The second part of this work entailed the problem of controlling cancer progression and its formulation within a Stochastic Hybrid Automaton (SHA) framework. Leveraging the fact that cell-biologic changes necessary for cancer development may



be schematized as a series of discrete steps, we proposed an integrative closed-loop framework for describing the progressive development of cancer and determining optimal personalized therapies. Our contributions to this end were twofold: first, we addressed the problem of cancer heterogeneity by proposing a novel Mixed Integer Linear Program (MILP) formulation that integrated somatic mutation and gene expression data. We tested this formulation using both simulated and real breast cancer data from The Cancer Genome Atlas (TCGA). By applying our MILP, we were able to infer the order in which genes mutate and, simultaneously, the changes they produce at the gene expression level during cancer progression. Additionally, we identified known causal relationships between mutations and gene expression changes in important breast cancer pathways. Second, we proposed a methodology applicable to stochastic models of cancer progression and illustrated our analysis with a case study of optimal Intermittent Androgen Suppression (IAS) therapy design for advanced prostate cancer. We developed a threshold-based policy for optimal IAS therapy design that is parameterized by lower and upper Prostate-Specific Antigen (PSA) threshold values and is associated with a cost metric that combines clinically relevant measures of therapy success. Results obtained by applying this methodology to clinical data from real prostate cancer patients suggest that optimal IAS treatment schemes are those in which both the lower and upper PSA thresholds take values as small as possible.

We subsequently extended our analysis to explore the tradeoff between system

optimality and robustness (or, equivalently, fragility), thus providing valuable insights on modeling and control of cancer progression. We performed sensitivity analysis with regards to the proliferation and apoptosis constants of the Hormone Sensitive Cell (HSC) and Castration Resistant Cell (CRC) subpopulations and found the system to be more sensitive to changes in the HSC constants than changes in the CRC constants. Moreover, we also identified a set of model parameter values for which the simulated IAS therapy scheme is essentially curative, as well as a set of parameter values for which the prostate tumor grows in an uncontrollable manner. Finally, assuming that an underlying, and most likely poorly understood, equilibrium of cancer cell subpopulation dynamics exists at suboptimal therapy settings, we found that relaxing the optimality condition in favor of increased robustness to modeling errors provides an alternative objective to therapy design for at least some patients.

## 7.1 Future Directions

In what follows, an outline is given of future research possibilities that extend the work presented in this thesis.

***Quasi-dynamic TLC.*** Possible future research directions include extending the proposed controller to incorporate bidirectional and left/right turn traffic, as well as acceleration/deceleration due to light switches. Assuming that traffic lights can communicate with each other, it is also possible to extend our methodology to a network of multiple intersections, in which a downstream

light is endowed with the ability to predict an impending flow of vehicles and adjust its light cycle within the proposed quasi-dynamic framework. Finally, it is worth acknowledging the emergence of a virtual traffic light setting (Dressler et al., 2014), in which case IPA techniques are equally applicable to the switching control of a virtual rather than actual traffic light.

***Modeling and Control of Cancer Progression.*** Possible future research directions include extending our MILP formulation to other sets of genes of interest, as well as other types of cancer. For instance, cancer data sets that provide somatic mutation and gene expression measurements of the same patient, such as TCGA colorectal cancer, glioblastoma, lung squamous cell carcinoma, and ovarian cancer could be analyzed. It would also be worthwhile to leverage the temporal sequence of events proposed by our MILP formulation by correlating it with additional patient data. In particular, it would be interesting to study whether meaningful correlations can be detected between our proposed phases of cancer progression and e.g., patient survival rates. Moreover, it is also possible to extend the SHA framework presented in Chapter 5 to analyze different potentially interesting controllable parameters, such as different drugs and/or dosages, in order to yield information on the effect of e.g., mixing different medication components or timing therapy periods, on the overall effectiveness of the treatment. Given that there exist several other potentially critical parameters in our SHA model of prostate cancer evolution, extending the sensitivity anal-

ysis study to other model parameters constitutes an additional future research topic. Finally, it would also be interesting to extend our methodology not only to other types of cancer, but also to other diseases that are known to progress in stages (e.g., tuberculosis).

## Appendix A

# IPA for Stochastic Hybrid Systems

We present here an introduction to Infinitesimal Perturbation Analysis (IPA) in the setting of Stochastic Hybrid Systems (SHS), as introduced in (Wardi et al., 2010),(Cassandras et al., 2010). Since an SHS is frequently described by means of a Stochastic Hybrid Automaton (SHA), we begin by defining an SHA and then proceed to contextualize the use of IPA within this framework.

An SHA may be obtained from a timed automaton with guards by replacing its clock structure with time-driven dynamics characterizing continuous state variables (Cassandras and Lafortune, 2008). There are generally several ways in which we can incorporate randomness into a hybrid automaton model: we may describe the time-driven dynamics through stochastic differential equations; we may define a stochastic clock structure for the events that control discrete state transitions; we may determine the next mode (resulting from a state transition) probabilistically. In this context, an SHA is defined as the eleventuple

$$G = (Q, X, E, U, f, \phi, Inv, guard, \rho, q_0, \mathbf{x}_0)$$

where

$Q \subset \mathbb{Z}^+$  is a set of discrete states;  
 $X$  is a continuous state space;  
 $E$  is a finite set of events;  
 $U$  is a set of admissible controls;  
 $f$  is a continuous vector field,  $f : Q \times X \times U \rightarrow X$ ;  
 $\phi$  is a discrete state transition function,  $\phi : Q \times X \times E \rightarrow Q$ ;  
 $Inv$  is a set defining an invariant condition,  $Inv \subseteq Q \times X \times U$ ;  
 $guard$  is a set defining a guard condition,  $guard \subseteq Q \times Q \times X$ ;  
 $\rho$  is a reset function,  $\rho : Q \times Q \times X \times E \rightarrow X$ ;  
 $q_0$  is an initial discrete state;  
 $\mathbf{x}_0$  is an initial continuous state.

Let us define  $\theta \in \Theta$  to be the control parameter vector of  $G$ , where  $\Theta \subset \mathbb{R}^n$  is a compact and convex set. As such,  $\theta$  may denote a system design parameter, a parameter of the underlying stochastic processes, or a parameter that characterizes the system's control policy. In the ensuing analysis, we assume that all stochastic processes are defined over a common probability space  $(\Omega, F, P)$ . For any given value of  $\theta$ , we can generate a sample path of the SHS, denoted by  $\omega \in \Omega$ , over a time interval  $[0, T]$ . We can further denote the event times on this sample path  $\omega$  by  $\tau_k(\theta, \omega)$ ,  $k = 1, 2, \dots$ , which we will write as  $\tau_k$  when no confusion arises. Over any interevent interval  $[\tau_k, \tau_{k+1})$  the system remains at a given state  $q_k \in Q$  and evolves according to continuous dynamics of the form

$$\dot{x} = f_k(x, u, \theta, t) \tag{A.1}$$

where  $\dot{x} \equiv \frac{dx}{dt}$ . In this context, IPA efficiently captures how changes in  $\theta$  affect the event times and the state of the SHA, and can ultimately be used to infer the effect

that a perturbation in  $\theta$  will have on the system's performance.

When an event takes place at time  $\tau_{k+1}$ , the system enters a new state  $q_{k+1}$ , but such discrete state transition may not be accompanied by a change in the system's continuous dynamics. For instance, the system's performance may be measured differently in state  $q_{k+1}$ , while  $f_{k+1} = f_k$ . Furthermore, the interactions between time-driven and event-driven system dynamics depend not only on the event times, but also on the types of events that occur. In the case of a linearized system, such interactions will be shown to depend on the derivatives of the event times with respect to the control parameters, i.e.  $\frac{\partial \tau_k}{\partial \theta}$ . Due to the fact that variations in  $\theta$  may change the sequence of events, such event time derivatives are generally not continuous in  $\theta$  for all  $\theta \in \Theta$ . Nevertheless, it is shown in (Cassandras and Lafortune, 2008) that the derivatives  $\frac{\partial \tau_k}{\partial \theta}$  exist w.p.1 under mild technical conditions, and we will discuss this in greater depth further on.

Now consider the performance function of the control parameter  $\theta$  to be

$$J(T, \theta, x(0, \theta)) = E_{\omega} [L(T, \theta, x(0, \omega), \omega)] \quad (\text{A.2})$$

where  $L(T, \theta, x(0, \omega), \omega)$  is a sample cost function of interest evaluated over  $[0, T]$  with initial conditions  $x(0, \omega)$ . For notational simplicity, we will write  $L(\theta)$  and  $J(\theta)$ . Let us further assume that all underlying input stochastic processes are piecewise

continuously differentiable w.p. 1, so that we can write

$$L(\theta) = \sum_{k=0}^N \int_{\tau_k}^{\tau_{k+1}} L_k(t, x, \theta) dt \quad (\text{A.3})$$

where  $N$  corresponds to the number of events occurring in the interval  $[0, T]$ , so that  $\tau_0 = 0$  and  $\tau_{N+1} = T$ . At this point it is important to mention that it is also possible to consider free-time cost functions, and that we restrict our analysis of  $J(\theta)$  to a finite horizon  $T$  for simplicity. We also note that it is infeasible to derive a closed-form expression of  $J(\theta)$  without full knowledge of the random processes that characterize the discrete or continuous disturbance inputs in the SHA model. As a result, the search for optimality must be driven by estimates of the cost function gradient with respect to the parameter of interest, i.e. we must rely on estimating  $\frac{dJ(\theta)}{d\theta}$  based on sample path data. Such gradient estimates can then be used to improve current operating conditions or (under certain conditions) to compute an optimal  $\theta^*$  through an iterative optimization algorithm of the form

$$\theta_{n+1} = \theta_n - \rho_n H_n(\theta_n, x(0, \theta), T, \omega_n), \quad n = 0, 1, \dots \quad (\text{A.4})$$

where  $\rho_n$  is the step size at the  $n$ th iteration and  $\omega_n$  denotes a sample path from which data are extracted and used to compute  $H_n(\cdot)$ , which is an estimate of  $\frac{dJ(\theta)}{d\theta}$ . The success of the IPA approach relies, however, on the unbiasedness of  $\frac{dL(\theta)}{d\theta}$ , i.e. on the following condition:

$$\mathbb{E} \left[ \frac{dL(\theta, \omega)}{d\theta} \right] = \frac{d\mathbb{E}[L(\theta, \omega)]}{d\theta} = \frac{dJ(\theta)}{d\theta} \quad (\text{A.5})$$



In the case of an SHS, the unbiasedness condition (A.5) is guaranteed under the following assumptions:

**Assumption A.1** *W.p. 1 all underlying input stochastic processes are piecewise analytic in the interval  $[0, T]$ .*

**Assumption A.2** *W.p. 1 and for every  $\theta \in \Theta$ , two events cannot occur at exactly the same time, unless the occurrence of one causes the other to take place at the same time.*

**Assumption A.3** *W.p. 1 there is a finite number of events observed in the sample path.*

Throughout the work presented in this thesis, we assume that the above assumptions hold, so that our IPA estimators are unbiased estimators of  $\frac{dJ(\theta)}{d\theta}$ . Let us then denote the state and event time derivatives with respect to parameter  $\theta$  as

$$x'(\theta, t) \equiv \frac{\partial x(t, \theta)}{\partial \theta}, \tau'_k(\theta) \equiv \frac{\partial \tau_k(\theta)}{\partial \theta}, k = 0, \dots, N \quad (\text{A.6})$$

Although  $\theta$  is included as an argument in the expressions above to stress the dependence on the control parameter, we will subsequently drop this for ease of notation as long as no confusion arises. The dynamics of  $x(t)$  are fixed over any interevent interval  $[\tau_k, \tau_{k+1})$ , so that taking derivatives of (A.1) with respect to  $\theta$  yields

$$\frac{d}{dt}x'(t) = \frac{\partial f_k(t)}{\partial x}x'(t) + \frac{\partial f_k(t)}{\partial \theta} \quad (\text{A.7})$$

with the following boundary condition (Cassandras et al., 2010):

$$x'(\tau_k^+) = x'(\tau_k^-) + [f_{k-1}(\tau_k^-) - f_k(\tau_k^+)] \cdot \tau'_k \quad (\text{A.8})$$

when  $x(\theta, t)$  is continuous in  $t$  at  $t = \tau_k$ . Otherwise,

$$x'(\tau_k^+) = \frac{d\rho(q, q', x, e)}{d\theta} \quad (\text{A.9})$$

where  $\rho(q, q', x, e)$  is the reset function defined in (A).

Given the initial condition  $x'(\tau_k^+)$ , it is possible to solve (A.7) and thus compute the linearized state trajectory  $x'(t)$  over  $[\tau_k, \tau_{k+1})$  as follows:

$$x'(t) = e^{\int_{\tau_k}^t \frac{\partial f_k(s)}{\partial x} ds} \left[ \int_{\tau_k}^t \frac{\partial f_k(v)}{\partial \theta} e^{-\int_{\tau_k}^v \frac{\partial f_k(\tau)}{\partial x} d\tau} dv + x'(\tau_k^+) \right] \quad (\text{A.10})$$

In order to evaluate (A.8), we must first determine  $\tau'_k$ , whose expression depends on the type of event that takes place at time  $\tau_k$ . As detailed in (Cassandras et al., 2010), the following three types of events are defined for a general SHS:

(i) *Exogenous Events*. These events are typically associated with the occurrence of uncontrolled random changes in the input processes. Exogenous events cause a discrete state transition which is independent of parameter  $\theta$  and, as a result,

$$\tau'_k = 0 \quad (\text{A.11})$$

(ii) *Endogenous Events*. In this case, there exists a continuously differentiable function  $g_k : \mathbb{R}^+ \times X \times \Theta \rightarrow \mathbb{R}$  such that  $\tau_k = \min \{t > \tau_{k-1} : g_k(t, x, \theta) = 0\}$ , where the function  $g_k$  usually corresponds to a guard condition in a hybrid automaton. Taking derivatives with respect to  $\theta$ , it is straightforward to obtain

$$\tau'_k = - \left[ \frac{\partial g_k}{\partial x} f_{k-1}(\tau_k^-) \right]^{-1} \left( \frac{\partial g_k}{\partial \theta} + \frac{\partial g_k}{\partial x} x'(\tau_k^-) \right) \quad (\text{A.12})$$

with  $\frac{\partial g_k}{\partial x} f_{k-1}(\tau_k^-) \neq 0$ .

(iii) *Induced Events.* Such an event occurs at time  $\tau_k$  if it is triggered by the occurrence of another event at time  $\tau_m \leq \tau_k$ , so that the expression of  $\tau'_k$  depends on that of  $\tau'_m$  (details can be found in (Cassandras et al., 2010)).

As a result, IPA estimators of  $\frac{dJ(\theta)}{d\theta}$  may be obtained by differentiating (A.3) with respect to  $\theta$  as follows:

$$\frac{dL(\theta)}{d\theta} = \sum_{k=0}^N \frac{d}{d\theta} \int_{\tau_k}^{\tau_{k+1}} L_k(t, x, \theta) dt$$

so that, applying the Leibnitz rule for  $k = 0, \dots, K$ , we obtain

$$\begin{aligned} \frac{dL(\theta)}{d\theta} &= \sum_{k=0}^N \left[ L_k(\tau_{k+1}, x, \theta) \tau'_{k+1} - L_k(\tau_k, x, \theta) \tau'_k \right] \\ &\quad + \sum_{k=0}^N \int_{\tau_k}^{\tau_{k+1}} \left[ \frac{\partial L_k}{\partial x}(t, x, \theta) x'(t) + \frac{\partial L_k}{\partial \theta}(t, x, \theta) \right] dt \end{aligned} \quad (\text{A.13})$$

In the case of an SHS, the IPA estimator given by (A.13) can often be greatly simplified. For one, under the conditions given in Lemma A.1 (Yao and Cassandras, 2011b), only the first part of (A.13) needs to be computed. Additionally, if Lemma A.2 is also satisfied, it may be possible to evaluate  $x'(\tau_k^+)$  without knowledge of the state trajectory prior to time  $\tau_k$ . Finally, as will be discussed later, the perturbation process may eventually be reset, meaning that the effect of  $\theta$  is forgotten, i.e.  $x'(\tau_k^+) = 0$ , which considerably simplifies the bookkeeping required for computing the gradient estimate.

**Lemma A.1** *If condition (i) or (ii) below holds,  $\frac{dL(\theta)}{d\theta}$  depends only on information available at even times  $\tau_k$ ,  $k = 0, \dots, K$ :*

(i)  $L_k(t, x, \theta)$  is independent of  $t$  over  $[\tau_k, \tau_{k+1})$  for all  $k = 0, \dots, N$ .

(ii)  $L_k(t, x, \theta)$  is only a function of  $x$  and the following condition holds for all  $t \in [\tau_k, \tau_{k+1})$ ,  $k = 0, \dots, N$ :

$$\frac{d}{dt} \frac{\partial l_k}{\partial x} = \frac{d}{dt} \frac{\partial f_k}{\partial x} = \frac{d}{dt} \frac{\partial f_k}{\partial \theta} = 0$$

**Lemma A.2** Suppose an endogenous event with switching function  $g_k(x, \theta)$  occurs at event time  $\tau_k$ . If  $f_k(\tau_k^+) = 0$ , then  $x'(\tau_k^+)$  is independent of  $f_{k-1}$ . If, in addition,  $\frac{\partial g_k}{\partial \theta} = 0$ , we have that  $x'(\tau_k^+) = 0$ .

## Appendix B

# IPA Algorithm for TLC with Fixed Light Cycles

The IPA algorithm developed for the TLC problem with fixed light cycle lengths is presented below.

**if** EVENT  $\zeta_1$

1. Estimate  $\alpha_1(\tau_k)$
2. Compute event time derivatives

$$\tau'_{k,1} = \frac{1-x'_{1,1}(\tau_k^-)}{\alpha_1(\tau_k)}$$

$$\tau'_{r,2} = -\frac{x'_{1,2}(\tau_k^-)}{\alpha_1(\tau_k)}$$

3. Check conditions for light switch ( $R2G_1/G2R_2$ )

**if**  $x_1 \geq s_1$  and  $x_2 < s_2$  and  $z_2 > \theta_{2,\min}$

- 3.1. Update  $\sigma$ -dynamics

$$\sigma'_{j,1} = \tau'_{k,1}$$

$$\sigma'_{j,2} = \tau'_{k,2}$$

- 3.2. Update state derivatives

$$x'_{1,1}(\tau_k^+) = x'_{1,1}(\tau_k^-) + h_1 \cdot \sigma'_{j,1}$$

$$x'_{1,2}(\tau_k^+) = x'_{1,2}(\tau_k^-) + h_1 \cdot \sigma'_{j,2}$$

*if* road 2 in *NEP*

$$x'_{2,1}(\tau_k^+) = x'_{2,1}(\tau_k^-) - h_2 \cdot \sigma'_{j,1}$$

$$x'_{2,2}(\tau_k^+) = x'_{2,2}(\tau_k^-) - h_2 \cdot \sigma'_{j,2}$$

*if* road 2 in *EP*

Estimate  $\alpha_2(\tau_k)$

$$x'_{2,1}(\tau_k^+) = x'_{2,1}(\tau_k^-) - \alpha_2(\tau_k) \cdot \sigma'_{j,1}$$

$$x'_{2,2}(\tau_k^+) = x'_{2,2}(\tau_k^-) - \alpha_2(\tau_k) \cdot \sigma'_{j,2}$$

**if** EVENT  $\zeta_2$

1. Estimate  $\alpha_2(\tau_k)$

2. Compute event time derivatives

$$\tau'_{k,1} = -\frac{x'_{2,1}(\tau_k^-)}{\alpha_2(\tau_k)}$$

$$\tau'_{r,2} = \frac{1-x'_{2,2}(\tau_k^-)}{\alpha_2(\tau_k)}$$

3. Check conditions for light switch ( $G2R_1/R2G_2$ )

**if**  $x_1 < s_1$  and  $x_2 \geq s_2$  and  $z_1 > \theta_{1,\min}$

3.1. Update  $\sigma$ -dynamics

$$\sigma'_{j,1} = \tau'_{k,1}$$

$$\sigma'_{j,2} = \tau'_{k,2}$$

3.2. Update state derivatives

*if* road 1 in  $NEP$

$$x'_{1,1}(\tau_k^+) = x'_{1,1}(\tau_k^-) - h_1 \cdot \sigma'_{j,1}$$

$$x'_{1,2}(\tau_k^+) = x'_{1,2}(\tau_k^-) - h_1 \cdot \sigma'_{j,2}$$

*if* road 1 in  $EP$

Estimate  $\alpha_1(\tau_k)$

$$x'_{1,1}(\tau_k^+) = x'_{1,1}(\tau_k^-) - \alpha_1(\tau_k) \cdot \sigma'_{j,1}$$

$$x'_{1,2}(\tau_k^+) = x'_{1,2}(\tau_k^-) - \alpha_1(\tau_k) \cdot \sigma'_{j,2}$$

$$x'_{2,1}(\tau_k^+) = x'_{2,1}(\tau_k^-) + h_2 \cdot \sigma'_{j,1}$$

$$x'_{2,2}(\tau_k^+) = x'_{2,2}(\tau_k^-) + h_2 \cdot \sigma'_{j,2}$$

**if** EVENT  $\gamma_1$

1. Estimate  $\alpha_1(\tau_k)$
2. Compute event time derivatives

$$\tau'_{k,1} = \frac{1 - x'_{1,1}(\tau_k^-)}{\alpha_1(\tau_k) - h_1}$$

$$\tau'_{r,2} = -\frac{x'_{1,2}(\tau_k^-)}{\alpha_1(\tau_k) - h_1}$$

3. Check conditions for light switch ( $G2R_1/R2G_2$ )

**if**  $x_1 < s_1$  and  $x_2 \geq s_2$  and  $z_1 > \theta_{1,\min}$

3.1. Update  $\sigma$ -dynamics

$$\sigma'_{j,1} = \tau'_{k,1}$$

$$\sigma'_{j,2} = \tau'_{k,2}$$

3.2. Update state derivatives

$$x'_{1,1}(\tau_k^+) = x'_{1,1}(\tau_k^-) - h_1 \cdot \sigma'_{j,1}$$

$$x'_{1,2}(\tau_k^+) = x'_{1,2}(\tau_k^-) - h_1 \cdot \sigma'_{j,2}$$

$$x'_{2,1}(\tau_k^+) = x'_{2,1}(\tau_k^-) + h_2 \cdot \sigma'_{j,1}$$

$$x'_{2,2}(\tau_k^+) = x'_{2,2}(\tau_k^-) + h_2 \cdot \sigma'_{j,2}$$

**if** EVENT  $\gamma_2$

1. Estimate  $\alpha_2(\tau_k)$

2. Compute event time derivatives

$$\tau'_{k,1} = -\frac{x'_{2,1}(\tau_k^-)}{\alpha_2(\tau_k) - h_2}$$

$$\tau'_{r,2} = \frac{1 - x'_{2,2}(\tau_k^-)}{\alpha_2(\tau_k) - h_2}$$

3. Check conditions for light switch ( $R2G_1/G2R_2$ )

**if**  $x_1 \geq s_1$  and  $x_2 < s_2$  and  $z_2 > \theta_{2,\min}$

3.1. Update  $\sigma$ -dynamics

$$\sigma'_{j,1} = \tau'_{k,1}$$

$$\sigma'_{j,2} = \tau'_{k,2}$$

3.2. Update state derivatives

$$x'_{1,1}(\tau_k^+) = x'_{1,1}(\tau_k^-) + h_1 \cdot \sigma'_{j,1}$$

$$x'_{1,2}(\tau_k^+) = x'_{1,2}(\tau_k^-) + h_1 \cdot \sigma'_{j,2}$$

$$x'_{2,1}(\tau_k^+) = x'_{2,1}(\tau_k^-) - h_2 \cdot \sigma'_{j,1}$$

$$x'_{2,2}(\tau_k^+) = x'_{2,2}(\tau_k^-) - h_2 \cdot \sigma'_{j,2}$$



**if** EVENT  $\lambda_1$

1. Check conditions for light switch ( $G2R_1/R2G_2$ )

**if**  $x_1 < s_1$  and  $x_2 \geq s_2$  and  $z_1 > \theta_{1,\min}$

1.1. No change to  $\sigma$ -dynamics

$$\sigma'_{j,1} = \sigma'_{j-1,1}$$

$$\sigma'_{j,2} = \sigma'_{j-1,2}$$

1.2. Update state derivatives

*if* road 1 in  $NEP$

$$x'_{1,1}(\tau_k^+) = x'_{1,1}(\tau_k^-) - h_1 \cdot \sigma'_{j,1}$$

$$x'_{1,2}(\tau_k^+) = x'_{1,2}(\tau_k^-) - h_1 \cdot \sigma'_{j,2}$$

*if* road 1 in  $EP$

Estimate  $\alpha_1(\tau_k)$

$$x'_{1,1}(\tau_k^+) = x'_{1,1}(\tau_k^-) - \alpha_1(\tau_k) \cdot \sigma'_{j,1}$$

$$x'_{1,2}(\tau_k^+) = x'_{1,2}(\tau_k^-) - \alpha_1(\tau_k) \cdot \sigma'_{j,2}$$

$$x'_{2,1}(\tau_k^+) = x'_{2,1}(\tau_k^-) + h_2 \cdot \sigma'_{j,1}$$

$$x'_{2,2}(\tau_k^+) = x'_{2,2}(\tau_k^-) + h_2 \cdot \sigma'_{j,2}$$

**if** EVENT  $\lambda_2$

1. Check conditions for light switch ( $R2G_1/G2R_2$ )

**if**  $x_1 \geq s_1$  and  $x_2 < s_2$  and  $z_2 > \theta_{2,\min}$

1.1. No change to  $\sigma$ -dynamics

$$\sigma'_{j,1} = \sigma'_{j-1,1}$$

$$\sigma'_{j,2} = \sigma'_{j-1,2}$$

## 1.2. Update state derivatives

$$x'_{1,1}(\tau_k^+) = x'_{1,1}(\tau_k^-) + h_1 \cdot \sigma'_{j,1}$$

$$x'_{1,2}(\tau_k^+) = x'_{1,2}(\tau_k^-) + h_1 \cdot \sigma'_{j,2}$$

*if* road 2 in  $NEP$

$$x'_{2,1}(\tau_k^+) = x'_{2,1}(\tau_k^-) - h_2 \cdot \sigma'_{j,1}$$

$$x'_{2,2}(\tau_k^+) = x'_{2,2}(\tau_k^-) - h_2 \cdot \sigma'_{j,2}$$

*if* road 2 in  $EP$

Estimate  $\alpha_2(\tau_k)$

$$x'_{2,1}(\tau_k^+) = x'_{2,1}(\tau_k^-) - \alpha_2(\tau_k) \cdot \sigma'_{j,1}$$

$$x'_{2,2}(\tau_k^+) = x'_{2,2}(\tau_k^-) - \alpha_2(\tau_k) \cdot \sigma'_{j,2}$$

**if** EVENT  $\mu_1(G2R_1/R2G_2)$

1. No change to  $\sigma$ -dynamics

$$\sigma'_{j,1} = \sigma'_{j-1,1}$$

$$\sigma'_{j,2} = \sigma'_{j-1,2}$$

## 2. Update state derivatives

*if* road 1 in  $NEP$

$$x'_{1,1}(\tau_k^+) = x'_{1,1}(\tau_k^-) - h_1 \cdot \sigma'_{j,1}$$

$$x'_{1,2}(\tau_k^+) = x'_{1,2}(\tau_k^-) - h_1 \cdot \sigma'_{j,2}$$

*if* road 1 in  $EP$

Estimate  $\alpha_1(\tau_k)$

$$x'_{1,1}(\tau_k^+) = x'_{1,1}(\tau_k^-) - \alpha_1(\tau_k) \cdot \sigma'_{j,1}$$

$$x'_{1,2}(\tau_k^+) = x'_{1,2}(\tau_k^-) - \alpha_1(\tau_k) \cdot \sigma'_{j,2}$$

*if* road 2 in  $NEP$

$$x'_{2,1}(\tau_k^+) = x'_{2,1}(\tau_k^-) + h_2 \cdot \sigma'_{j,1}$$

$$x'_{2,2}(\tau_k^+) = x'_{2,2}(\tau_k^-) + h_2 \cdot \sigma'_{j,2}$$

*if* road 2 in  $EP$

Estimate  $\alpha_2(\tau_k)$

$$x'_{2,1}(\tau_k^+) = x'_{2,1}(\tau_k^-) + \alpha_2(\tau_k) \cdot \sigma'_{j,1}$$

$$x'_{2,2}(\tau_k^+) = x'_{2,2}(\tau_k^-) + \alpha_2(\tau_k) \cdot \sigma'_{j,2}$$

**if** EVENT  $\mu_2(R2G_1/G2R_2)$

1. No change to  $\sigma$ -dynamics

$$\sigma'_{j,1} = \sigma'_{j-1,1}$$

$$\sigma'_{j,2} = \sigma'_{j-1,2}$$

2. Update state derivatives

*if* road 1 in  $NEP$

$$x'_{1,1}(\tau_k^+) = x'_{1,1}(\tau_k^-) + h_1 \cdot \sigma'_{j,1}$$

$$x'_{1,2}(\tau_k^+) = x'_{1,2}(\tau_k^-) + h_1 \cdot \sigma'_{j,2}$$

*if* road 1 in  $EP$

Estimate  $\alpha_1(\tau_k)$

$$x'_{1,1}(\tau_k^+) = x'_{1,1}(\tau_k^-) + \alpha_1(\tau_k) \cdot \sigma'_{j,1}$$

$$x'_{1,2}(\tau_k^+) = x'_{1,2}(\tau_k^-) + \alpha_1(\tau_k) \cdot \sigma'_{j,2}$$

*if* road 2 in  $NEP$

$$x'_{2,1}(\tau_k^+) = x'_{2,1}(\tau_k^-) - h_2 \cdot \sigma'_{j,1}$$

$$x'_{2,2}(\tau_k^+) = x'_{2,2}(\tau_k^-) - h_2 \cdot \sigma'_{j,2}$$

*if* road 2 in  $EP$

Estimate  $\alpha_2(\tau_k)$

$$x'_{2,1}(\tau_k^+) = x'_{2,1}(\tau_k^-) - \alpha_2(\tau_k) \cdot \sigma'_{j,1}$$

$$x'_{2,2}(\tau_k^+) = x'_{2,2}(\tau_k^-) - \alpha_2(\tau_k) \cdot \sigma'_{j,2}$$

## Appendix C

# Mathematical Proofs

### C.1 Chapter 2

#### C.1.1 Proof of Lemma 2.1

We begin with a  $G2R$  light switching event. This event is induced by one of four possible endogenous events, which we analyze separately in what follows.

1. *Event  $\zeta_1$  occurs at time  $\sigma_j$ .* In this case, a  $G2R_2$  event occurs, hence also an  $R2G_1$  event. Since road 1 must be undergoing a RED cycle within an NEP, it follows from (A.12) with  $g_j = x_1 - s_1$  and (2.6) that  $\sigma'_{j,1} = \frac{1-x'_{1,1}(\sigma_j^-)}{\alpha_1(\sigma_j)}$  and  $\sigma'_{j,2} = \frac{-x'_{1,2}(\sigma_j^-)}{\alpha_1(\sigma_j)}$ .

2. *Event  $\zeta_2$  occurs at time  $\sigma_j$ .* This results in a  $G2R_1$  event and the same reasoning as above applies to verify that  $\sigma'_{j,1} = \frac{-x'_{2,1}(\sigma_j^-)}{\alpha_2(\sigma_j)}$  and  $\sigma'_{j,2} = \frac{1-x'_{2,2}(\sigma_j^-)}{\alpha_2(\sigma_j)}$ .

3. *Event  $\gamma_1$  occurs at time  $\sigma_j$ .* This results in a  $G2R_1$  event. Moreover, since this a light switching event, it follows from (2.3) that  $x_1(\sigma_j^-) > s_1$  and  $x_1(\sigma_j) = s_1$ , which means that road 1 must be in an NEP with  $\beta_1(\sigma_j) > 0$ . As a result, it follows from (A.12) with  $g_j = x_1 - s_1$  and (2.6) that  $\sigma'_{j,1} = \frac{1-x'_{1,1}(\sigma_j^-)}{\alpha_1(\sigma_j)-h_1(\sigma_j)}$  and  $\sigma'_{j,2} = \frac{-x'_{1,2}(\sigma_j^-)}{\alpha_1(\sigma_j)-h_1(\sigma_j)}$ .

4. *Event  $\gamma_2$  occurs at time  $\sigma_j$ .* This results in a  $G2R_2$  event and the same reasoning as above applies to verify that  $\sigma'_{j,1} = \frac{-x'_{2,1}(\sigma_j^-)}{\alpha_2(\sigma_j)-h_2(\sigma_j)}$  and  $\sigma'_{j,2} = \frac{1-x'_{1,2}(\sigma_j^-)}{\alpha_2(\sigma_j)-h_2(\sigma_j)}$ .

5. *Event  $\lambda_n$ ,  $n = 1, 2$ , occurs at time  $\sigma_j$ .* Let  $\Delta_j = \sigma_j - \sigma_{j-1}$ ,  $j = 1, 2, \dots$ , where

(without loss of generality) we set  $\sigma_0 = 0$ . Therefore, we can write  $\sigma_j = \sigma_{j-1} + \Delta_j$ ,  $j = 1, 2, \dots$ . Recall that, by definition, whenever a light switching event is induced by  $\lambda_n$  we must have  $\Delta_j = \theta_{n,\min}$ , which is independent of  $s_1, s_2$ . Therefore,  $\sigma'_{j,i} = \sigma'_{j-1,i}$  for all  $j = 1, 2, \dots$  and  $i = 1, 2$ .

6. *Event  $\mu_n$ ,  $n = 1, 2$ , occurs at time  $\sigma_j$ .* This is similar to the previous case with  $\Delta_j = \theta_{n,\max}$  and once again we have  $\sigma'_{j,i} = \sigma'_{j-1,i}$  for all  $j = 1, 2, \dots$  and  $i = 1, 2$ .

This concludes the proof for a  $G2R_n$  light switching event. The analysis for an  $R2G_n$  event is similar, due to the fact that the end of a RED cycle on road  $n$  ( $R2G_n$  event) must coincide with the start of a RED cycle on road  $\bar{n}$  ( $G2R_{\bar{n}}$  event).

## C.2 Chapter 3

### C.2.1 Proof of Lemma 3.1

We begin by considering the occurrence of a  $G2R_n$  light switching event, which may be induced by one of four different endogenous events. Each of these cases will be analyzed separately in what follows.

1. *Event  $\zeta_1$  occurs at time  $\sigma_j$*

This is an endogenous event with  $g_j = x_1 - s_1 = 0$ , so that  $\frac{\partial g_j}{\partial x_1} = 1$ ,  $\frac{\partial g_j}{\partial v_5} = -1$ , and all remaining partial derivatives are equal to zero. Since  $x_1(\sigma_j^-) < s_1$  and  $x_1(\sigma_j^+) = s_1$ , road 1 is necessarily in NEP when this event takes place. Furthermore, the fact that road 1 is undergoing a RED cycle at time  $\sigma_j^-$  but will be undergoing a GREEN cycle at  $\sigma_j^+$  means that  $f_{1,j-1}(\sigma_j^-) = \alpha_1(\sigma_j)$  and  $f_{1,j}(\sigma_j^+) = \alpha_1(\sigma_j) - h_1(\sigma_j)$ . As a result, it

is simple to verify that (A.12) reduces to

$$\sigma'_{j,i} = \begin{cases} \frac{1-x'_{1,i}(\sigma_j^-)}{\alpha_1(\sigma_j)} & \text{if } i = 5 \\ -\frac{x'_{1,i}(\sigma_j^-)}{\alpha_1(\sigma_j)} & \text{otherwise} \end{cases} \quad (\text{C.1})$$

2. *Event  $\zeta_2$  occurs at time  $\sigma_j$*

This is an endogenous event with  $g_j = x_2 - s_2 = 0$ , resulting in a  $G2R_1$  event.

The same reasoning as above applies to verify that (A.12) becomes

$$\sigma'_{j,i} = \begin{cases} \frac{1-x'_{2,i}(\sigma_j^-)}{\alpha_2(\sigma_j)} & \text{if } i = 6 \\ -\frac{x'_{2,i}(\sigma_j^-)}{\alpha_2(\sigma_j)} & \text{otherwise} \end{cases} \quad (\text{C.2})$$

3. *Event  $\gamma_1$  occurs at time  $\sigma_j$*

This is an endogenous event with  $g_j = x_1 - s_1 = 0$ , resulting in a  $G2R_1$  event.

In order for this event to take place at time  $\sigma_j$ , we must have  $x_1(\sigma_j^-) > s_1$  and  $x_1(\sigma_j^+) = s_1$ , which means that road 1 must be in an NEP with outflow. Furthermore, the occurrence of this event will only induce a light switch if  $x_2(\sigma_j) \geq s_2$ , which means that road 2 must also be in NEP at  $\sigma_j$ . Since road 1 is undergoing a GREEN cycle at time  $\sigma_j^-$  but will be undergoing a RED cycle at  $\sigma_j^+$ , we will have that  $f_{1,j-1}(\sigma_j^-) = \alpha_1(\sigma_j) - h_1(\sigma_j)$  and  $f_{1,j}(\sigma_j^+) = \alpha_1(\sigma_j)$ . As a result, (A.12) can be seen to become

$$\sigma'_{j,i} = \begin{cases} \frac{1-x'_{1,i}(\sigma_j^-)}{\alpha_1(\sigma_j)-h_1(\sigma_j)} & \text{if } i = 5 \\ -\frac{x'_{1,i}(\sigma_j^-)}{\alpha_1(\sigma_j)-h_1(\sigma_j)} & \text{otherwise} \end{cases} \quad (\text{C.3})$$

4. *Event  $\gamma_2$  occurs at time  $\sigma_j$*

This is an endogenous event with  $g_j = x_2 - s_2 = 0$ , resulting in a  $G2R_2$  event.

The same reasoning as above applies to verify that (A.12) reduces to

$$\sigma'_{j,i} = \begin{cases} \frac{1-x'_{2,i}(\sigma_j^-)}{\alpha_2(\sigma_j)-h_2(\sigma_j)} & \text{if } i = 6 \\ -\frac{x'_{2,i}(\sigma_j^-)}{\alpha_2(\sigma_j)-h_2(\sigma_j)} & \text{otherwise} \end{cases} \quad (\text{C.4})$$

5. *Event  $\lambda_1$  occurs at time  $\sigma_j$*

This is an endogenous event with  $g_j = z_1 - \theta_{1,\min} = 0$ , resulting in a  $G2R_1$  event. Let  $\tau_p$  be the time of occurrence of the last  $R2G_1$  event before  $\lambda_1$  takes place at time  $\sigma_j$ . We have shown that  $\frac{d}{dt}z'_{1,i}(t) = 0$ ,  $i = 1, \dots, 6$  and it thus follows that  $z'_{1,i}(\sigma_j^-) = z'_{1,i}(\tau_p^+)$ . Furthermore, the fact that road 1 is undergoing a RED cycle at time  $\tau_p^-$  but will be undergoing a GREEN cycle at  $\tau_p^+$  means that  $f_{1,p-1}(\tau_p^-) = 0$  and  $f_{1,p}(\tau_p^+) = 1$ . Let also  $\tau_r$  be the time of occurrence of the last  $G2R_1$  event before  $\tau_p$ , so that we will have that  $z'_{1,i}(\tau_p^-) = z'_{1,i}(\tau_r^+)$ . Since  $z_1(t)$  is reset to zero whenever a  $G2R_1$  event takes place, we will have that  $z'_{1,i}(\tau_r^+) = 0$ . As a result, (A.8) can be easily seen to yield  $z'_{1,i}(\tau_p^+) = -\tau'_{p,i}$ ,  $i = 1, \dots, 6$ . Using a similar reasoning to the one applied for determining the change in state dynamics due to an  $R2G_1$  event at  $\tau_p$ , it is simple to verify that  $f_{1,j-1}(\sigma_j^-) = 1$  and  $f_{1,j}(\sigma_j^+) = 0$ . By substituting these expressions into (A.12), and recalling that  $\tau_p = \sigma_{j-1}$ , we obtain

$$\sigma'_{j,i} = \begin{cases} 1 + \sigma'_{j-1,1} & \text{if } i = 1 \\ \sigma'_{j-1,1} & \text{otherwise} \end{cases} \quad (\text{C.5})$$

6. *Event  $\lambda_2$  occurs at time  $\sigma_j$*

This is an endogenous event with  $g_j = z_2 - \theta_{2,\min} = 0$ , resulting in a  $G2R_2$  event. Let  $\tau_r$  be the time of occurrence of the last  $G2R_1$  event before  $\lambda_2$  takes place at time



$\sigma_j$ . The same reasoning as above applies to verify that  $z'_{2,i}(\sigma_j^-) = z'_{2,i}(\tau_r^+)$ ,  $i = 1, \dots, 6$ . Furthermore, since light switches are coupled, road 2 is undergoing a RED cycle at time  $\tau_r^-$  but will be undergoing a GREEN cycle at  $\tau_r^+$ , so that  $f_{2,r-1}(\tau_r^-) = 0$  and  $f_{2,r}(\tau_r^+) = 1$ . As a result, (A.8) can be easily seen to yield  $z'_{2,i}(\tau_r^+) = -\tau'_{r,i}$ . By substituting these expressions into (A.12), and recalling that  $\tau_p = \sigma_{j-1}$ , we obtain

$$\sigma'_{j,i} = \begin{cases} 1 + \sigma'_{j-1,1} & \text{if } i = 3 \\ \sigma'_{j-1,1} & \text{otherwise} \end{cases} \quad (\text{C.6})$$

7. *Event  $\mu_1$  occurs at time  $\sigma_j$*

This is an endogenous event with  $g_j = z_1 - \theta_{1,\max} = 0$ , resulting in a  $G2R_1$  event.

The same reasoning as in case 5 applies to verify that (A.12) reduces to

$$\sigma'_{j,i} = \begin{cases} 1 + \sigma'_{j-1,1} & \text{if } i = 2 \\ \sigma'_{j-1,1} & \text{otherwise} \end{cases} \quad (\text{C.7})$$

8. *Event  $\mu_2$  occurs at time  $\sigma_j$*

This is an endogenous event with  $g_j = z_2 - \theta_{2,\max} = 0$ , resulting in a  $G2R_2$  event.

The same reasoning as in case 6 applies to verify that (A.12) reduces to

$$\sigma'_{j,i} = \begin{cases} 1 + \sigma'_{j-1,1} & \text{if } i = 4 \\ \sigma'_{j-1,1} & \text{otherwise} \end{cases} \quad (\text{C.8})$$

This concludes the proof for a  $G2R_n$  light switching event. The analysis for an  $R2G_n$  event is similar, due to the fact that the end of a RED cycle on road  $n$  ( $R2G_n$  event) must coincide with the start of a RED cycle on road  $\bar{n}$  ( $G2R_{\bar{n}}$  event).

## C.3 Chapter 5

### C.3.1 Proof of Lemma 5.1

We begin with an occurrence of event  $e_1$  which causes a transition from state  $q^{ON}$  to state  $q^{OFF}$  at time  $\tau_j$ . This implies that  $g_j(x, \theta) = x_1 + x_2 - \theta_1 = 0$ . As a result,  $\frac{\partial g_k}{\partial x_1} = \frac{\partial g_k}{\partial x_2} = 1$ ,  $\frac{\partial g_k}{\partial x_3} = \frac{\partial g_k}{\partial z_i} = \frac{\partial g_k}{\partial \theta_2} = 0$ ,  $i = 1, 2$ , and  $\frac{\partial g_k}{\partial \theta_1} = -1$ , and it is simple to verify that (6.48) follows from (A.12).

Next, consider event  $e_2$  at time  $\tau_j$ , leading to a transition from state  $q^{OFF}$  to state  $q^{ON}$ . In this case,  $g_j(x, \theta) = x_1 + x_2 - \theta_2 = 0$ , so that  $\frac{\partial g_k}{\partial x_1} = \frac{\partial g_k}{\partial x_2} = 1$ ,  $\frac{\partial g_k}{\partial x_3} = \frac{\partial g_k}{\partial z_i} = \frac{\partial g_k}{\partial \theta_1} = 0$ ,  $i = 1, 2$ , and  $\frac{\partial g_k}{\partial \theta_2} = -1$ . Substituting into (A.12) once again yields (6.48).

### C.3.2 Proof of Theorem 5.1

We assume, without loss of generality, that the start of our sample path will coincide with the start of the first on-treatment period. Note also that we choose to end our sample path at time  $T$ , and that this choice is independent of  $\theta_i$ ,  $i = 1, 2$ . Consequently, we will have  $[0, T] \equiv [\xi_1, \eta_{K_T}]$ , which implies that  $\frac{\partial \xi_1}{\partial \theta_i} = \frac{\partial \eta_{K_T}}{\partial \theta_i} = 0$ ,  $i = 1, 2$ . Recall that the sample path of our SHA will consist of alternating on and off-treatment periods.

Since  $z_1(t) = 0$  when  $q(t) = q^{OFF}$ , we can rewrite (5.12) as

$$\begin{aligned} L(\theta, x(0), z(0), T) &= \frac{W}{T} \sum_{k=1}^{K_T} \int_{\xi_k}^{\eta_k} \left[ \frac{x_1(\theta, t) + x_2(\theta, t)}{PSA_{init}} \right] dt \\ &\quad + \frac{(1-W)}{T} \left[ \sum_{m=1}^{M_T} \int_{\xi_m}^{\eta_m} \frac{z_1(t)}{T} dt + \int_{\xi_{M_T+1}}^T \frac{z_1(t)}{T} dt \right] \end{aligned} \tag{C.9}$$

Note that our sample path can either (a) end with an incomplete on-treatment

period, or (b) end with an incomplete off-treatment period. In (C.9), we assume that (a) holds, since (b) is a special case of (a) for which  $\int_0^T \frac{z_1(t)}{T} dt = \sum_{m=1}^{M_T} \int_{\xi_m}^{\eta_m} \frac{z_1(t)}{T} dt$ . Observe that the end of an on-treatment period is coupled with the start of the subsequent off-treatment period, i.e.,  $x_i(\eta_k) = x_i(\xi_{k+1})$ ,  $i = 1, 2$ ,  $k = 1, \dots, K_T - 1$ .

Using this notation and taking the derivative of (C.9) yields

$$\begin{aligned}
\frac{dL(\theta)}{d\theta_i} &= \frac{W}{T \cdot PSA_{init}} \sum_{k=1}^{K_T-1} \int_{\xi_k}^{\xi_{k+1}} [x'_{1,i}(\theta, t) + x'_{2,i}(\theta, t)] dt \\
&+ \frac{W}{T \cdot PSA_{init}} \sum_{k=1}^{K_T-1} [x_1(\xi_{k+1}) + x_2(\xi_{k+1})] \frac{\partial \xi_{k+1}}{\partial \theta_i} \\
&- \frac{W}{T \cdot PSA_{init}} \sum_{k=1}^{K_T-1} [x_1(\xi_k) + x_2(\xi_k)] \frac{\partial \xi_k}{\partial \theta_i} \\
&+ \frac{W}{T \cdot PSA_{init}} \int_{\xi_{K_T}}^T [x'_{1,i}(\theta, t) + x'_{2,i}(\theta, t)] dt \\
&+ \frac{W}{T \cdot PSA_{init}} [x_1(T) + x_2(T)] \frac{\partial T}{\partial \theta_i} \\
&- \frac{W}{T \cdot PSA_{init}} [x_1(\xi_{K_T}) + x_2(\xi_{K_T})] \frac{\partial \xi_{K_T}}{\partial \theta_i} \\
&+ \frac{(1-W)}{T} \sum_{m=1}^{M_T} \left[ \int_{\xi_m}^{\eta_m} \frac{z'_{1,i}(t)}{T} dt + \frac{z_1(\eta_m^-)}{T} \frac{\partial \eta_m}{\partial \theta_i} - \frac{z_1(\xi_m^+)}{T} \frac{\partial \xi_m}{\partial \theta_i} \right] \\
&+ \frac{(1-W)}{T} \int_{\xi_{M_T+1}}^T \frac{z'_{1,i}(t)}{T} dt + \frac{z_1(T^-)}{T} \frac{\partial T}{\partial \theta_i} - \frac{z_1(\xi_{M_T+1}^+)}{T} \frac{\partial \xi_{M_T+1}}{\partial \theta_i}
\end{aligned} \tag{C.10}$$

Observe that multiple cancelations of the second, third and sixth terms in (C.10)

simplify to

$$\begin{aligned}
&\sum_{k=1}^{K_T-1} [x_1(\xi_{k+1}) + x_2(\xi_{k+1})] \frac{\partial \xi_{k+1}}{\partial \theta_i} \\
&- \sum_{k=1}^{K_T-1} [x_1(\xi_k) + x_2(\xi_k)] \frac{\partial \xi_k}{\partial \theta_i} \\
&= [x_1(\xi_{K_T}) + x_2(\xi_{K_T})] \frac{\partial \xi_{K_T}}{\partial \theta_i}
\end{aligned} \tag{C.11}$$

Further note that the sixth term in (C.10) cancels out with the second term on the right hand side of (C.11). Moreover, it is clear from (5.5) that  $z_1(\xi_{M_T+1}^+) = z_1(\xi_m^+) = 0$  and  $z_1(\eta_m^-) = \eta_m - \xi_m$ ,  $m = 1, \dots, M_T$ . Since  $z'_{j,i}(t) = z'_{j,i}(\tau_k^+)$ ,  $j, i = 1, 2$ , over any interevent interval  $[\tau_k, \tau_{k+1})$ , and recalling that  $\frac{\partial T}{\partial \theta_i} = \frac{\partial \xi_1}{\partial \theta_i} = 0$ , the last two terms in

(C.10) simplify to

$$\begin{aligned} & \frac{(1-W)}{T^2} \left[ \sum_{m=1}^{M_T} z'_{1,i}(\xi_m^+) (\eta_m - \xi_m) + (\eta_m - \xi_m) \frac{\partial \eta_m}{\partial \theta_i} \right] \\ & + \frac{(1-W)}{T^2} z'_{1,i}(\xi_{M_T+1}^+) (T - \xi_{M_T+1}) \end{aligned}$$

Recall that  $\xi_m$  is the start of the  $m$ th on-treatment period, which necessarily corresponds to the  $(m-1)$ th occurrence of event  $e_2$ . Hence,  $z'_{1,i}(\xi_m^+) = -\xi'_{m,i}$ ,  $m = 1, \dots, M_{T+1}$  from (6.47). As a result, (C.10) can be further simplified to

$$\begin{aligned} \frac{dL(\theta)}{d\theta_i} &= \frac{W}{T \cdot PSA_{init}} \sum_{k=1}^{K_T-1} \int_{\xi_k}^{\xi_{k+1}} [x'_{1,i}(\theta, t) + x'_{2,i}(\theta, t)] dt \\ &+ \frac{W}{T \cdot PSA_{init}} \int_{\xi_{K_T}}^T [x'_{1,i}(\theta, t) + x'_{2,i}(\theta, t)] dt \\ &+ \frac{(1-W)}{T^2} \left[ \sum_{m=1}^{M_T} -\xi'_{m,i} (\eta_m - \xi_m) + (\eta_m - \xi_m) \eta'_{m,i} \right] \\ &- \frac{(1-W)}{T^2} \xi'_{M_T+1} (T - \xi_{M_T+1}) \end{aligned} \tag{C.12}$$

The result in (C.12) is obtained under the assumption that our sample path ends with an incomplete on-treatment period, i.e.,  $K_T$  is odd. If this is not the case, the last term in (C.12) can be disregarded. It is then straightforward to verify that (C.12) can be rewritten as (6.51).

## References

- (2007). National traffic signal report card. Technical report, National Traffic Operations Coalition. available at [www.ntoctalks.com /ntocmembers.php](http://www.ntoctalks.com/ntocmembers.php).
- Abdulhai, B., Pringle, R., and Karakoulas, G. (2003). Reinforcement learning for true adaptive traffic signal control. *Journal of Transportation Engineering*, 129(3):278–285.
- Ahrendt, S., Hu, Y., Buta, M., McDermott, M. P., Benoit, N., Yang, S. C., Wu, L., and Sidransky, D. (2003). p53 mutations and survival in stage i non-small-cell lung cancer: Results of a prospective study. *JNCI Journal of the National Cancer Institute*, 95(13):961–970.
- Alla, H., Cavaille, J.-B., Bail, J. L., and Bel, G. (1992). Les systemes de production par lot: une approche discret-continu utilisant le reseaux de petri hybrides. *Automatisation des Procedes Mixtes Continus et Sequentiels: Les Processus Discontinus; 29-30 janvier 1992 = Automation of Mixed Continuous and Sequential Processes*. Paris: Ministere de la Recherche et de la Technologie.
- Alla, H. and David, R. (1998). Continuous and hybrid petri nets. *Journal of Circuits, Systems and Computers*, 8(1):159–188.
- Alrefaei, M. (1999). A simulated annealing algorithm with constant temperature for discrete stochastic optimization. *Management Science*, 45(5):748–764.
- Alur, R., Courcoubetis, C., Halwachs, N., Henzinger, T., Ho, P., Nicollin, X., Olivero, A., Sifakis, J., and Yovine, S. (1995). The algorithmic analysis of hybrid systems. *Theoretical Computer Science*, 138:3–34.
- Alvarez, I. and Poznyak, A. (2010). Game theory applied to urban traffic light control problem. In *ICCAS 2010: International Conference on Control, Automation and Systems*, pages 2164–2169. Piscataway, NJ: IEEE.
- Bail, J. L., Alla, H., and David, R. (1991). Hybrid petri nets. pages 1472–1477. Paris: Hermes.
- Barton, R. and Ivey, J. (1996). Nelder-mead simplex modifications for simulation optimization. *Management Science*, 42(7):954–973.

- Bazzan, A. (2009). Opportunities for multiagent systems and multiagent reinforcement learning in traffic control. *Autonomous Agents and Multi-Agent Systems*, 18(3):342–375.
- Bedard, P., Hansen, A., Ratain, M., and Siu, L. (2013). Tumor heterogeneity in the clinic. *Nature*, 501:355–364.
- Beerenwinkel, N., Antal, T., Dingli, D., Traulsen, A., Kinzler, K., Velculescu, V., Vogelstein, B., and Nowak, M. (2007). Genetic progression and the waiting time to cancer. *PLoS Computational Biology*, 3(11):2239–2246.
- Bertsekas, D. (2005). *Dynamic Programming and Optimal Control*. Athena Scientific.
- Boesel, J., Nelson, B., and Ishii, N. (2003). A framework for simulation-optimization software. *IEEE Transactions*, 35(3):221–229.
- Bruchovsky, N., Klotz, L., Crook, J., Malone, S., Ludgte, C., Morris, W., Gleave, M., Goldenberg, S., and Rennie, P. (2006). Final results of the Canadian prospective phase II trial of intermittent androgen suppression for men in biochemical recurrence after radiotherapy for locally advanced prostate cancer. *Cancer*, 107:389–395.
- Bruchovsky, N., Klotz, L., Crook, J., Malone, S., Ludgte, C., Morris, W., Gleave, M., Goldenberg, S., and Rennie, P. (2007). Locally advanced prostate cancer biochemical results from a prospective phase II study of intermittent androgen suppression for men with evidence of prostate-specific antigen recurrence after radiotherapy. *Cancer*, 109:858–867.
- Bujorianu, L. (2012). *Stochastic Reachability Analysis of Hybrid Systems*. Springer.
- Cassandras, C. (2015). Event-driven control and optimization in hybrid systems. In *Event-based control and signal processing*. CRC Press/Taylor and Francis.
- Cassandras, C. and Lafortune, S. (2008). *Introduction to Discrete Event Systems*. Springer.
- Cassandras, C. and Lygeros, J., editors (2007). *Stochastic Hybrid Systems*. CRC Press.
- Cassandras, C., Wardi, Y., Melamed, B., Sun, G., and Panayiotou, C. (2002). Perturbation analysis for on-line control and optimization of stochastic fluid models. *IEEE Transactions on Automatic Control*, 47(8):1234–1248.
- Cassandras, C., Wardi, Y., Panayiotou, C., and Yao, C. (2010). Perturbation analysis and optimization of stochastic hybrid systems. *European Journal of Control*, 6(6):642–664.

- Chen, C. and Lee, L. (2010). *Stochastic Optimization: An Optimal Computing Budget Allocation*. World Scientific.
- Chiu, S. (1992). Adaptive traffic signal control using fuzzy logic. *Proceedings of the Intelligent Vehicles '92 Symposium*, pages 98–107. Piscataway, NJ: IEEE Service Center.
- Choi, W., Yoon, H., Kim, K., Chung, I., and Lee, S. (2002). A traffic light controlling FLC considering the traffic congestion. In Pal, N. and Sugeno, M., editors, *Advances in Soft Computing. AFSS 2002. 2002 AFSS International Conference on Fuzzy Systems*, volume 2275 of Lecture Notes in Computer Science, pages 69–75. Berlin, New York: Springer.
- Chou, C. and Teng, J. (2002). A fuzzy logic controller for traffic junction signals. *Information Sciences*, 143(1):73–97.
- David, R. and Alla, H. (1987). Continuous petri nets. In *Papers Presented at the 8th European Workshop on Application and Theory of Petri Nets, Zaragoza, Spain*, pages 275–294.
- David, R. and Alla, H. (2001). On hybrid petri nets. *Discrete Event Dynamic Systems: Theory and Applications*, 11:9–40.
- Dexter, D. and Leith, J. (1986). Tumor heterogeneity and drug resistance. *Journal of Clinical Oncology*, 4(2):244–257.
- Dingli, D., Traulsen, A., and Pacheco, J. (2007). Stochastic dynamics of hematopoietic tumor stem cells. *Cell Cycle*, 6(4):461–466.
- Dong, C. (2004). Area traffic signal timing optimization based on chaotic and genetic algorithm approach. *Computer Engineering and Applications*, 40(29):32–34.
- Dong, C. (2006). Chaos-particle swarm optimization algorithm and its application to urban traffic control. *International Journal of Computer Science and Network Security*, 61(1):97–101.
- Dong, C., Liu, Z., and Qiu, Z. (2005). Urban traffic signal timing optimization based on multi-layer chaos neural networks involving feedback. In Wang, L., Chen, K., and Ong, Y., editors, *Advances in Natural Computation. First International Conference. ICNC 2005*, volume 3610-3612 of Lecture Notes in Computer Science, pages 340–344. Berlin, New York: Springer.
- Dressler, F., Hartenstein, H., Altintas, O., and Tonguz, O. (2014). Inter-vehicle communication Quo Vadis. *IEEE Communications Magazine*, 52(6):170–177.

- Dubois, E. and Alla, H. (1993). Hybrid petri nets with a stochastic discrete part. In Nieuwenhuis, J., Praagman, C., and Trentelman, H., editors, *Proceedings of the Second European Control Conference. ECC '93*. Netherlands.
- Dujardin, Y., Boillot, F., Vanderpooten, D., and Vinant, P. (2011). Multiobjective and multimodal adaptive traffic light control on single junctions. *2011 14th International IEEE Conference on Intelligent Transportation Systems (ITSC)*, pages 1361–1368. Piscataway, NJ: IEEE.
- Findle, N., Surender, S., and Catrava, S. (1997). On-line decision about permitted/protected left-hand turns in distributed traffic signal control. *Engineering Applications of Artificial Intelligence*, 10(3):315–320.
- Findler, N. and Strapp, J. (1992). A distributed approach to optimized control of street traffic signals. *Journal of Transportation Engineering*, 118(1):99–110.
- Fu, M. and Howell, W. (2003). Application of perturbation analysis to traffic light signal timing. *42nd IEEE Conference on Decision and Control: Proceedings*, pages 4837–4840. Piscataway, NJ: IEEE.
- Fu, M. and Hu, J. (1997). Applications of perturbation analysis to the design and analysis of control charts. *Technical Report*. available at <http://drum.lib.umd.edu/handle/1903/5893>.
- Gartner, N., Pooran, F., and Andrews, C. (2002). Implementation and field testing of the OPAC adaptive control strategy in RT-TRACS. *Journal of the Transportation Research Board*, pages 148–156.
- Geng, Y. (2013). *Optimization Methods for Intelligent Transportation Systems in Urban Settings*. PhD thesis, Boston University.
- Geng, Y. and Cassandras, C. (2012). Traffic light control using infinitesimal perturbation analysis. *In IEEE 51st Annual Conference on Decision and Control (CDC)*, pages 7001–7006. Piscataway, NJ: IEEE.
- Geng, Y. and Cassandras, C. (2013). Quasi-dynamic traffic light control for a single intersection. *2013 IEEE 52nd Annual Conference on Decision and Control (CDC)*, pages 880–885. Piscataway, NJ: IEEE.
- Geng, Y. and Cassandras, C. (2015). Multi-intersection traffic light control with blocking. *Journal of Discrete Event Dynamic Systems*, 25(1):7–30.
- Gentry, S. and Jackson, T. (2013). A mathematical model of stem cell driven tumor initiation: Implications of niche size and loss of homeostatic regulatory mechanisms. *PLoS ONE*, 8(8):e71128.



- Gerstung, M., Eriksson, N., Lin, J., Vogelstein, B., and Beerenwinkel, N. (2011). The temporal order of genetic and pathway alterations in tumorigenesis. *PLoS ONE*, 6(11):e27136.
- Glasserman, P. (1991). *Gradient Estimation via Perturbation Analysis*. Kluwer Academic.
- Hanahan, D. and Weinberg, R. (2011). Hallmarks of cancer: The next generation. *Cell*, 144:646–674.
- Head, L., Ciarallo, F., and Kaduwela, D. (1996). A perturbation analysis approach to traffic signal optimization. *INFORMS National Meeting*.
- Henry, J. and Farges, J. (1990). *PRODYN control, computers, communications in transportation*. Pergamon Press.
- Henry, J., Farges, J., and Gallego, J. (1998). Neuro-fuzzy techniques for traffic control. *Control Engineering Practice*, 6:755–761.
- Hirata, Y., Bruchovsky, N., and Aihara, K. (2010a). Development of a mathematical model that predicts the outcome of hormone therapy for prostate cancer. *Journal of Theoretical Biology*, 264:517–527.
- Hirata, Y., di Bernardo, M., Bruchovsky, N., and Aihara, K. (2010b). Hybrid optimal scheduling for intermittent androgen suppression of prostate cancer. *Chaos*, 20:045125.
- Ho, Y. and Cao, X. (1991). *Perturbation Analysis of Discrete Event Dynamic Systems*. Kluwer Academic.
- Hollstein, M. and Hainaut, P. (2010). Massively regulated genes: the example of tp53. *The Journal of Pathology*, 220(2):164–173.
- Hu, J., Fu, M., and Marcus, S. (2008). A model reference adaptive search method for stochastic global optimization. *Communications Information Systems*, 8(3):245–276.
- Hunt, P., Robertson, D., and Bretherton, R. (1982). The SCOOT on-line traffic signal optimization technique. *Traffic Engineering and Control*, 23:190–192.
- Huzarski, T., Cybulski, C., Wokolorczyk, D., Jakubowska, A., Byrski, T., Gronwald, J., Domagaa, P., Szwiec, M., Godlewski, D., Kilar, E., Marczyk, E., Sioek, M., Winiowski, R., Janiszewska, H., Surdyka, D., Sibilski, R., Sun, P., Lubiski, J., and Narod, S. (2014). Survival from breast cancer in patients with chek2 mutations. *Breast Cancer Research and Treatment*, 144(2):397–403.

- Ideta, A., Tanaka, G., Takeuchi, T., and Aihara, K. (2008). A mathematical model for intermittent androgen suppression for prostate cancer. *Journal of Nonlinear Science*, 18:593–614.
- Jackson, T. (2004a). A mathematical investigation of the multiple pathways to recurrent prostate cancer: comparison with experimental data. *Neoplasia*, 6:697–704.
- Jackson, T. (2004b). A mathematical model of prostate tumor growth and androgen-independent replace. *Discrete and Continuous Dynamical Systems. Series B*, 4:187–201.
- Kanehisa, M. and Goto, S. (2000). Kyoto encyclopedia of genes and genomes. *Nucleic Acids Research*, 28:27–30.
- Kanehisa, M., Goto, S., Sato, Y., Kawashima, M., Furumichi, M., and Tanabe, M. (2014). Data, information, knowledge and principle: back to metabolism in kegg. *Nucleic Acids Research*, 42:D199–D205.
- Kebarighotbi, A. and Cassandras, C. (2009). Revisiting the optimality of  $c\mu$  rule with stochastic flow models. *Proceedings of 48th IEEE Conference on Decision and Control, 2009*, pages 2304–2309.
- Kebarighotbi, A. and Cassandras, C. (2011a). Optimal scheduling of parallel queues using stochastic flow models. *Journal of Discrete Event Dynamic Systems*, 21:547–576.
- Kebarighotbi, A. and Cassandras, C. (2011b). Timeout control in distributed systems using perturbation analysis. *2011 50th IEEE Conference on Decision and Control and European Control Conference (CDC-ECC)*, pages 5437–5442. Piscataway, NJ: IEEE.
- Kim, S. and Zhang, D. (2010). Convergence properties of direct search methods for stochastic optimization. *Proceedings of the 2010 Winter Simulation Conference*, pages 1003–1011. Piscataway, NJ: IEEE.
- Leder, K., Pitter, K., LaPlant, Q., Hambardzumyan, D., Ross, B., Chan, T., Holland, E., and Michor, F. (2014). Mathematical modeling of PDGF-driven glioblastoma reveals optimized radiation dosing schedules. *Cell*, 156:603–616.
- Lee, A. and Swanton, C. (2012). Tumor heterogeneity and drug resistance: Personalising cancer medicine through functional genomics. *Biochemical Pharmacology*, 83:1013–1020.
- Lee, J., Lee, K., and Lee-Kwang, H. (1995). Fuzzy controller for intersection group. *1995 International IEEE/IAS Conference on Industrial Automation and Control. Emerging Technologies*, pages 367–382. Piscataway, NJ: IEEE.

- Liberzon, D. (2003). *Switching in Systems and Control*. Birkhauser.
- Little, J., Kelson, M., and Gartner, N. (1981). Maxband: a program for setting signals on arteries and triangular networks. *Transportation Research Record*, 795:40–46.
- Liu, B., Kong, S., Gao, S., Zuliani, P., and Clarke, E. (2015). Towards personalized cancer therapy using delta-reachability analysis. *HSCC’15: 18th ACM International Conference on Hybrid Systems, Computation and Control*. New York: ACM.
- Liu, Z. (2007). A survey of intelligent methods in urban traffic signal control. *International Journal of Computer Science and Network Security*, 7(7):105–112.
- Liu, Z., Wu, J., Li, X., and Wan, B. (1997). Hierarchical fuzzy neural network control for large scale urban traffic systems. *Information and Control*, 26(6):441–448.
- Longo, D., Fauci, A., Kasper, D., Hauser, S., Jameson, J., and Loscalzo, J., editors (2012). *Harrison’s principles of internal medicine*. McGraw-Hill, Medical Pub. Division, New York, 18th edition.
- Loohuis, L. (2013). *Cancer Progression: Model, Therapy and Extraction*. PhD thesis, The City University of New York.
- Loohuis, L., Caravagna, G., Graudenzi, A., Ramazzotti, D., Mauri, G., Antoniotti, M., and Mishra, B. (2014). Inferring causal models of cancer progression with a shrinkage estimator and probability raising. *preprint available at <http://biorxiv.org>*.
- Lowrie, P. (1982). The sydney co-ordinated adaptive traffic system - principles, methodology, algorithms. *International Conference on Road Traffic Signaling*, pages 67–70. London; New York: Institution of Electrical Engineers.
- Lygeros, J., Tomlin, C., and Sastry, S. (2008). Hybrid systems: Modeling, analysis and control. Lecture Notes, UC Berkeley.
- Maksimenko, J., Irmejs, A., Nakazawa-Miklasevica, M., Melbarde-Gorkusa, I., Trofimovics, G., Gardovskis, J., and Miklasevics, E. (2013). Prognostic role of BRCA1 mutation in patients with triple-negative breast cancer. *Oncology Letters*, 7(1):278–284.
- Michor, F., Iwasa, Y., and Nowak, M. (2004). Dynamics of cancer progression. *Nature Reviews Cancer*, 4:197–205.
- Murat, Y. and Gedizlioglu, E. (2005). A fuzzy logic multi-phased signal control model for isolated junctions. *Transportation Research Part C*, 18:19–36.

- Nakatsuyama, M., Nagahashi, H., and Nishizuka, N. (1984). Fuzzy logic phase controller for traffic junctions in the one-way arterial road. In Gertler, J. and Kevicky, L., editors, *A Bridge Between Control Science and Technology: Proceedings of the Ninth Triennial World Congress of IFAC*, pages 2865–2870. Oxford; New York: Published for IFAC by Pergamon Press.
- Ng, S., Collisson, E. A., Sokolov, A., Goldstein, T., Gonzalez-Perez, A., Lopez-Bigas, N., Benz, C., Haussler, D., and Stuart, J. M. (2012). Paradigm-shift predicts the function of mutations in multiple cancers using pathway impact analysis. *Bioinformatics*, 28(18):i640–i646.
- Nicolini, F., Corm, S., L, Q., Roche-Lestienne, C., and Preudhomme, C. (2007). The prognosis impact of bcr-abl p-loop mutations: worse or not worse. *Leukemia*, 21:193–194.
- Niittymäki, J., Nevala, R., and Turunen, E. (2002). Fuzzy traffic signal control and a new interface method for maximal fuzzy similarity. *Proceedings of the 13th Mini-EURO Conference Handling Uncertainty in the Analysis of Traffic and Transportation Systems*, pages 716–728. Bari: Polytechnic University of Bari.
- Panayiotou, C. (2004). On-line resource sharing in communication networks using infinitesimal perturbation analysis of stochastic fluid models. *Proceedings of 43rd IEEE Conference on Decision and Control, 2004. CDC*, pages 563–568.
- Panayiotou, C., Howell, W., and Fu, M. (2005). Online traffic light control through gradient estimation using stochastic flow models. *Proceedings of the 16th IFAC World Congress*. Oxford: Elsevier Ltd.
- Papageorgiou, M., Diakaki, C., Dinopoulou, V., Kotsialos, A., and Wang, Y. (2003). Review of road traffic control strategies. *Proceedings of the IEEE*, 91(12):2043–2067.
- Pappis, C. and Mamdani, E. (1977). A fuzzy logic controller for a traffic junction. *IEEE Transactions on Systems, Man, and Cybernetics SMC-7*, 7(10):707–717.
- Park, J., Neve, R., Szollosi, J., and Benz, C. (2008). Unravelling the biologic and clinical complexities of HER2. *Clinical Breast Cancer*, 8(5):392–401.
- Payne, S. R. and Kemp, C. J. (2005). Tumor suppressor genetics. *Carcinogenesis*, 26(12):2031–2045.
- Porche, I., Sampath, M., Sengupta, R., Chen, Y.-L., and Lafortune, S. (1996). A decentralized scheme for real-time optimization of traffic signals. *Proceedings of the 1996 IEEE International Conference on Control Applications*, pages 582–589. New York: IEEE.

- Prashant, L. and Bhatnagar, S. (2011). Reinforcement learning with function approximation for traffic signal control. *IEEE Transactions on Intelligent Transportation Systems*, 12(2):412–421.
- Raphael, B. and Vandin, F. (2015). Simultaneous inference of cancer pathways and tumor progression from cross-sectional data. *Journal of Computational Biology*, 22(6):510–527.
- Robertson, D. (1969). TRANSYT method for area traffic control. *Traffic Engineering and Control*, 10:276–281.
- Rodriguez-Brenes, I., Komarova, N., and Wodarz, D. (2011). Evolutionary dynamics of feedback escape and the development of stem-cell-driven cancers. *Proceedings of the National Academy of Sciences of the United States of America*, 108(47):18983–18988.
- Rodriguez-Brenes, I., Komarova, N., and Wodarz, D. (2014). Cancer-associated mutations in healthy individuals: assessing the risk of carcinogenesis. *Cancer Research*, doi:10.1158/008-5472.CAN-13-1452.
- Rubinstein, R. and Shapiro, A. (1993). *Discrete Event Systems: Sensitivity Analysis and Stochastic Optimization by the Score Function Method*. Wiley.
- Sahinidis, N. (2004). Optimization under uncertainty: State-of-the-art and opportunities. *Computers and Chemical Engineering*, 28:971–983.
- Schutter, B. D. (1999). Optimal traffic light control for a single intersection. *Proceedings of the 1999 American Control Conference*, 3:2195–2199. Piscataway, NJ: IEEE.
- Schutter, B. D., Heemels, W., Lunze, J., and Prieur, C. (2009). Survey of modeling, analysis, and control of hybrid systems. In Lunze, J. and Lamnabhi-Lagarigue, F., editors, *Handbook of Hybrid Systems Control - Theory, Tools, Applications*. Cambridge University Press.
- Sen, S. and Head, L. (1997). Controlled optimization of phases at an intersection. *Transportation Science*, 31:5–17.
- Shelby, S., Bullock, D., Gettman, D., Ghaman, R., Sabra, Z., and Soyke, N. (2008). Overview and performance evaluation of ACS lite - a low cost adaptive signal control system. no. 08-0334. In TRB 87th Annual Meeting: Compendium of Papers DVD. Washington, D.C.: Transportation Research Board.
- Shimada, T. and Aihara, K. (2008). A nonlinear model with competition between prostate tumor cells and its application to intermittent androgen suppression therapy of prostate cancer. *Mathematical Biosciences*, 214:134–139.

- Somasundaram, R., Villanueva, J., and Herlyn, M. (2012). Intratumoral heterogeneity as a therapy resistance mechanism: Role of melanoma subpopulations. *Advances in Pharmacology*, 65:335–359.
- Spall, J. and Chin, D. (1997). Traffic-responsive signal timing for system wide traffic control. *Transportation Research Part C: Emerging Technologies*, 5(3):153–163.
- Stevanovic, A. (2010). Adaptive traffic light control systems: Domestic and foreign state of practice. *Transportation Research Board NCHRP Synthesis 403*.
- Sun, G., Cassandras, C., and Panayiotou, C. (2004a). Perturbation analysis and optimization of stochastic flow networks. *IEEE Transactions on Automatic Control*, 49(12):2113–2128.
- Sun, G., Cassandras, C., and Panayiotou, C. (2004b). Perturbation analysis of multiclass stochastic fluid models. *Journal of Discrete Event Dynamic Systems*, 14(3):267–307.
- Sun, G., Cassandras, C., Panayiotou, C., and Wardi, Y. (2003). Perturbation analysis and control of two-class stochastic fluid models for communication networks. *IEEE Transactions on Automatic Control*, 48(5):770–782.
- Suzuki, T., Bruchovsky, N., and Aihara, K. (2010). Piecewise affine systems modelling for optimizing therapy of prostate cancer. *Philosophical Transactions of the Royal Society of London. Series A*, 368:5045–5059.
- Tanaka, G., Hirata, Y., Goldenberg, S., Bruchovsky, N., and Aihara, K. (2010). Mathematical modelling of prostate cancer growth and its application to hormone therapy. *Philosophical Transactions of the Royal Society of London. Series A*, 368:5029–5044.
- Tao, Y., Guo, Q., and Aihara, K. (2010). A mathematical model of prostate tumor growth under hormone therapy with mutation inhibitor. *Journal of Nonlinear Science*, 20:219–240.
- TCGA (2008). Comprehensive genomic characterization defines human glioblastoma genes and core pathways. *Nature*, 455:1061–1068.
- TCGA (2014). Comprehensive molecular profiling of lung adenocarcinoma. *Nature*, 511:543–550.
- The Cancer Genome Atlas Research Network (2012a). Comprehensive genomic characterization of squamous cell lung cancers. *Nature*, 489(7417):519–525.
- The Cancer Genome Atlas Research Network (2012b). Comprehensive molecular characterization of human colon and rectal cancer. *Nature*, 487(7407):330–337.

- The Cancer Genome Atlas Research Network (2012c). Comprehensive molecular portraits of human breast tumours. *Nature*, 490(11412):61–70.
- The Cancer Genome Atlas Research Network (2014). Comprehensive molecular profiling of lung adenocarcinoma. *Nature*, 511(7511):543–550.
- Thorpe, T. (1997). Vehicle traffic light control using SARSA. Master’s thesis, Department of Computer Science, Colorado State University.
- Trabia, M., Kaseko, M., and Ande, M. (1996). A two-stage fuzzy logic controller for traffic signals. *Transportation Research Part C*, 7(16):353–367.
- Turner, N. and Reis-Filho, J. (2012). Genetic heterogeneity and cancer drug resistance. *Lancet Oncology*, 13:e178–e185.
- Ukkusuri, S., Ramadurai, G., and Patil, G. (2010). A robust transportation signal control problem accounting for traffic dynamics. *Computers & Operations Research*, 37(5):869–879.
- Vaske, C., Benz, S., Sanborn, J., Earl, D., Szeto, C., Zhu, J., Haussler, D., and Stuart, J. (2010). Inference of patient-specific pathway activities from multi-dimensional cancer genomic data using paradigm. *Bioinformatics*, 26:i237–i245.
- Vassilev, L. T., Vu, B. T., Graves, B., Carvajal, D., Podlaski, F., Filipovic, Z., Kong, N., Kammlott, U., Lukacs, C., Klein, C., Fotouhi, N., and Liu, E. A. (2004). In vivo activation of the p53 pathway by small-molecule antagonists of mdm2. *Science*, 303(5659):844–848.
- Vogel, C., Cobleigh, M., Tripathy, D., Gutheil, J., Harris, L., Fehrenbacher, L., Slamon, D., Murphy, M., Novotny, W., Burchmore, M., Shak, S., and Stewart, S. (2001). First-line, single-agent herceptin(c) (trastuzumab) in metastatic breast cancer. *European Journal of Cancer*, 37(Suppl.1):25–29.
- Vogelstein, B. and Kinzler, K. (2004). Cancer genes and the pathways they control. *Nature Medicine*, 10(8):789–799.
- Vogelstein, B., Papadopoulos, N., Velculescu, V., Zhou, S., Jr., L. D., and Kinzler, K. (2013). Cancer genome landscapes. *Science*, 339:1546–1558.
- Wadhwa, P., Zielske, S., Roth, J., Ballas, C., Bowman, J., and Gerson, S. (2002). Cancer gene therapy: Scientific basis. *Annual Review of Medicine*, 53:437–452.
- Wardi, Y., Adams, R., and Melamed, B. (2010). A unified approach to infinitesimal perturbation analysis in stochastic flow models: the single-stage case. *IEEE Transactions on Automatic Control*, 55(1):89–103.

- Wei, W., Zhang, Y., Mbede, J., Zhang, Z., and Song, J. (2001). Traffic signal control using fuzzy logic and MOGA. In Bahill, T., editor, *2001 IEEE International Conference on Systems, Man, and Cybernetics*, pages 1335–1340. Piscataway, NJ: IEEE.
- Weinstein, J. N., Collisson, E. A., Mills, G. B., Shaw, K. R. M., Ozenberger, B. A., Ellrott, K., Shmulevich, I., Sander, C., and Stuart, J. M. (2013). The cancer genome atlas pan-cancer analysis project. *Nature genetics*, 45(10):1113–1120.
- Wen, W. and Hsu, H. (2006). A dynamic and automatic traffic light control system for solving the road congestion problem. *WIT Transactions on the Built Environment*, 89:307–316.
- Wen, Y. and Wu, T. (2005). Reduced-order rolling horizon optimization of traffic control based on ant algorithm. *Journal of Zhejiang University (Engineering Science)*, 39(6):835–839.
- Werner, B., Dingli, D., Lenaerts, T., Pacheco, J., and Traulsen, A. (2011). Dynamics of mutant cells in hierarchical organized tissues. *PLoS Computational Biology*, 7(12):e100290.
- Werner, B., Dingli, D., and Traulsen, A. (2013). A deterministic model for the occurrence and dynamics of multiple mutations in hierarchically organized tissues. *Journal of the Royal Society, Interface*, 10:20130349.
- Wey, W.-M. (2000). Model formulation and solution algorithm of traffic light control in an urban network. *Computers, Environment and Urban Systems*, 24:355–377.
- Wiering, M., Vennen, J., and Koopman, A. (2004). Intelligent traffic light control. Technical Report UU-CS-2004.
- Xu, D., Fang, J., and Shao, S. (1992). A fuzzy controller of traffic systems and its neural network implementation. *Information and Control*, 21(2):74–78.
- Yao, C. and Cassandras, C. (2011a). Perturbation analysis of stochastic hybrid systems and applications to resource contention games. *Frontiers of Electric and Electronic Engineering China*, 6:453–467.
- Yao, C. and Cassandras, C. (2011b). Resource contention games in multiclass stochastic flow models. *Nonlinear Analysis:Hybrid Systems*, 5(2):301–319.
- Yu, H. and Cassandras, C. (2006). Perturbation analysis and feedback control of communication networks using stochastic hybrid models. *Journal of Nonlinear Analysis*, 65(6):1251–1280.
- Yu, X.-H. and Recker, W. (2006). Stochastic adaptive control model for traffic light systems. *Transportation Research Part C: Emerging Technology*, 14:263–282.



- Zahreddine, H. and Borden, K. (2013). Mechanisms and insights into drug resistance in cancer. *Frontiers in Pharmacology*, 4:1–8.
- Zhao, X. and Chen, Y. (2003). Traffic light control method for a single intersection based on hybrid systems. *Proceedings of the 2003 IEEE International Conference on Intelligent Transportation Systems. Vol. 2*, pages 1105–1109. Piscataway, NJ: IEEE.

# CURRICULUM VITAE

**Julia Lima Fleck**

jffleck@bu.edu

## EDUCATION

**Boston University, Boston, MA**

Ph.D. in Systems Engineering - Expected May 2016

Current Research: Design of personalized cancer therapy using Infinitesimal Perturbation Analysis

Related Coursework: Optimization Theory, Dynamic Programming, Nonlinear Systems and Control, Discrete Event and Hybrid Systems

Related Skills: Algorithm development, Programming in Matlab and C/C#

**Catholic University (PUC-Rio), Rio de Janeiro, Brazil**

M.S. in Mechanical Engineering - August 2008

Thesis: “Artificial Neural Network Modeling for Quality Inference of a Polimerization Process”

**Federal University of Rio de Janeiro (UFRJ), Rio de Janeiro, Brazil**

B.Eng. in Chemical Engineering - August 2006

Areas of Concentration: Modeling and control of dynamical systems

## HONORS AND AWARDS

National Institute of Cancer Travel Award - sponsored speaker at the Systems Approaches to Cancer Biology Meeting, Woods Hole, MA - April 2016

Center for Information and Systems Engineering Award - 1st prize, Boston University - April 2015

Boston University Women’s Guild Scholarship, Boston University - May 2014

Full Tuition Academic Scholarship, Catholic University - August 2006 - August 2008

## RELATED EXPERIENCE

**Boston University, Boston, MA**

Graduate Research Assistant - May 2012 - Present

Graduate Teaching Assistant - September 2011 - May 2012

**Tecgraf/Catholic University (PUC-Rio), Rio de Janeiro, Brazil**

Researcher - September 2008 - August 2011

**Catholic University (PUC-Rio), Rio de Janeiro, Brazil**

Graduate Teaching Assistant - January 2007 - June 2007

**Chemtech - A Siemens Company, Rio de Janeiro, Brazil**

Engineering Intern - October 2005 - September 2006

**Federal University of Rio de Janeiro (UFRJ), Rio de Janeiro, Brazil**

Undergraduate Teaching Assistant - January 2002 - June 2005

Undergraduate Research Assistant - March 2003 - July 2004

**PAPERS AND PUBLICATIONS**

Fleck, J.L., Pavel, A.B., and Cassandras, C.G. Integrating mutation and gene expression cross-sectional data to infer cancer progression, *BMC Systems Biology*, DOI 10.1186/s12918-016-0255-6, 2016.

Fleck, J.L. and Cassandras, C.G. Optimal design of personalized prostate cancer therapy design using Infinitesimal Perturbation Analysis, *Nonlinear Analysis: Hybrid Systems*, under review.

Fleck, J.L. and Cassandras, C.G. Personalized cancer therapy design: Robustness vs. Optimality, *55th IEEE Conference on Decision and Control*, submitted.

Fleck, J.L. and Cassandras, C.G. Infinitesimal Perturbation Analysis for personalized cancer therapy design, *Proceedings of the 5th IFAC Conference on Analysis and Design of Hybrid Systems*, p. 205-210, 2015.

Fleck, J.L., Cassandras, C.G., and Geng, Y. Adaptive quasi-dynamic traffic light control, *IEEE Transactions on Control Systems Technologies*, to appear.

Fleck, J.L. and Cassandras, C.G. Infinitesimal Perturbation Analysis for quasi-dynamic traffic light controllers, *Proceedings of the 2014 Intl. Workshop on Discrete Event Systems*, p. 235-240, 2014.

**PROJECTS****Cancer Hybrid Automaton - New York University, New York, NY - July 2014**

The Cancer Hybrid Automaton (CHA) is a formalism to model the progression of cancer through various stages based on the concept of hybrid automata. Involvement encompassed developing control theory associated with the CHA.

**IBM Smarter Cities Challenge - Boston, MA - June 2012**

The Smarter Cities Challenge is a program launched by IBM to help cities become more instrumented, interconnected, and intelligent. Involvement encompassed developing a common data model and implementing preliminary visualizations of analyzed data.

## ORGANIZATIONS

### **West End House Boys & Girls Club, Boston, MA - Mentor - September 2014 - May 2015**

The Girls Science Club is an outreach program organized by Graduate Women in Science and Engineering (GWSE), a student organization at Boston University that seeks to strengthen the role of women in science and technology. Mentors (female STEM students from Boston University) use fun, hands-on activities to convey important concepts from the STEM field to elementary school girls.

### **Student Association of Graduate Engineers, Boston University, Boston, MA - Vice president, Systems Engineering Representative - September 2012 - May 2014**

The Student Association of Graduate Engineers (SAGE) is a student organization whose members and officers are graduate students in the College of Engineering at Boston University. The goal of SAGE is to address the issues and concerns of engineering graduate students. SAGE officers act as liaisons between the graduate student body and university officials and also organize non-academic activities that foster interactions between students.

## LANGUAGES

English - bilingual proficiency

French - full professional proficiency

German - professional working proficiency

Portuguese - bilingual proficiency